MASTER EN INVESTIGACIÓN MATEMÁTICA

The nuclear magnetic resonance and the magnetic resonance imaging process. Introducing random differential equation systems for Bloch equations model.

TFM submitted by César Catalán Capaccioni.

Supervised by:
Dr. Juan Carlos Cortés López and Dr. Rafael Jacinto Villanueva Micó.

Contents

I remember when I was 17 years old, where mathematics, physics and machines were so attractive to me, for this reason I decided to begging the Master's Degree in Industrial Engineering (electrical and mechanical fields) here at the U.P.V. university. I have developed my professional profile into several branches such as automotive, agri-food industry, aesthetic medicine, aquariums, building sector and the last ten years within the hospital engineering branch.

Motivated by educational maths due to, both my own children, I decided continue to learn advanced maths two years ago, I also took in mind embark into a mathematical doctorate programme, so I enrolled and coursed the Master's Degree in Mathematical Research, **INVESTMAT**, at U.V. & U.P.V. located in Valencia because of it I present the current work.

As we have told above, during the last ten years I have just dedicated my professional adventure into the medical field. I participated as a MEP (Mechanical-Electrical-Plumber) engineer manager in the construction of an Hospital near Valencia. Over there, I had the opportunity to implant all different medical equips including a **1,5T Magnetic Resonance**, which was possibility the most complicated and technological efforts so far taken in this regard. Physical, chemical and all engineering systems and installations take place in this installation: electromagnetic homogeneity requirements, the magnetic shield of the room for safety purposes, temperature and humidity specifications should have high levels of accuracy and reliability, three different air cooling systems for the room and a cryo-cooler compressor water cooling, for refrigerating the superconductor magnet and gradients, the acoustic and vibration requirements within the rooms in which the patients and technicians are impacted by the noise of the MR system as the gradients are pulsed and the acoustic noise transmitted to other spaces via airborne and structureborne paths, ventilation and an exhaust fan set-up system for evacuating gas Helio from inside the room, the slab stability for supporting the weight of the magnet (around 4.000 Kg/m^2) and as well its composition to avoid external, internal magnetic

interferences and other ones.

But after the commissioning of the **Magnetic Resonance** I observed at the operator workspace several images related to brains and knees obtained through the scanner and I asked myself: how is it possible to obtain these high quality images only with a magnet or an electromagnetic field?, how does it work?

The interest of these questions returned during this postgraduate, therefore I took the decision to write a review and expose the maths significance in this area and the recent researches, furthermore we introduce and solve the matrix Bloch random equations system which govern this process computing the 1-p.d.f. by using the Random Variable Transformation (R.V.T.) method.

I would like to thank my wife, Ana, for supporting me over this last years on weekends, in the evenings, nights and holidays. Many thanks for the supervisors Juan Cortés and Rafael Jacinto for all of their guidance through this process.

I would also like to thank all academics, doctors and coordinators belong to this Master's Degree in Mathematical Research, INVESTMAT, which have been motivating and encouraging me for these years in order to open me eyes towards the mathematical research.

Chapter 1

Introduction.

The **MRI** (Magnetic Resonance Imaging) is a noninvasive diagnostic procedure employed in the **NMR** (Nuclear Magnetic Resonance) scanner to obtain detailed sectional images of the internal structure of the body. This technique has played a major role in the revolution over the last 30 years. In this sense, the influence and development of Mathematics are essential for making it possible understanding and eliminating the **Artifacts** of the images, **quickly**, with accurate and efficiency. Thus, this is necessary for recovering as soon as possible the investment of the medical equipments and make a diagnosis using right and precise images.

In this work we will introduce the **Bloch equation** which govern the **MRI** process and how the perturbation fields, inhomogeneities and dynamic flow affect to the image results. We overview the tend researches to solve the nonlinear differential equation systems and some numerical, discretization and convergence methods for modelling and resolving it [1], [2].

But the main purpose of this work is to introduce and solve the basic Bloch equations model as a random differential equation systems and obtain conclusions about of their possible applications.

Magnetic Resonance Imaging (**MRI**) is a method that generates exquisite images of the soft tissue anatomy of the human body. The principle of MRI is to record the variations of the nuclear magnetization of the biological tissues by using different kinds of magnetic fields. A static magnetic field $\vec{\mathbf{B}}_0$ is used to generate a macroscopic nuclear magnetisation $\vec{\mathbf{M}}$ in the body to be imaged; typically $\vec{\mathbf{B}}_0$ has a strength around 1,5 - 5 Tesla, but technology and

magnets are increasing quickly. To shift the magnetisation vector $\vec{\mathbf{M}}$ from its equilibrium position, a radio-frequency magnetic field (RF field) $\vec{\mathbf{B}}_1$ is applied at every characteristic pulsation determined by the Larmor frequency,

$$\omega_0 = \gamma \|\vec{B_0}\| \tag{1.1}$$

where γ is a constant called the gyro-magnetic ratio ($\gamma = 42.58$ MHz by Tesla for proton for the hydrogen atom), thus if we applied a magnetic field of 1 Tesla ($\|\vec{B_0}\| = 1$ T), the *Larmor frequency* $\omega_0 \simeq 42.58$ MHz for proton. In MRI this phenomenon is known as resonance process. The position of the magnetisation vector at the end of the resonance process is determined by the duration of the RF field $\vec{\mathbf{B}}_1$. Typically this duration is chosen so that the angle between the initial position and the resulting one is $\frac{\pi}{2}$ or π. When the RF field $\vec{\mathbf{B}}_1$ is stopped, the magnetisation tends to return to its equilibrium position in a process called the relaxation. During the relaxation process the magnetisation creates an induced electric signal in an antenna set in a plane perpendicular to $\vec{\mathbf{B}}_0$. This signal is acquired for subsequent processing and gives rise to the image. Moreover, magnetic field gradients (static magnetic field aligned with $\vec{\mathbf{B}}_0$) are applied during the imaging process to set up a spatial correspondence between position in the boy and position in the image through a frequency encoding of the MRI signal.

Any perturbation of the magnetic fields involved in MRI can disturb the imaging process. The result is a local deformation of the image (called *artifact*) that may render the image inaccurate and useless for medical diagnostics. Sources of perturbation of magnetic fields are various and can be classified mainly in four groups: the one connected to the static magnetic field and the gradients, the one connects to the RF field, the external one and those attached to the dynamic of the fluids and tissues inside the body. Moreover one can distinguish between defects that are properties of the MRI device (e.g. non uniformity of the magnetic fields over the whole imaging area) and perturbations of the magnetic fields due to the patient himself. Since they are fixed properties of the MRI device, the first ones can handled with efficiency, either by the use of additional components or by taking into account their effect in the reconstruction of the algorithm. It is much more difficult to deal with the other ones as they are no identical from one experiment to the other. Common causes of such magnetic field perturbations are changes of magnetic properties in the sample due to metallic implanted objects, such as dental prostheses, hip prostheses, vascular clips, internal orthopaedic devices, metallic surgical instruments used in interventional MRI, etc. On other hand the existing dynamic processes inside a body (vessels, heart, blood, angiographic techniques,

etc.) require to introduce new phisical concepts for interpreting and reduce the artifact images.

Artifacts produced by the magnetic susceptibility of metallic implants have been widely studied in the literature using an experimental approach, as well as using mathematical modelling and numerical simulation. In the last decade attention has been paid to MRI artifacts caused by *eddy currents* in conducting metallic implants. Eddy currents may originate either from RF field $\vec{\mathbf{B}}_1$, from the field gradients or form external or electrical or magnetic field divergences. However it has been found that artifacts due to eddy currents from the magnetic field gradients are not significant.

For simple test objects (cylindersm spheres or ellipsoids) analytical expresions for the RF perturbation are known. In general a precise calculation of the RF field perturbation involves a boundary value problem with partial differential equation derived from Maxwell's equations and requires the use of PDE aproximations schemes. Among the classical methods are the finite element method, the finite difference method and the boundary element method.

In chapter 2 we first explain and introduce the Bloch equation and the processes involving MRI, in chapter 5 we expose an efficient and accurate model for solving of RF artifacts due to eddy current [1] and at the end of this chapter we will expose the well-possedness of the Bloch model for dinamical flow and its associated semi-discrete equation [2].

1.1 The NMR history.

In **1946** nuclear magnetic resonance (NMR) in condensed matter was discovered simultaneously by **Edward Purcell** at Harvard and **Felix Bloch** at Stanford using different instrumentaton and techniques. Both groups, however, observed the response of magnetic nuclei, placed in an uniform magnetic field, to a continuous wave (CW) radio frequency magnetic field as the field was tuned through resonance. This discovery opened up a new form of spectroscopy which has become one of the most important tools for physicists, chemists, geologists, and biologists.

In **1950 Erwin Hahn**, a young postdoctoral fellow at the University of Illinois, explored the response of magnetic nuclei in condensed matter to pulse burst of these same radio frequency (**RF**) magnetic fields. Hahn was interested in observing transient effects on the magnet nuclei after the RF burst. During these experiments he observed a spin echo signal; that is, a signal from the magnetic nuclei that occurred after a two pulse sequence at a time equal to

the delay time between the two pulses. This discovery, and his brillant analysis of the experiments, gave birth to a new technique for studying magnetic resonance. This pulse method originally had only a few practitioners, but now it is the method of choise for most laboratories. For the first twenty years after its discovery, continuous wave (CW) magnetic resonance apparatus was used in almost every research chemistry laboratory, and no commercial pulsed NMR instrument were available. However, since **1966** when **Ernst** and **Anderson** showed that high resolution NMR spectroscopy can be achieved using Fourier transforms of the transient response, and cheap fast computers made this calculation practical, pulsed NMR has become the dominant commercial instrumentation for most research applications.

This technology has also found its way into medicine, **Paul C. Lauterbur** (died in 2007) shared the Nobel Prize in Medicine in **2003** for developing magnetic resonance imaging into a way to look inside living organisms.He was a real pioneer in the study of the nucleus of the carbon atom. Dr. Lauterbur became interested in possible biological applications of nuclear magnetic resonance after reading a paper in 1971 by Raymond V. Damadian, who described how some cancerous tissues responded differently to the magnetic fields than normal tissue. Until then, most scientists placed the samples in a uniform magnetic field, and the radio signals emanated from the entire sample. Dr. Lauterbur realized that if a nonuniform magnetic field were used, then the radio signals would come from just one slice of the sample, allowing a two-dimensional image to be created. Dr. Lauterbur shared the Nobel Prize with Sir **Peter Mansfield** of the University of Nottingham in England, who also came up with the idea of using a non-uniform magnetic field and developed mathematical techniques for analyzing the data. The images can be stacked together to form a three-dimensional view.

When NMR imaging became common for medical uses, the name was tweaked to magnetic resonance imaging (MRI), the nuclear dropped for fear that patients might think radioactive elements are used. MRI (magnetic resonance imaging) scans are revolutionizing radiology. This imaging technique seems to be completely noninvasive, produces remarkable three dimensional imagens, and has the potential to give physicians detailed information about the inner working of living systems. For example, preliminary work has already shown that blood flow patterns in both the brain and the heart can be studied without dangerous catheterization or injection of radioactive isotopes. Someday, MRI scans may be able to pinpoint malignant tissue without biop-

sies. MRI is in its infancy, and we will see many more applications of this diagnostic tool in the coming years [18].

1.2 The MR physical principle.

In clinical MRI the image is formed by the signals from protons in water and lipid. At the atomic level, since a proton is a charged particle which spins around an internal axis of rotation with a given value of angular momentum $\vec{P}$, it also has a magnetic moment μ, and therefore can be thought of as a very small magnet with a north and south pole.

The internal rotation of a proton creates a magnetic moment, and so the proton acts as a magnet with north and south pole as shown in Figure 1.1.
The hydrogen nucleus with one proton is the nucleus of choice in MRI because it possesses the strongest magnetic moment and its abundance in organic tissues.
The magnitude of the proton's magnetic moment is proportional to the magnitude of the angular momentum $\|\vec{\mu}\| = \gamma\|\vec{P}\|$.

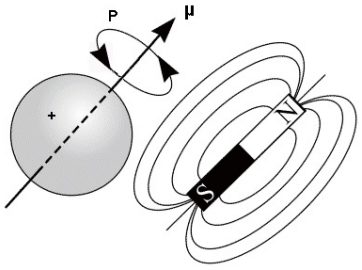

Figure 1.1: proton acts as a magnet.

As a result, the magnitude of the magnetic moment has a single, fixed value and in absence of an external magnetic field ($\vec{\mathbf{B}}_0$), as shown in Figure 1.2, the magnitude of the magnetic moment of every proton in our bodies is fixed, but the orientation is completely random. Therefore, the net magnetization ($\mathbf{M_0}$), i.e. the sum of all the individual magnetic moments in our bodies is zero.

The situation changes with the application of an external magnetic field ($\vec{\mathbf{B}}_0$). From quantum mechanics, the component of the magnetic moment in the direction of ($\vec{\mathbf{B}}_0$) can have only two possible discrete values, which results in the magnetic moments being aligned with respect to ($\vec{\mathbf{B}}_0$) in the same direction as we can see in Figure 1.3.

The relative number of protons in the parallel and anti-parallel configurations depend upon the value of $\vec{\mathbf{B}}_0$. Protons in the parallel configuration are

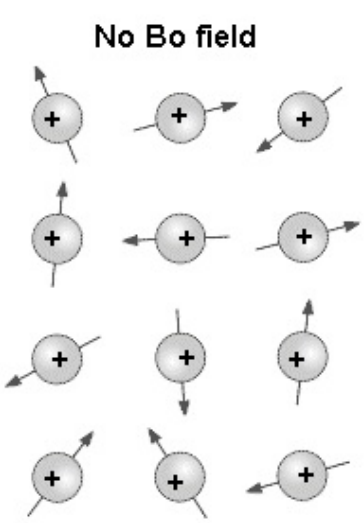

Figure 1.2: orientation of protons in absence of B_0.

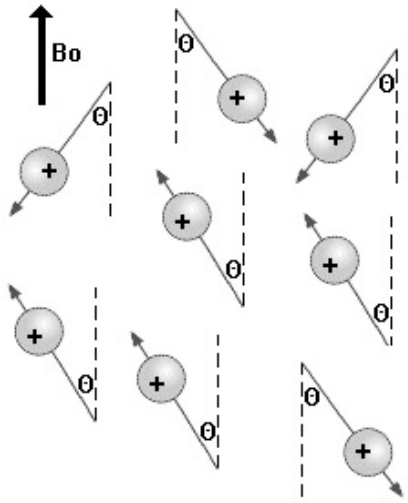

Figure 1.3: orientation of protons when a strong magnetic field B_0 is applied.

preferred because it guarantees the lowest energy state (see Figure 1.4) and the energy difference is given by

$$\Delta E = \frac{\gamma h B_0}{2\pi} \quad \text{with } h \equiv \text{Plank's constant} = 6.63 \cdot 10^{-34} Js. \tag{1.2}$$

It is possible to calculate the relative number of protons in each of the two configurations with the Boltzmann equation:

$$\frac{N_{anti-parallel}}{N_{parallel}} = e^{-\frac{\Delta E}{kT}}, \tag{1.3}$$

with $k \equiv$ Boltzmann's constant $k = 1.38 \cdot 10^{-23}$ J/K and T is temperature in K, and we notice that the exponent $\frac{\Delta E}{kT}$ is very small $\rightarrow e^{-x} \approx 1 - x$, therefore

$$\frac{N_{anti-parallel}}{N_{parallel}} = 1 - \frac{\Delta E}{kT}, \tag{1.4}$$

thus

$$N_{parallel} - N_{anti-parallel} = N_{total} \frac{\Delta E}{kT} = N_{total} \frac{\gamma h B_0}{2\pi kT}, \tag{1.5}$$

where N_{total} represent the total number of protons. Equation 1.5 shows that the MRI signal depends upon the difference in populations between the two

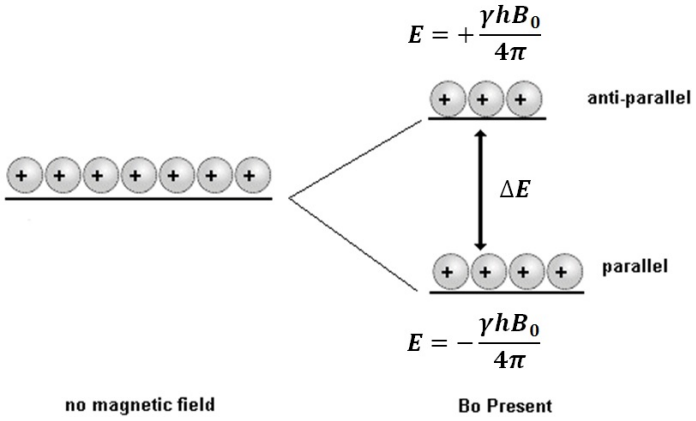

Figure 1.4: orientation of protons in absence of B_0.

energy levels. It is important to note that MRI can detect only the difference in populations between $N_{paralllel}$ and $N_{antiparallel}$, and not the total number of protons.

By superimposing all proton magnetic moments we can represent the net magnetization in a simple vector form, with slightly more protons in the parallel than anti-parallel state. The total magnetization can be calculated by a simple vector sum of the individual components $\vec{\mu}_i$. The net magnetization has only a z-component since the vector sum of the components has only a z-component, since the vector sum of the components on the x- and y-axes is zero.

Thus the net magnetization vector $\vec{\mathbf{M}}_0$ for of the sample is defined as:

$$\vec{\mathbf{M}}_0 = \sum_{Vol(V)} \vec{\mu}_{zn} = \frac{\gamma h \vec{B_0}}{4\pi}(N_{parallel} - N_{anti-parallel}) = N_{total}\frac{\gamma^2 h^2 \vec{B_0}}{16\pi^2 kT}. \quad (1.6)$$

1.3 The Larmor frequency.

We have determined that the proton magnetic moments are all aligned at an angle θ with respect to the direction of $\vec{\mathbf{B}}_0$. The motion of these magnetic moments can most easily be described using classical mechanics in a macroscopic scope, so the $\vec{\mathbf{B}}_0$ field attempts to align the macroscopic magnetic moment $\vec{\mathbf{M}}$ with itself, and this action create a torque, $\vec{\mathbf{C}}$, given by the cross product of

the two magnetic fields:

$$\vec{C} = \vec{M} \times \vec{B}_0 = \|\vec{M}\| \cdot \|\vec{B}_0\| \cdot \sin\theta \cdot \vec{\imath}_N, \tag{1.7}$$

where $\vec{\imath}_N$ is a unit vector normal to both $\vec{\mathbf{M}}$ and $\vec{\mathbf{B}}_0$.The direction of the torque is tangential to the $\vec{\mathbf{M}}$ direction and so causes the proton to "precess" around the axis of the magnetic field $\vec{\mathbf{B}}_0$. See Figure 1.5.

To calculate how fast a proton precesses, we use the fact that the torque is defined as the rate of change of the proton's angular momentum, thus

$$\vec{C} = \frac{\partial \vec{P}}{\partial t} = \vec{M} \times \vec{B}_0.$$

From Figure 1.5, the magnitude of the component of the angular momentum which precesses in the plane perpendicular to $\vec{\mathbf{B}}_0$ (plane xy) is given by $\|\vec{\mathbf{P}}\| \cdot \sin\theta$. In a short time ∂t, $\vec{\mathbf{M}}$ precesses through an angle $\partial\alpha$ resulting in a change $\partial\vec{P}$ in the angular momentum. By trigonometry in plane xy it is possible to give the relationship that

$$\sin(\partial\alpha) = \frac{\partial \vec{P}}{\|\vec{P}\| sin\theta} = \frac{\vec{C} \cdot \partial t}{\|\vec{P}\| \sin\theta}, \tag{1.8}$$

thus, from equation (1.8) we use the approximation $\sin(\partial\alpha) \approx \partial\alpha$ to obtain the angular precession frequency $\omega_0 = \frac{\partial\alpha}{\partial t}$ when a magnetic field $\vec{B}_0$ is applied.

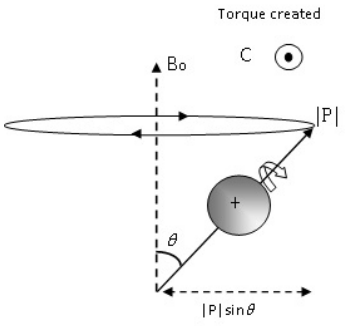

Figure 1.5: precession motion.

$$\omega = \frac{\partial\alpha}{\partial t} = \frac{\vec{C}}{\|\vec{P}\| \sin\theta} = \frac{\vec{M} \times \vec{B}_0}{\|\vec{P}\| \sin\theta} = \frac{\gamma\vec{P} \times \vec{B}_0}{\|\vec{P}\| \sin\theta} = \frac{\gamma\|\vec{P}\|\|\vec{B}_0\| \sin\theta}{\|\vec{P}\| \sin\theta} = \gamma\|\vec{B}_0\|.$$

1.4 Bloch equation and the oscillator model.

As we will expose in chapter 2 the time evolution of the macroscopic magnetization, in presence of an external static magnetic field $\vec{B}_0$ can be obtained from Bloch model (equation 2.1) by averaging the magnetic moments over a continuum volume (1.6).

$$\frac{\partial \vec{M}}{\partial t} = \gamma \vec{M} \times \vec{B}. \tag{1.9}$$

Equation (1.9) is based on the implicit assumption that the protons are non-interacting.

So if we apply a radio frequency magnetic field B_1 to "excite" a uniformly magnetized sample, the magnetization vectors tip over and experience transversal precession at the know Larmor frequency.

The magnetization in the transverse plane is very often described using a complex notation as

$$\vec{M}_{xy}(t) = M_x(t) + iM_y(t) = \|\vec{M}_{xy}(t)\| e^{i(\omega+\psi)} = M_{xy}(t) e^{i(\omega+\psi)}. \tag{1.10}$$

To get a response from an object going through an NMR experiment, the orientation of the longitudinal magnetization is altered by applying an oscillating magnetic field $\vec{B}_1(t) = B_{1x}(t)\vec{e}_x + B_{1y}(t)\vec{e}_y$ from a nearby RF transmit coil.

If the resonance condition is fulfilled, the $\vec{B}_1$ field tilts the magnetization towards the transverse plane (Figure 4.1).

The RF excitation field in the transverse plane is specified by the shape and the duration τ_p of the envelope function $\vec{B}_1(t)$, the excitation carrier frequency ω_1 and the initial phase ψ_1 of the RF pulse, expressed in the complex notation as

$$\vec{B}_1(t) = B_{1x}(t) + iB_{1y}(t) = \|\vec{B}_1(t)\| e^{i(\omega_1+\psi_1)} = B_1(t) e^{i(\omega_1+\psi_1)}. \tag{1.11}$$

$B_1(t)$ determines the flip angle θ of the magnetization due to the RF pulse by the following relation

$$\theta(\tau_p) = \gamma \int_0^{\tau_p} B_1(t) dt. \tag{1.12}$$

Immediately after $\vec{M}$ is tilted from its equilibrium position, the spins inside the excited volume mutually interact among themselves and with the surrounding to precess towards the equilibrium state again.

The precession of the spins towards the equilibrium position, as depicted in

Figure 4.1, is characterized by two phenomenologically determined intrinsic time constants called T_1 and T_2 times (see section 2.1) and initial Bloch equation (1.9) transforms into

$$\frac{\partial \vec{M}}{\partial t} = \gamma \vec{M} \times \vec{B} - \frac{M_x \vec{e}_x + M_y \vec{e}_y}{T_2} - \frac{(M_z + \tau_0)\vec{e}_z}{T_1}. \tag{1.13}$$

After the RF excitations time evolution of magnetizations are governed by the relaxation and the presence of the static magnetic field. The time evolution of transverse and longitudinal magnetizations can be expressed and solved as we expose in chapter 3, taking initial condition as the magnetization result finishing the RF process, where $M_{0xy} = M_{xy}(\tau_p)$ and $M_{0z} = M_z(\tau_p)$ (see chapter 4).

1.5 The gradient fields.

The amount and direction of the rate of change in space of the magnetic field strength. In the magnetic resonance system, gradient amplifiers generated by coils are used to vary the magnetic field strength in the x, y, and z planes. Figure 1.6 shows three different coils used in the MR.

On top of that magnetic field gradients need to be applied to obtain cross-sectional images. The location and thickness of the slice is determined by applying a slice-selection gradient G_z. After that, the object is spatially encoded via the application of additional magnetic field gradients G_x, G_y in the transversal directions. The magnitude and time of application of magnetic gradients G depend on the experimental requirements, see [8] for the description of a typical pulse sequence.

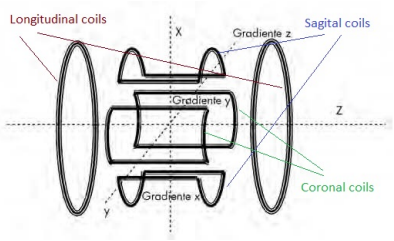

Figure 1.6: Gradient coils in the MR.

When we turn on a linear magnetic gradient field, G_x, along the line segment at the instant we begin recording signal in the current loop, thus a new magnetic field flux $B_{G_x} = xG_x$ appears. Therefore, for a time τ we can measure this magnitude as

$$B_{G_x}(t) = \int_0^t xG_x d\tau. \tag{1.14}$$

1.6 The signal.

Fundamentally, MRI is based on the following two steps:

(i) Manipulation of the equilibrium magnetization to create a detectable signal from the object of interest.

(ii) The reconstruction of an image of the object from the detected signal using a suitable reconstruction method.

When we exposed a tissue to $\vec{B}_0$; the sample becomes polarized at a rate determined by T_1. Once the sample is polarized, a $\vec{B}_1$ field, of the form given in (indicar figura), is turned on for a finite time τ. This is called an RF-excitation and is turned off, usually when the flip angle ($\theta(\tau) = \pi/2$).

Definition 1. *Faraday's law*
Faraday's law states that the electromotive force (ϵ) is also given by the rate of change of the magnetic flow (in a loop of wire according to the relation):

$$\varepsilon = -\frac{\partial \Phi_B}{\partial t}. \tag{1.15}$$

Definition 2. *Magnetic flux.*
The magnetic flux through a surface is defined by

$$\Phi_B = \iint_{\Sigma(t)} \vec{B} \partial \vec{S}. \tag{1.16}$$

where $\vec{S}$ is the hypothetical surface $\Sigma(t)$ whose boundary is a wire loop and $\vec{B}$ is the magnetic flux density into the surface.

The transverse components of $\vec{M}$ are a rapidly varying magnetic field, which, according to Faraday's law, induce a current in a loop of wire. Moreover, the reciprocity law indicates that "*the detector hears what the source sends*" and since all the vectors are oscillating ar frequency ω by using several such loops to form a receive coil, we can measure a signal of the form

$$s_r(t) = M(t)e^{-i\omega t}. \tag{1.17}$$

Emitted energy due to the precession of the magnetizations is converted into an electric signal in the receiver coil of an MRI system which is manipulated further for image reconstruction. The received signal can be expressed

as

$$s_r(t) = \int_\Omega M_{xy}(r,t) e^{-i\gamma B_0 t} e^{-i\gamma \int_0^t (xG_x + yG_y) d\tau} dr. \tag{1.18}$$

Let us suppose that we have a 2D sample in the xy plane which we would like to image. We turn on the y-gradient G_y for a time t_y and, we turn on the x-gradient G_x for a time t, so that the signal sent by the position oscillator at time t after t_y be applied is

$$s_r(t) = e^{-i\gamma B_0 t} \int_\Omega M_{xy}(x,y,t) e^{-2\pi i \left(\frac{\gamma \int_0^t (xG_x d + yG_y) d\tau}{2\pi} \right)} dxdy. \tag{1.19}$$

Up to the carrier frequency $e^{-i\gamma B_0 t}$, this is just a 2D Fourier transform.

Fourier analysis assumes an important role in functional analysis and signal processing.

Definition 3. *Let $f : \mathbb{R} \to \mathbb{C}$ be integrable. The Fourier transform is defined as:*

$$\mathcal{F}(f)(\xi) := \hat{f}(\xi) := \int_{-\infty}^{+\infty} f(x) e^{-2\pi i x \xi} dx, \ \xi \in \mathbb{R}. \tag{1.20}$$

If $\hat{f}$ is also integrable, then f can by recovered by the inverse Fourier transform according to the Fourier inversion theorem.

$$\mathcal{F}^{-1}(\hat{f})(x) := f(x) := \int_{-\infty}^{+\infty} \hat{f}(x) e^{2\pi i x \xi} d\xi, \ x \in \mathbb{R}. \tag{1.21}$$

The pair of analytical function and its Fourier transform that is relevant to this work are the top-hat function $\chi_{[-1/2,1/2]}$ and the sinc function. We will see them in section 1.7.

To obtain a sufficient collection of data for reconstruction, it is needed to measure many values of this signal for several time (t). There are many possible ways to do this. These rectangular partition is called the **k-space**.

For conceptual advantages, the spatial encoding is often expressed in a k-space formalism as

Definition 4. *k-space.*

$$k_x := \frac{\gamma}{2\pi} \int_0^t G_x d\tau, \tag{1.22}$$

$$k_y := \frac{\gamma}{2\pi} \int_0^t G_y d\tau. \tag{1.23}$$

Therefore the receiver signal shows as

$$s_r(t) = e^{-i\gamma B_0 t} \int_\Omega M_{xy}(x,y,t) e^{-2\pi i(xk_x + yk_y)} dxdy. \tag{1.24}$$

In principle, the k-space trajectories can be arbitrary. Figure 1.7 shows only two popular k-space trajectories.

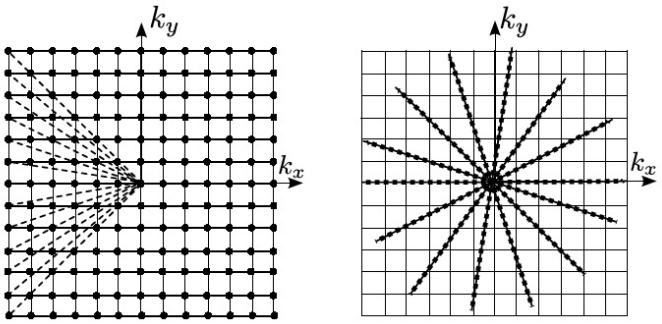

Figure 1.7: Schematic illustration of typical k-space trajectories in MRI. (Left) Cartesian. (Right) Radial [10].

To achieve these trajectories it is necessary to turn on the gradients G_x and G_y in different time sequences. In the real case, coils have physical characteristics and it is needed to define the $Cr(\vec{r})$ as the detection sensitivity of the receiver coil. Remember we coils in several axes, so we define the sensitibity of these coils with the complex notation as

$$C_{r,xy} = C_{r,x} + iC_{r,y}, \tag{1.25}$$

$$s_r(t) = e^{-i\gamma B_0 t} \int_\Omega C_{r,xy} M_{xy}(x,y,t) e^{-2\pi i(xk_x + yk_y)} dxdy. \tag{1.26}$$

Equation (1.26) shows that the received signal in k-space is the Fourier transform of the dot product between transverse magnetizations and the coil sensitivity map.

Numerically, this is a fantastic situation since FFT algorithm give an extremely fast, stable method for computing the approximate inverse Fourier transform and well known results from discrete Fourier theory can be applied to improve reconstruction and signal quality.

Figure 1.8 shows the MRI signal reconstruction process.

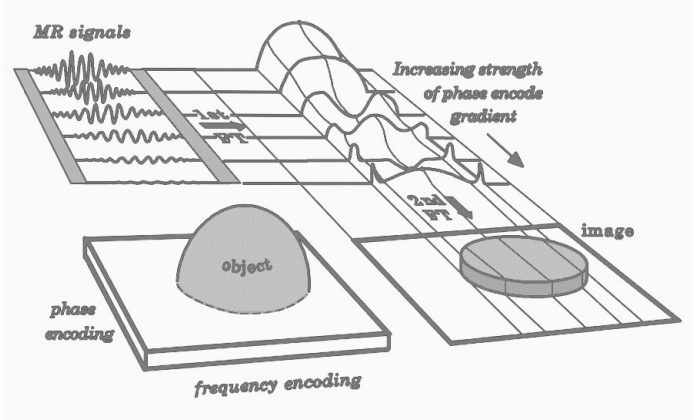

Figure 1.8: signal reconstruction process.

The received signals are typically demodulated in frequency by γB_0 using phase-sensitive detection before being used for image reconstruction. The resultant signal expression after demodulation is

$$s_d(t) = s_r(t)e^{i\gamma B_0 t}. \tag{1.27}$$

The demodulated signal corresponds to the solution of the Bloch equation in a frame rotating clockwise about z-axis with an angular frequency $\omega_0 = \gamma\|\vec{B_0}\|$.

We denoted the rotation frame with unitary vectors $(\vec{e}_1, \vec{e}_2, \vec{z})$ and the laboratory frame with $(\vec{x}, \vec{y}, \vec{z})$ unitary vectors, see Definition 5.

1.7 The RF pulse. Slide selection.

An RF excitation pulse with limited bandwidth of $\Delta\omega_p$ will only excite spins within a matching frequency range. For a slice selective excitation, a linear field gradient is applied corresponding to the limited bandwidth of the RF pulse as illustrated in Figure 1.9. The frequency bandwidth should be a rectangular function $\Pi(\omega)$ in order to get a perfectly rectangular slice profile so that the excitation pulse will excite spins equally within the slice of the sample leaving the surrounding spins in equilibrium state.

Although the RF excitation pulse $B_1(t)$ is accurately proportional to the

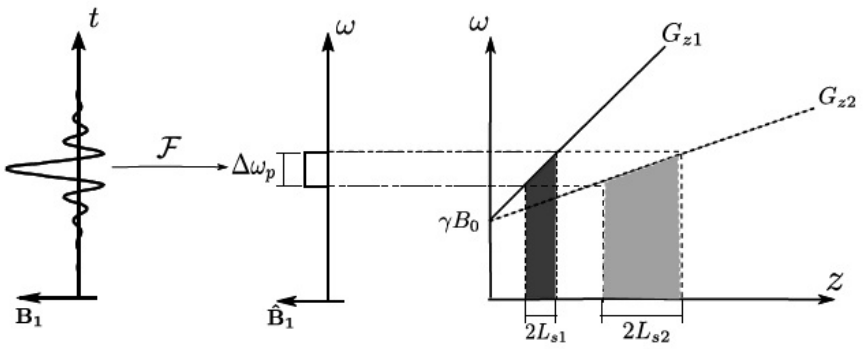

Figure 1.9: Schematic diagram depicting the relations of slice selection gradient, RF sinc pulse and the slice thickness. Different gradient strengths (G_1 and G_2) create slices of different thickness at different positions ($2L_{s1}$ and $2L_{s2}$) for same envelope $B_1(t)$ functions of a sinc pulse. $\mathcal{F}$ refers to the Fourier transform [10].

Fourier transform of the frequency bandwidth for small flip angles (θ), the same relation is acceptable to a very good approximation even for high flip angles. The identity $\frac{1}{a}\Pi(\frac{f}{a}) \xrightarrow{\mathcal{F}} sinc(at)$ implies that a sinc function which has an unlimited support is necessary to get a perfectly rectangular slice profile.

As only pulses with finite durations are feasible, a truncated sinc pulse is used which results in a distorted slice profile. Windowing functions are very often used with the truncated sinc pulse to reduce the distortion of the slice profile. The explicit expression of the envelope function of the sinc pulse is given by

$$B_1(t) = \begin{cases} \omega(t) B_1 sinc[\pi(t - Nt_0)/Nt_0] & 0 \leq t \leq \tau_p, \\ 0 & \text{otherwise}, \end{cases} \tag{1.28}$$

where $\omega(t)$ is a window function, N represents twice the zero-crossing of the sinc-pulse and t_0 one half the width. Depending on the shape of the $\omega(t)$ function (see Table 1.1) we have several shapes as we show in Figure 1.10.

Table 1.1: Window functions.

window function	$\omega(t)$
rectangular	1
Hamming	$0.50 + 0.50\cos(\pi(t - Nt_0)/Nt_0)$
Hanning	$0.54 + 0.46\cos(\pi(t - Nt_0)/Nt_0)$
Blackman	$0.42 + 0.50\cos(\pi(t - Nt_0)/Nt_0) - 0.08\cos(2\pi(t - Nt_0)/Nt_0)$

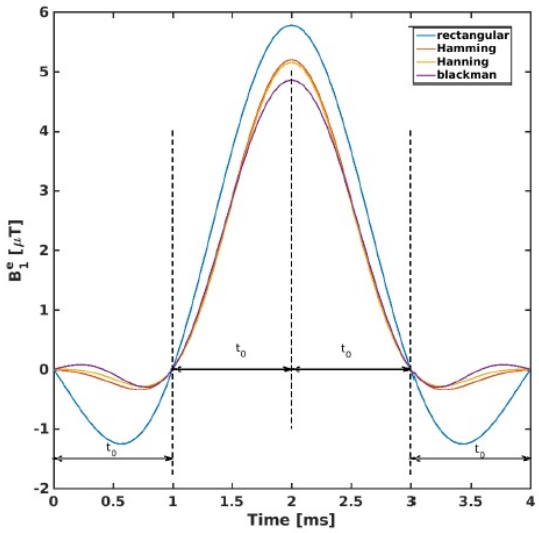

Figure 1.10: Envelope function of the sinc-pulses with different window functions for RF pulse duration of 4 ms and 4 zero-crossings [10].

To create a slice profile of thickness $2L_s$, the required slice selection gradient G_z is given by

$$G_z = \frac{\pi \Delta f}{\gamma L_s} \text{ where } \Delta f = \frac{\Delta\omega}{2\pi}\frac{1}{t_0}. \tag{1.29}$$

1.8 MRI. Image sequence.

A generic spoiled GE sequence for 2D imaging is shown in Figure 1.11. A slice selection gradient is applied along with a ω_1 pulse and ϕ_1 RF phase for selective excitations. After that a rewinder gradient is applied in the slice direction to avoid undesirable signal loss as a result of the phase shift caused by

the application of the slice selection gradient. A phase encoding gradient and a pre-phasing gradient are applied in the direction of phase encoding (y) and readout (x) respectively to accelerate the FID signal decay.Then the dephased spins are rephased by applying a gradient of opposite polarity in the direction of readout.

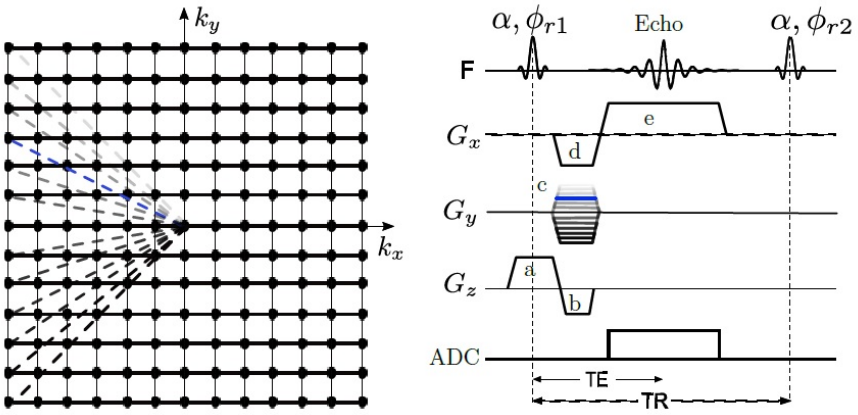

Figure 1.11: Generic spoiled gradient echo sequence diagram. Gradients: (a) slice selection (b) rewinder (c) phase encoding (d) prephasing in read direction (e) readout. The colored line in the phase encoding direction corresponds to the colored line in the k-space [10].

When the gradient moment of the readout gradient equals the gradient moment of the prephasing gradient in the direction of readout gradient, the spins are completely rephased and form an echo. The time between the center of the RF pulse and the peak of the signal induced is known as echo time (**TE**) and the time duration from RF pulse to the next RF pulse is defined as repetition time (**TR**).

Each GE sequence consists of a train of excitation pulses separated by a TR period. Between successive excitation pulses, the spatial encoding is performed with switched gradients in read, phase and slice direction and one line in k-space is acquired with each repetition of RF. Excitation pulse in the next TR acts on the modified magnetization and the process of precession is repeated again and again.

Figure 1.12 illustrates a GE sequence with radial trajectories. The fundamental diference of radial with Cartesian trajectory is that radial trajectory

consists of a readout gradient in two directions unlike one phase encoding and one readout as in Cartesian trajectory.

An other difference is that in case of Cartesian sampling, the inverse Fourier transform is applied directly to the sampled k-space data to obtain an image, but in radial trajectories, however the sampled k-space data are neither on a Cartesian grid nor equidistant. Thus, the image reconstruction with radial sampled data require advance techniques like non-uniform fast Fourier transform (NUFFT) or interpolation of the data onto a Cartesian grid.

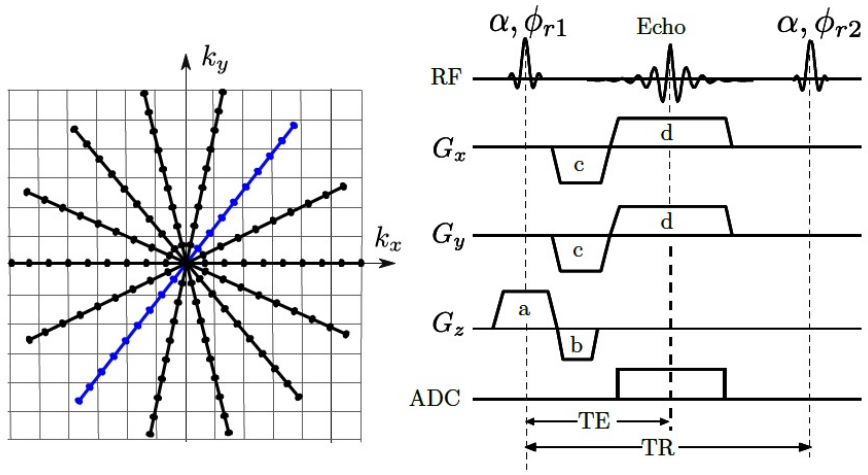

Figure 1.12: Generic spoiled gradient echo sequence with radial trajectory. Gradients: (a) slice selection, (b) rewinder, (c) prephasing, (d) readout. The colored line in the k-space corresponds to the current repetition [10].

Radial encoding scheme is gaining interest in last decade because of a number of interesting advantages:

- radial encoding is relatively more resistant to undersampling than Cartesian encoding. Moreover, undersampling artifacts appear as streaks at the edge of the image while the main structure of the object is maintained.

- the readout gradient in radial GE allows oversampling along both readout directions without additional measuring time. This oversampling enlarges the circular-supported **FOV** and hence reduces undersampling artifacts.

- radial encoding is intrinsically robust against motion. Due to the absence of phase encoding, motion-induced ghost artifacts are eliminated as seen very often in Cartesian trajectory.

Note: section 1.6, section 1.7, section 1.8 are basically a resume available in [10].

1.9 FOV. field of view.

To avoid aliasing artifacts, the sample spacings Δk_x and Δk_y must be chosen so that the excited portion of the sample is contained in a region of size Δk_x^{-1}xΔk_y^{-1}. This is called the field-of-view or **FOV**. Since we can only collect the signal for a finite period of time, the Fourier transform is sampled at frequencies lying in a rectangle with vertices $(\pm\Delta k_x^{-1}, \Delta k_y^{-1})$ where

$$k_{x,max} = \frac{n_x \Delta k}{2},\ k_{y,max} = \frac{n_y \Delta k}{2}, \tag{1.30}$$

The maximum frequencies sampled effectively determine the resolution available in the reconstructed image. Heuristically, this resolution limit equals half the shortest measured wavelength:

$$\Delta x \approx \frac{1}{2k_{max}} = \frac{FOV_x}{n_x}, \Delta y \approx \frac{1}{2k_{max}} = \frac{FOV_y}{n_y}, \tag{1.31}$$

where n_x, n_y represents the number of time sample points (base resolution) in a single data acquisition, k_{max} the maximal sampling distance from the centre in the k-space.

1.10 Contrast and resolution.

The single most distinctive feature of MRI is its extraordinarily large innate contrast. For two soft tissues, it can be on the order of several hundred percent. By comparison, contrast in X-ray imaging is a consequence of differences in the attenuation coefficients for two adjacent structures or tissues and is typically on the order of a few percent.The contrast between two regions, A and B, with signals S_A; S_B respectively, could be defined as different options

$$f_{contrast}(x) = -|C_1(x) - C_2(x)|, \tag{1.32}$$

or

$$f_{contrast}(x) = -\frac{|C_1(x) - C_2(x)|}{|C_1(x)|}, \tag{1.33}$$

where C_1 and C_2 are the contrast maps of the individual tissues and x is an element of the set of relevant sequence parameters.

For practical purposes, it may be more interesting to investigate the contrast-to-signal ratio as

$$f_{contrast}(x) = -\frac{|C_1(x) - C_2(x)|}{|C_1(x)| + |C_2(x)|}. \tag{1.34}$$

This way, the relative distinguish ability is maximized. A tissue combination that produces low signal with a high relative difference is easier to distinguish in practice than a tissue combination that produces high signals with low relative difference.

Run time is a critical factor for the sequence, and parameters that are key to the run time also often influence contrast. The desired trade-off can be controlled through the weighting factors of the objective function and the optimization is still fast. In this case the objective function is

$$f_{contrast}(x) = -|C_1(x) - C_2(x)| + g(t(x)), \tag{1.35}$$

where t is the runtime and g is a function that applies a weighting.

See [11] for more information of this subject.
Figure 1.13 shows differences between two tissues depending on the RF process used.

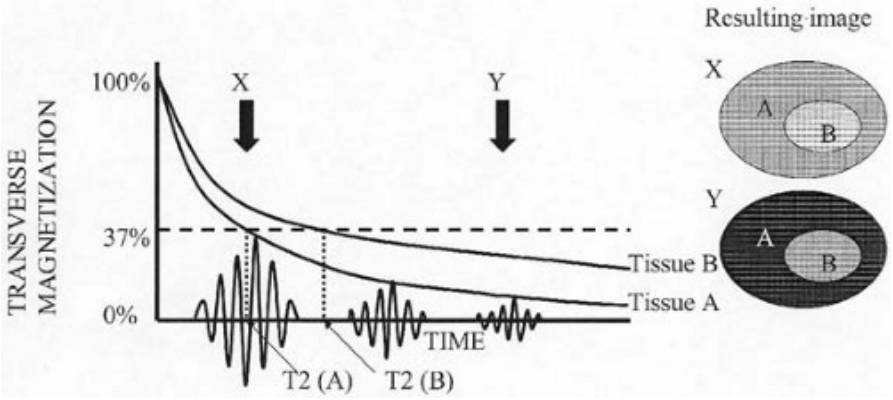

Figure 1.13: Contrast between tissues using different TE.

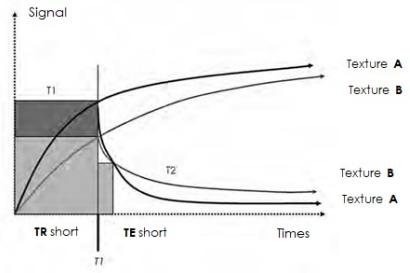

Figure 1.14: Contrast with a short TR and TE parameters,[16].

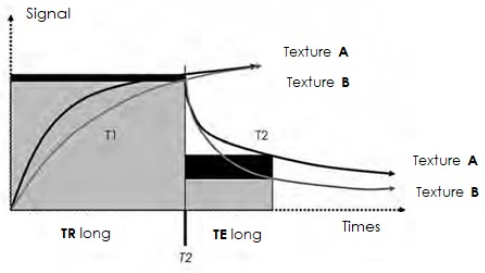

Figure 1.15: Contrast with a long TR and TE parameters,[16].

1.11 SNR. Signal to noise ratio.

In detecting an NMR signal, our primary goal is to use the induced EMF with minimal addition of noise. In other words, we aim to maximize the signal-to-noise ratio.A secondary goal when we are receiving comparatively large signals, such as are given by our example, is to minimize radiation damping without sacrifice of signal-to-noise ratio.

At a given spatial resolution, image quality is largely determined by the signal-to-noise ratio (**SNR**) and contrast between the different materials making up the imaging object. SNR in MRI is defined as the voxel signal amplitude divided by the noise standard deviation. The noise in the NMR signal, in general, is Gaussian distributed with zero mean [14]. Ignoring contributions from quantization, for example, due to limitations of the analog-to-digital converter, the noise voltage of the signal can be ascribed to random thermal fluctuations in the receive circuit and the variance is given by (see [17])

$$\sigma^2_{termal} = 4k_B T R \Delta\nu, \tag{1.36}$$

where k_B is Boltzmann's constant $(1,3806488(13)10^{23} JK^{-1})$,T is the absolute temperature measured in ^oK, R is the effective resistance resulting from both receive coil R_c and object R_o (measured in Oms (Ω)). $\Delta\nu$ is the receive bandwidth. Both R_c and R_o are frequency dependent, with $R_c \propto \omega^{\frac{1}{2}}$ and $R_o \propto \omega$. Their relative contributions to overall circuit resistance depend in a complicated manner on coil geometry, and the imaging object's shape, size and conductivity. Hence, at high magnetic field, and for large objects, as in most medical applications, the resistance from the object dominates and the

noise scales linearly with frequency. Since the signal is proportional to ω^2; in MRI, the SNR increases in proportion to the field strength.

As the reconstructed image is complex valued, it is customary to display the magnitude rather than the real component. Doing so, however, has some consequences on the noise properties. In regions where the signal is much larger than the noise, the Gaussian approximation is valid. However, in regions where the signal is low, rectification causes the noise to assume a Raleigh distribution, see [26]. Random complex numbers whose real and imaginary components are independently and identically distributed Gaussian with equal variance and zero mean. In that case, the absolute value of the complex number is Rayleigh-distributed, which has the following probability density function

$$f_X(x;\sigma) = \frac{x}{\sigma^2} e^{\frac{-(x^2)}{2\sigma^2}}, \tag{1.37}$$

Let be N_r and N_i the noise in the real and imaginary channels, when the signal is large compared to noise, one finds that the variance $\sigma_m^2 = \sigma^2$, In the other extreme of nearly zero signal, one obtains for the mean and variance,

$$\mu(X) = \sigma\sqrt{\frac{\pi}{2}} \cong 1.253\sigma, \tag{1.38}$$

$$\sigma^2(X) = \sigma^2(4 - \frac{\pi}{2}) \cong 0.655\sigma^2, \tag{1.39}$$

Of particular practical significance is the SNR dependence on the imaging parameters. The voxel noise variance is reduced by the total number of samples collected during the data acquisition process, i.e.

$$\sigma_m^2 = \frac{\sigma^2}{N}, \tag{1.40}$$

where $N = N_x N_y$ in a 2d spin-warp experiment. Incorporating the contributions to thermal noise variance we obtain $u = 4Nk_BTR\Delta$,

$$\sigma_m^2 = \frac{4k_BTR\Delta\nu}{N_xN_yN_{avg}}. \tag{1.41}$$

Here N_{avg} is the number of signal averages collected at each phase-encoding step. We obtain a simple formula for SNR per voxel of volume $\Delta V = \Delta_x\Delta_y d_z$,

$$SNR = C\rho\Delta_x\Delta_y d_z\sqrt{\frac{N_xN_yN_{avg}}{4k_BTR\Delta\nu}}, \tag{1.42}$$

where $\Delta_x; \Delta_y$ are defined in 1.31, d_z is the thickness of the slab selected by the sliceselective RF pulse, and ρ denotes the spin density weighted by effects determined by the (spatially varying) relaxation times T_1 and T_2 and the pulse sequence timing parameters.

For advanced researches about SNR see [11].

Chapter 2

The Bloch equation model and the MRI process.

Time dependence of the macroscopic nuclear magnetization $\vec{\mathbf{M}}$ under the influence of a magnetic flux density $\vec{\mathbf{B}}$ is modelled by the following differential equation proposed in 1946 by F. Bloch:

$$\boxed{\frac{\partial \vec{M}}{\partial t} = \gamma \vec{M} \times \vec{B} - \frac{M_x \vec{\imath} + M_y \vec{\jmath}}{T_2} - \frac{(M_z + \tau_0)\vec{k}}{T_1}} \tag{2.1}$$

where $\vec{\mathbf{M}} = (M_x, M_y, M_z)$ denotes the components of the magnetisation $\vec{\mathbf{M}}$ we want to solve, $\mathbf{T_1}$ is the named "longitudinal relaxation time", "spin-lattice relaxation time" or "thermal relaxation time" and $\mathbf{T_2}$ is known as the " transverse relaxation time" or "spin-spin relaxation time". $\mathbf{T_1}$ is the time constant for regrowth of longitudinal magnetization (Mz) and $\mathbf{T_2}$ is the time constant for decay/dephasing of transverse magnetization (Mxy). $\vec{\tau}_0$ is the strength of the equilibrium magnetisation.

This equation is valid during the **resonance process** as well as during the **relaxation process**, provided that the correct form for the total magnetic flux density $\vec{\mathbf{B}}$ is taken. Show that $\vec{B} = \vec{B_0} + \vec{B_1}$ during the resonance process and $\vec{B} = \vec{B_0}$ during the relaxation process when the RF field is stopped. As well, Bloch equation (2.1) is valid for time dependent fields and for whatever perturbation fields ($\vec{\mathbf{B}'}$),

$$\vec{B} = \vec{B_0} + \vec{B_G} + \vec{B_1} + \vec{B'}. \tag{2.2}$$

We denote the vector components of $\vec{\mathbf{B}}$ as (B_x, B_y, B_z) and we consider the magnet field $\vec{\mathbf{B}}_0$ has $(0, 0, B_0)$ direction.

In the ideal case where no disturbance of the RF field $\overrightarrow{\mathbf{B}}_1$ occurs, the Bloch equation reduces to a ordinary differential equation (**O.D.E.**) system with constant coefficients. Therefore the position of the magnetisation at the end of the resonance process can be determined in a straightforward quickly and with accuracy.

The differential equation system for Bloch equation is:

$$\begin{cases} \frac{\partial M_x(t)}{\partial t} = \gamma(M_y(t)B_z(t) - M_z(t)B_y(t)) - \frac{M_x(t)}{T_2}, \\ \frac{\partial M_y(t)}{\partial t} = \gamma(M_z(t)B_x(t) - M_x(t)B_z(t)) - \frac{M_y(t)}{T_2}, \\ \frac{\partial M_z(t)}{\partial t} = \gamma(M_x(t)B_y(t) - M_y(t)B_x(t)) - \frac{M_z(t)-\tau_0}{T_1}. \end{cases} \tag{2.3}$$

Therefore, defining $\tau_1 = \frac{1}{T_1}$ and $\tau_2 = \frac{1}{T_2}$ as "relaxation rates", the matrix form of the Bloch equation system can be expressed as

$$\frac{\partial}{\partial t}\begin{pmatrix} M_x(t) \\ M_y(t) \\ M_z(t) \end{pmatrix} = \begin{pmatrix} -\tau_2 & \gamma B_z(t) & -\gamma B_y(t) \\ -\gamma B_z(t) & -\tau_2 & \gamma B_x(t) \\ \gamma B_y(t) & -\gamma B_x(t) & -\tau_1 \end{pmatrix}\begin{pmatrix} M_x(t) \\ M_y(t) \\ M_z(t) \end{pmatrix} + \begin{pmatrix} 0 \\ 0 \\ \tau_1\tau_0 \end{pmatrix},$$

Thus, in matrix form the Bloch equation reads

$$\frac{\partial \mathbf{M(t)}}{\partial \mathbf{t}} = \mathbf{A(t)M(t)} + \mathbf{b}, \tag{2.4}$$

$$\mathbf{M(0)} = \mathbf{M_0}, \tag{2.5}$$

with

$$\mathbf{M} = \begin{pmatrix} M_x(t) \\ M_y(t) \\ M_z(t) \end{pmatrix}, \quad \mathbf{A} = \begin{pmatrix} -\tau_2 & \gamma B_z & -\gamma B_y(t) \\ -\gamma B_z & -\tau_2 & \gamma B_x(t) \\ \gamma B_y(t) & -\gamma B_x(t) & -\tau_1 \end{pmatrix},$$

$$\mathbf{b} = \begin{pmatrix} 0 \\ 0 \\ \tau_1\tau_0 \end{pmatrix}, \quad \mathbf{M_0} = \begin{pmatrix} M_{0x} \\ M_{0y} \\ M_{0z} \end{pmatrix}.$$

2.1 Magnitudes and domain.

Before assuming several hypothesis it is required to know the range and domain of each one.

- $\mathbf{B_0} \in [1, 10]$ T. Superconducting scanner magnets are more and more powerful, nowadays 3-5 Tesla is a standard level value for a superconducting magnet.
- $\mathbf{M_0} \in [-10, 10]$ T.
- $\tau_\mathbf{0} \in [-10, 10]$ T.
- $\mathbf{G} \in [-0.05, 0.05]$ T/m and $\mathbf{B_G} \in [-0.025, 0.025]$ T. We are interested in create high gradient strengths for increasing constrast imaging.
- $\mathbf{B_1} \in [0.0001, 0.01]$ T. Remember that B_1 is the magnetic field created by the RF coils, which produce the RF signal and also can receive the response signal.
- $\mathbf{T_1} \in [0.1, 2]$ s $\rightarrow \tau_1 \in [0.5, 10]$. For biologial tissues with $B_0 = 1$ T, $T_1 = 750$ ms for muscle and $T_1 = 250$ ms for fat. T_1 experimental value for $B_0 = 1.5T$ $B_0 = 3T$ can be showed in tables, see Table 2.2.
- $\mathbf{T_2} \in [0.05, 0.5]$ s.$\rightarrow \tau_2 \in [2, 20]$. For biologial tissues with $B_0 = 1$ T, $T_2 = 50$ ms for muscle and $T_2 = 80$ ms for fat).T_2 experimental value for $B_0 = 1.5T$ $B_0 = 3T$ can be showed in tables, see Table 2.2.
- γ (giroscopic constat for hidrogen) = 42.58 MHz/T, thus $\omega_\mathbf{0} \in [42.575 \cdot 10^6, 212.875 \cdot 10^6]$ Hz. Remember that ω_0 depends of the B_0 magnet field, see equation 1.1.

2.2 Decay and recovery times. T_1 and T_2.

Longitudinal, T_1, and transverse, T_2, relaxation time measurements are relevant in understanding water molecular dynamics in biologic systems. T_1 and T_2 relaxation time depend on the chemical and physical environments of water protons in tissue. Moreover T_1 and T_2 provide quantitative assessment of tissue pathology, in particular, they offer additional information about the processes demyelination and axonal loss, inflammation, infarction, white matter edema, tumor malignancy and ischemia. Both tissue relaxation parameter estimates are important in designing MRI pulse sequences thataim to accentuate contrast between normal and pathological tissue.

In the relaxation process $M_{xy}(t) = M_0 e^{-\frac{t}{T_2}}$ and $M_z(t) = M_0(1 - e^{-\frac{t}{T_1}})$, therefore $\mathbf{T_1}$ can be viewed as the time required for the z-component of M, (M_z), to reach $(1 - \frac{1}{e})$ or about 63% of its maximum value, M_0. $\mathbf{T_2}$ is the time required for the transverse magnetization to fall to approximately 37% $(\frac{1}{e})$ of its initial value, M_0.
Figure 2.1 shows T_1 and T_2 graphical interpretation.

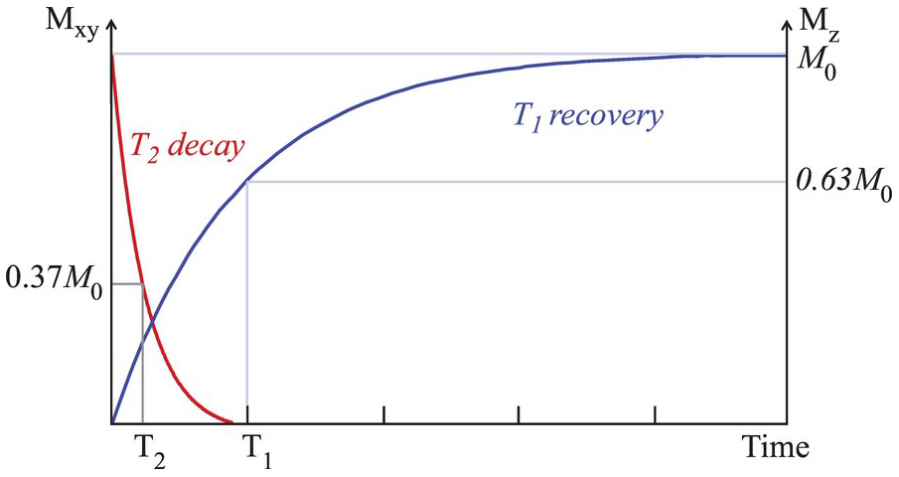

Figure 2.1: T_1 and T_2 parameters interpretation.

To explain the experimental methods for measuring the relaxation and magnetization transfer we will refer to [13] where they used the Carr-Purcell-Meiboom-Gill (CPMG) sequence for calculating T_1 and T_2 into a 1.5T and 3T magnetic resonance equipment. In this article they expose several experimental results that we are going to bear in mind and applied into Random Bloch equation assuming that T_1 and T_2 are random variables:

1. T_2 relaxation time was found to be independent of magnetic field (see Table 2.2).The measured values at 3 and 1.5T showed no significant differences within experimental error.

2. Longitudinal T_1 relaxation times increase with the strength of the magnetic field. Thus, T_1 depend on the applied $\vec{B}$.

Lars G. Hanson, [9], exposed clearly that the difference between T_1 and T_2 is due to a difference in the causes of relaxation. For the protons in firm matter, the spins will rapidly be dephased after excitation, meaning that they

Table 2.1: T_2 and T_1 Relaxation Times at $3T$ and $1.5T$ Measured at $37C$, [13].

TISSUE	T1[ms]-3T	T2[ms]-3T	TISSUE	T1[ms]-1.5T	T2[ms]-1.5T
Blood	1932±85	275±50	Blood	1441±120	290±30
Gray matter	1820±114	99±7	Gray matter	1124±50	95±8
Muscle	1412±13	50±4	Muscle	1008±20	44±6
Liver	812±64	42±3	Liver	576±30	46±6

will point in all directions perpendicular to the field (have all kinds of phases). This is caused by the small local contributions to the magnetic field that the individual spins are making, and that make the neighbouring nuclei precess at altered frequencies. In firm matter, these interactions are constant in time, while they vary in fluids, since nuclei are constantly experiencing new neighbours. Thus, the spins can remain in phase for relatively long (seconds) in fluids, while they loose their common orientation in a matter of milliseconds or less in firm matter. We can therefore conclude that T2 is short in firm matter.

The described process affects the individual spins Larmor frequency, but does not give rise to a change of the longitudinal magnetization, since the interaction of just two nuclei cannot alter the combined energy, which is proportional to the longitudinal magnetization. Therefore this type of nuclear interaction does not contribute T_1-relaxation that requires more drastic nuclear interactions that involve an exchange of energy with the surroundings. All processes that result in T_1-relaxation also result in T_2-relaxation, ensuring that T_1 is never smaller than T_2.

Generally T_2 becomes smaller with increasing firmness of the matter, but this does not apply to T_1, which is long in very firm matter and very fluid matter (e.g., several seconds), but is short for semi-firm matter.

2.3 Inhomogeneity as a source of signal loss, T_2^*.

Interactions between nuclei in the ever changing environment of molecules is the cause of radio signal loss on a timescale T_2 and longitudinal magnetization recovery on a longer timescale T_1. However, a loss of transversal magnetization is also observed because of inhomogeneity in the field, B', meaning variation

in B_0. As expressed through the Larmor-equation, the nuclei precess at a frequency depending on the magnetic field. If this varies over the investigated area, the nuclei will after some time, point in all directions transversally, even if they had some degree of alignment after excitation. This process is called dephasing.

Since the measured signal is proportional to the transversal net magnetization, inhomogeneity gives rise to a loss of signal. The larger the field inhomogeneity, the faster the dephasing. How quickly this happens in denoted by the time constant T_2^* (pronounced T_2-star). The degree of inhomogeneity depends partly on the scanners ability to deliver a uniform field (called a good "shim").T_1 and T_2, are tissue-dependent parameters for which normal values are published. This does not apply to T_2^* values, since they depend, for example, on the size of the voxel since the inhomogeneity increases with this.

Loss of signal due to interactions of nuclei is irreversible, but through a sly trick, signal lost due to inhomogeneity can be recovered. The inverse process of dephasing is called refocusing, and it involves gradual re-alignment of nuclei in the transversal plane. Refocusing is triggered by repeated use of radio waves. The recovered signal is known as an echo.

Figure 2.2 shows the graphical interpretation of T_2^*.

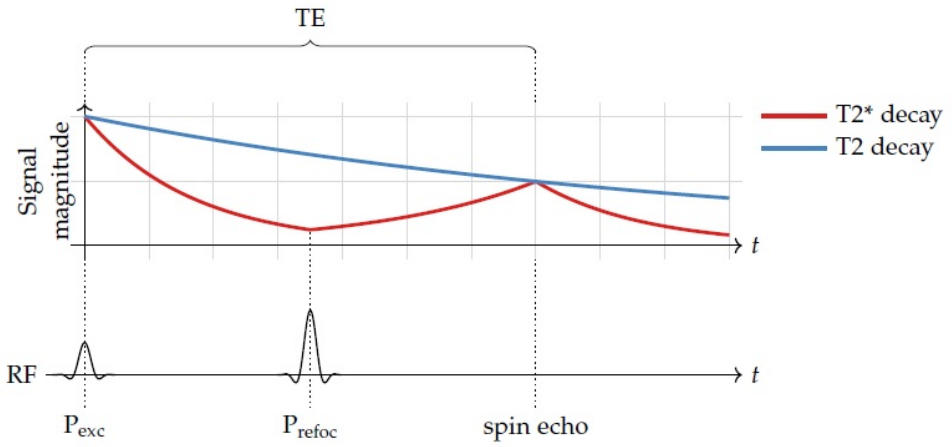

Figure 2.2: T_2^* lost of signal.

Chapter 3

Bloch equation in the relaxation process.

Remember the Bloch equation in matrix form:

$$\frac{\partial \vec{M}(t)}{\partial t} = A(t)\vec{M}(t) + \vec{b}, \quad (3.1)$$

$$\vec{M}(0) = \vec{M}_0. \quad (3.2)$$

Let us mention that during the relaxation process, the RF field $\vec{\mathbf{B}}_1$ is stopped ($\vec{B}_1 = 0$) and observe that if no perturbation fields are present ($\vec{B}' = 0$) the matrix $\mathbf{A}(t)$ is reduced to the constant matrix $\mathbf{A}$,

$$\mathbf{A} = \begin{pmatrix} -\tau_2 & \gamma B_0 & 0 \\ -\gamma B_0 & -\tau_2 & 0 \\ 0 & 0 & -\tau_1 \end{pmatrix}, \qquad \vec{\mathbf{b}} = \begin{pmatrix} 0 \\ 0 \\ \tau_1 \tau_0 \end{pmatrix}, \quad (3.3)$$

with

$$\vec{\mathbf{M}} = \begin{pmatrix} M_x(t) \\ M_y(t) \\ M_z(t) \end{pmatrix}, \qquad \vec{\mathbf{M}}_0 = \begin{pmatrix} M_{0x} \\ M_{0y} \\ M_{0z} \end{pmatrix}, \qquad \begin{array}{l} \tau_1 = \frac{1}{T_1}, \\ \tau_2 = \frac{1}{T_2}. \end{array}$$

3.1 Analytical solution into the relaxation process.

The equation differential system (3.1 and 3.2) can be solved analytically using standard results from differential equations theory [23]. Thus we obtain the eigenvalues which result in one real and two complex:

$$\begin{cases} \lambda_0 = -\tau_1, \\ \lambda_1 = -\tau_2 - i\gamma B_0, \\ \lambda_2 = -\tau_2 + i\gamma B_0, \end{cases} \tag{3.4}$$

and the eigenvectors associated to the three eigenvalues λ_0, λ_1, λ_2 are

$$\vec{v}_0 = \begin{pmatrix} 0 \\ 0 \\ 1 \end{pmatrix}, \vec{v}_1 = \begin{pmatrix} i \\ 1 \\ 0 \end{pmatrix}, \vec{v}_2 = \begin{pmatrix} -i \\ 1 \\ 0 \end{pmatrix}.$$

The solution to the homogeneous differential system associated to (3.1) and (3.2) is: $\vec{M}_h(t) = C_0 e^{\lambda_0 t}\vec{v}_0 + C_1 e^{\lambda_1 t}\vec{v}_1 + C_2 e^{\lambda_2 t}\vec{v}_2 \quad$ with $(C_0, C_1, C_2) \in \mathbb{C}^3$.

The solution of the magnetization vector during the relaxation process is an explicit and known solution and is given by

$$M = \begin{pmatrix} e^{-\tau_2 t}(C_1 \cos(\omega_0 t) + C_2 \sin(\omega_0 t)) \\ e^{-\tau_2 t}(C_2 \cos(\omega_0 t) - C_1 \sin(\omega_0 t)) \\ M_0 - C_3 e^{-\tau_1 t} \end{pmatrix}, \tag{3.5}$$

where the constants C_1, C_2 and C_3 are determined by the value of the magnetization vector at the beginning of the relaxation process.

We take the following initial conditions,

$$\vec{B} = \begin{pmatrix} B_x(t) \\ B_y(t) \\ B_z(t) \end{pmatrix} = \begin{pmatrix} 0 \\ 0 \\ B_0 \end{pmatrix}, \qquad \vec{M}_0(0) = \begin{pmatrix} 0 \\ M_0 \\ 0 \end{pmatrix},$$

and the analytical solution is:

$$\begin{aligned} M_x(t) &= M_0 \exp^{-t\tau_2} \sin(t\gamma B_0), \\ M_y(t) &= M_0 \exp^{-t\tau_2} \cos(t\gamma B_0), \\ M_z(t) &= \tau_0(1 - \exp^{-t\tau_1}). \end{aligned}$$

The strength of the transversal magnetization is defined as $M_{xy} = \|M_x(t) + iM_y(t)\|$ and represent the decay process (transverse magnetization value) and $M_z(t)$ represent the recovery process (longitudinal magnetization),

$$\begin{aligned} M_{xy}(t) &= M_0 \exp^{-t\tau_2}, \\ M_z(t) &= \tau_0(1 - \exp^{-t\tau_1}). \end{aligned} \tag{3.6}$$

As we show in Figures 3.2 and 3.1, the magnetisation field movement $\vec{M}(t)$ is like an inverse spiral which has the origin on plane xy and the end aligned to the magnetic field $\vec{B}_0$.

These equations predict that $\vec{M}$ will exhibit a spiraling precession around $\vec{B}_0$ at the Larmor frequency with decay of transverse components back to zero and regrowth of the longitudinal component to its original maximum value M_0. Because T_2 is always shorter than T_1, the transverse components typically decay completely before the longitudinal magnetization is fully restored.

Thus, we solve the Bloch equation with Mathematica software for different tissues. Defining the particular and real values for the relaxation process :

- $B_0 = 3$ T.
- $M_0 = 3$ T.
- $\tau_0 = M_0$ T.
- γ (giroscopic constat for hidrogen) = 42.58 MHz/T.

Figure 3.1 shows graphical interpretation for the M_{xy} decay time T_2 and M_z recovery time T_1 of the magnetization vector into the relaxation process.

Figure 3.2 shows graphical interpretation for the $\vec{M}$ magnetization vector and M_{xy} decay movement located on xy-plane into the relaxation process.

Figure 3.3 shows graphical interpretation for the $\vec{M}$ for several tissues (with different T_1 and T_2) of the magnetization vector into the relaxation process.

Figure 3.4 shows graphical interpretation for the transversal M_{xy} vector for several tissues (with different T_2) into the relaxation process.

And Figure 3.5 shows $M_{xy}(t)$ and $M_z(t)$ all together.

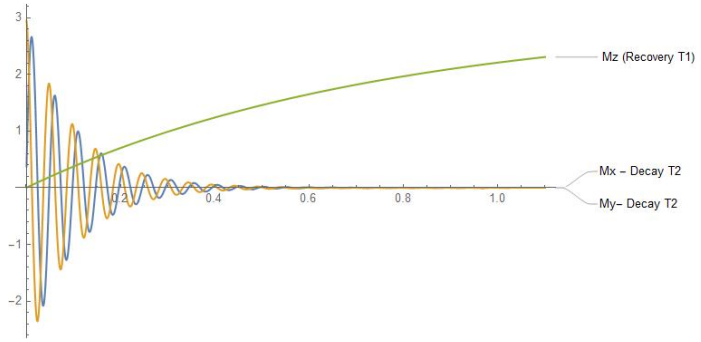

(a) $M_x(t), M_y(t), M_z(t)$.

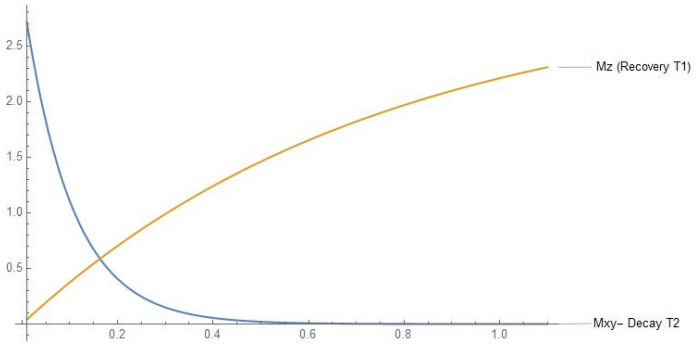

(b) $M_{xy}(t), M_z(t)$.

Figure 3.1: M_x, M_y, M_{xy} decay time T_2 and M_z recovery time T_1.

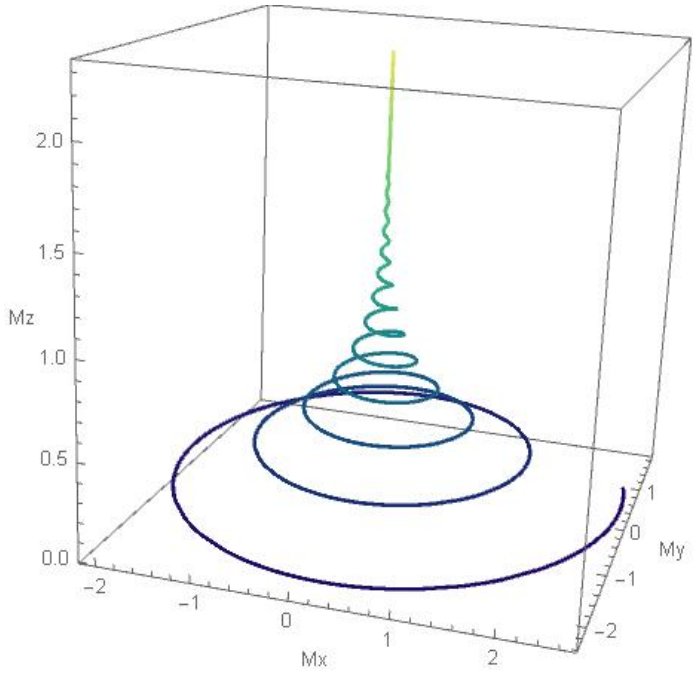

(a) $\vec{M}(t)$.

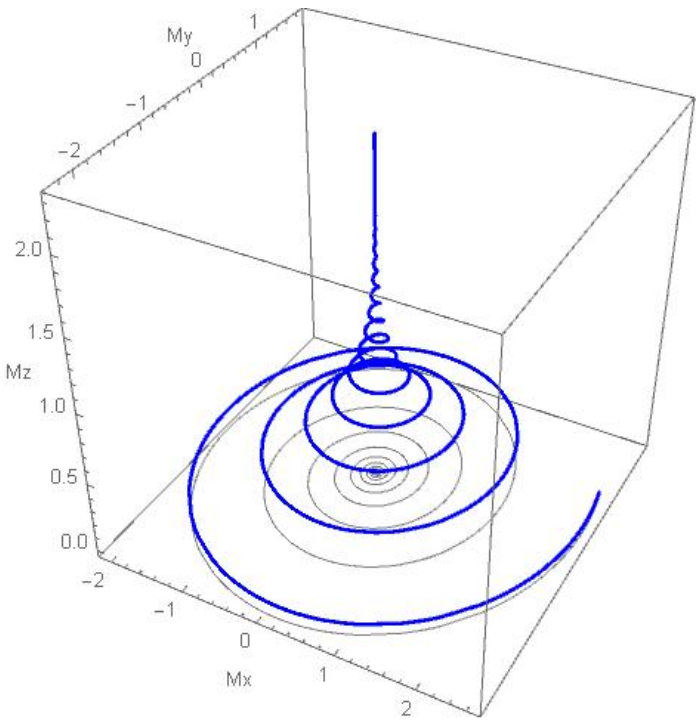

(b) $\vec{M}(t)$ and $M_{xy}(t)$.

Figure 3.2: Magnetization movement vector at relaxation process.

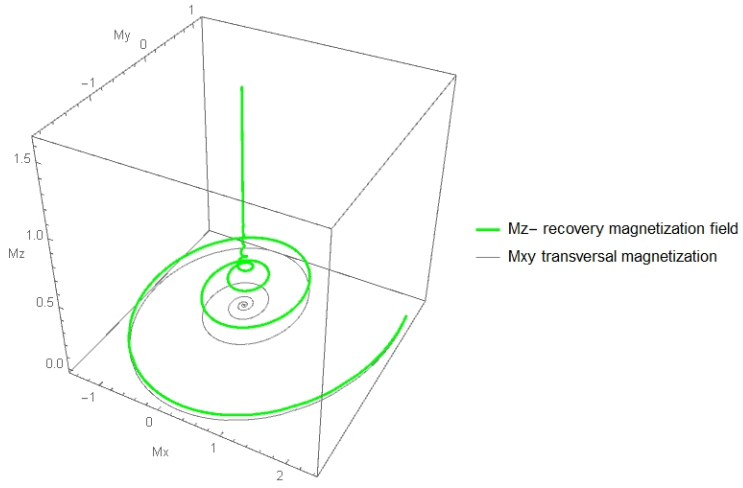

(a) $\vec{M}(t)$ and $M_{xy}(t)$-muscle.

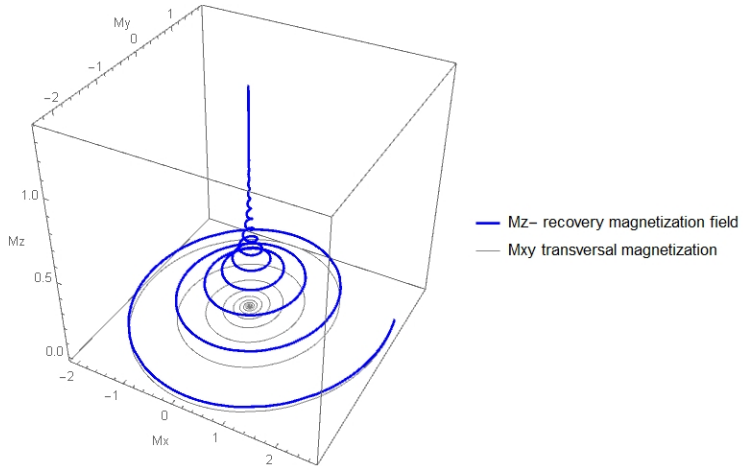

(b) $\vec{M}(t)$ and $M_{xy}(t)$-graymatter.

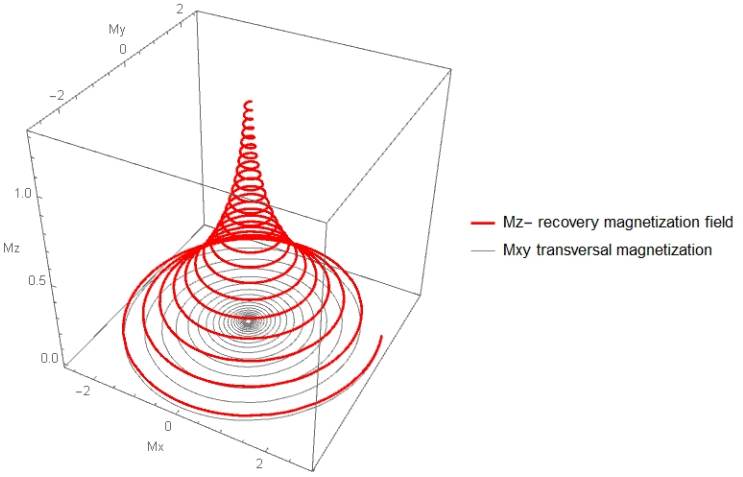

(c) $\vec{M}(t)$ and $M_{xy}(t)$-blood.

Figure 3.3: Magnetization movement vector at relaxation process for several tissues.

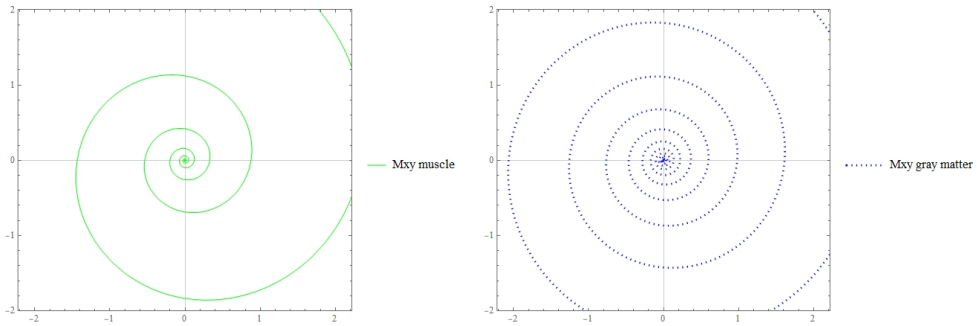

(a) $M_{xy}(t)$-muscle. (b) $M_{xy}(t)$-graymatter.

(c) $M_{xy}(t)$-blood. (d) $M_{xy}(t)$ all together.

Figure 3.4: Transversal magnetization vector at relaxation process for several tissues.

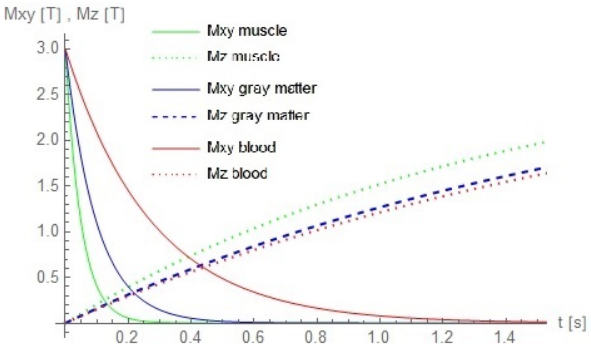

(a) $M_{xy}(t)$ and $M_y(t)$.

Figure 3.5: Transversal and longitudinal magnetization vector in the relaxation process for several tissues.

Chapter 4

Bloch equation in the radio-frequency pulse process.

Remember the Bloch equation in matrix form:

$$\frac{\partial \vec{M}(t)}{\partial t} = A(t)\vec{M}(t) + \vec{b}, \quad (4.1)$$

$$\vec{M}(0) = \vec{M}_0. \quad (4.2)$$

During the RF pulse $\vec{B}_1$ is not a null value ($\|\vec{B}_1\| \neq 0$) and the main magnetic field of the magnet is activated ($\vec{B}_0$). We observe that if no perturbation fields and gradient are present the matrix $A(t)$ is reduced to:

$$\mathbf{A} = \begin{pmatrix} -\tau_2 & \gamma B_0 & -\gamma B_y(t) \\ -\gamma B_0 & -\tau_2 & \gamma B_x(t) \\ \gamma B_y(t) & -\gamma B_x(t) & -\tau_1 \end{pmatrix}, \qquad \vec{\mathbf{b}} = \begin{pmatrix} 0 \\ 0 \\ \tau_1 \tau_0 \end{pmatrix}, \qquad (4.3)$$

with

$$\vec{\mathbf{M}} = \begin{pmatrix} M_x(t) \\ M_y(t) \\ M_z(t) \end{pmatrix}, \qquad \vec{\mathbf{M}}_0 = \begin{pmatrix} M_{0x} \\ M_{0y} \\ M_{0z} \end{pmatrix}, \qquad \vec{\mathbf{B}}_1 = \begin{pmatrix} B_1 \cos(\omega_1 t) \\ -B_1 \sin(\omega_1 t) \\ 0 \end{pmatrix}.$$

Thus, matrix A could be written as:

$$\mathbf{A} = \begin{pmatrix} -\tau_2 & \gamma B_0 & \gamma B_1 \sin(\omega_1 t) \\ -\gamma B_0 & -\tau_2 & \gamma B_1 \cos(\omega_1 t) \\ -\gamma B_1 \sin(\omega_1 t) & -\gamma B_1 \cos(\omega_1 t) & -\tau_1 \end{pmatrix}. \tag{4.4}$$

We are going to define the $\tilde{A}$ matrix form. In this way we will introduce the rotation frame and the laboratory frame.

Definition 5. *Laboratory and rotation frame of reference.*

*We denote the **laboratory frame** of reference a coordinate frame whose reference point in a fixed Cartesian coordinate system. It is represented with the orthonormal vectors* $(\vec{x}, \vec{y}, \vec{z})$.

*We denote the **rotation frame** of reference a coordinate frame of reference that rotates with the magnetization vector whirling at a Larmor frequency,* ω_0. *It is represented with the orthonormal vectors* $(\vec{e}_1, \vec{e}_2, \vec{z})$. *A frequency rotating clockwise correspond positive frequencies.*

S. Balac and L. Chupin [1] proposed to split the A matrix into a product of two different matrix's. In this way the coefficients $a_{12} = a_{21} = \gamma B_0$ are of magnitude $\approx 10^6$ whereas the others are of magnitude ≈ 1 (see Section 2.1).

Definition 6. *We define* $\vec{M}(t) = R(t)\vec{m}(t)$, *with* $R(t)$ *the following orthonormal and so on, invertible matrix rotation around axe z.*

$$\mathbf{R} = \begin{pmatrix} \cos(\omega_0 t) & \sin(\omega_0 t) & 0 \\ -\sin(\omega_0 t) & \cos(\omega_0 t) & 0 \\ 0 & 0 & 1 \end{pmatrix}, \tag{4.5}$$

then $\vec{m} = (m_1, m_2, m_3)^T$ satisfies the generalised differential system:

$$R(t)\frac{\partial \vec{m}}{\partial t} = \left(A(t)R(t) - \frac{\partial R}{\partial t} \right) \vec{m}(t) + \vec{b}.$$

Since $R^{-1}\vec{b} = \vec{b}$, then

$$\frac{\partial \vec{m}}{\partial t} = \tilde{A}(t)\vec{m}(t) + \vec{b}, \quad (4.6)$$
$$\vec{m}(0) = \vec{m}_0. \quad (4.7)$$

$$\tilde{A}(t) = \left(A(t)R(t) - \frac{\partial R}{\partial t} \right) = \begin{pmatrix} -\tau_2 & 0 & -\omega_a(t) \\ 0 & -\tau_2 & \omega_b(t) \\ \omega_a(t) & -\omega_b(t) & -\tau_1 \end{pmatrix}, \quad (4.8)$$

with

$$\begin{aligned} \omega_a(t) &= \gamma B_y(t)\cos(\omega_0 t) + \gamma B_x(t) sin(\omega_0 t), \\ \omega_b(t) &= \gamma B_x(t)\cos(\omega_0 t) - \gamma B_y(t) sin(\omega_0 t). \end{aligned} \quad (4.9)$$

As ω_a and ω_b are regular functions os time, by Cauchy-Lipschitz theorem (see [23]) that the first order linear differential system (equations 4.6 and 4.7) has unique solution under the initial condition $\vec{m}(0) = \vec{m}_0 = \vec{M}_0$.

4.1 Analytical solution of Bloch equation in the RF process.

Let us observe that without RF perturbation ($\|\vec{B}'\| = 0$) and as a consequence of the previous magnitude values, since B_0 is greater than B_1, it is possible to assume that $\mathbf{B_z} \simeq \mathbf{B_0}$. Then matrix's $\mathbf{A(t)}$ and $\mathbf{b}$ reduce to the following constant matrix's

$$\mathbf{A} = \begin{pmatrix} -\tau_2 & \gamma B_0 & -\gamma B_y(t) \\ \gamma B_0 & -\tau_2 & \gamma B_x(t) \\ \gamma B_y(t) & -\gamma B_x(t) & -\tau_1 \end{pmatrix}, \quad (4.10)$$

Let us assume the RF pulse has the form

$$\vec{B}_1(t) = B_1 \cos(\omega_0 t)\vec{x} - B_1 \sin(\omega_0 t)\vec{y}. \quad (4.11)$$

The Larmor frequency ω_0 is the frequency we want to send out into the scanner with an RF pulse ($\vec{B}_1$) so that the signal energy produced by the hydrogen protons reaches its maximum value.

Let us observe that without RF perturbation, the matrix $\tilde{A}(t)$ reduces to the following constant matrix

$$\tilde{\mathbf{A}} = \begin{pmatrix} -\tau_2 & 0 & 0 \\ 0 & -\tau_2 & \omega_1 \\ 0 & -\omega_1 & -\tau_1 \end{pmatrix}, \tag{4.12}$$

where $\omega_1 = \gamma B_1$, and the differential system (4.6) with initial condition (4.7) can be solved analytically using standard results from differential equations theory [23]. Thus we obtain the eigenvalues which result in one real and two imaginaries:

$$\begin{cases} \lambda_0 = -\tau_2, \\ \lambda_1 = -\frac{1}{2}(\tau_1+\tau_2) + \frac{1}{2}\mathrm{i}\sqrt{4\omega_1^2 - (\tau_1-\tau_2)^2}, \\ \lambda_2 = -\frac{1}{2}(\tau_1+\tau_2) - \frac{1}{2}\mathrm{i}\sqrt{4\omega_1^2 - (\tau_1-\tau_2)^2}. \end{cases} \tag{4.13}$$

We can show that $4\omega_1^2-(\tau_1-\tau_2)^2$ is always a positive value ($\omega_1 >>> \tau_1, \tau_2$) and the eigenvectors associated to the three eigenvalues λ_0, λ_1, λ_2 are

$$\vec{v}_0 = \begin{pmatrix} 1 \\ 0 \\ 0 \end{pmatrix}, \vec{v}_1 = \begin{pmatrix} 0 \\ -\tau_1 + \lambda_1 \\ -\omega_1 \end{pmatrix}, \vec{v}_2 = \begin{pmatrix} 0 \\ -\tau_1 + \lambda_2 \\ -\omega_1 \end{pmatrix}.$$

The solution to the homogeneous differential system associated to equation 4.6 is: $\vec{m}_h(t) = C_0 e^{\lambda_0 t}\vec{v}_0 + C_1 e^{\lambda_1 t}\vec{v}_1 + C_2 e^{\lambda_2 t}\vec{v}_2 \quad$ with $(C_0, C_1, C_2) \in \mathbb{C}^3$;

whereas a particular solution (for $t = 0$) is

$$m_p(t) = \begin{pmatrix} 0 \\ -\frac{\omega_1\tau_1}{\tau_1\tau_2+\omega_1^2} M_0 \\ -\frac{\tau_1\tau_2}{\tau_1\tau_2+\omega_1^2} M_0 \end{pmatrix}.$$

The global solution to the differential system (4.6)-(4.7) is then $m(t) = m_h(t) + m_p(t)$ where the constants C_0, C_1 and C_2 are determined through the initial magnetization value $\tilde{\mathbf{M}}_0$. We supposed $\tilde{\mathbf{M}}_0 = (0, 0, \tau_0)$, thus

$$\begin{cases} C_0 = 0, \\ C_1 = \frac{1}{\lambda_1-\lambda_2}\left(\frac{\omega_1\tau_1\tau_0}{\tau_1\tau_2+\omega_1^2} - \frac{\tau_1\tau_0\tau_2(\tau_1+\lambda_2)}{\omega_1(\tau_1\tau_2+\omega_1^2)}\right), \\ C_2 = \frac{\tau_1\tau_0\tau_2(\tau_1+\lambda_2)}{\omega_1(\tau_1\tau_2+\omega_1^2)} - C_1. \end{cases} \tag{4.14}$$

If we compare the physical magnitude of τ_1 given in (10), τ_2 given in (50) with ω_1 magnitude value (10^6), we show that it is possible to neglect τ_1 and τ_2, thus

$$\begin{cases} \lambda_0 = -\tau_2, \\ \lambda_1 = -\frac{1}{2}(\tau_1 + \tau_2) + \mathrm{i}\omega_1, \\ \lambda_2 = -\frac{1}{2}(\tau_1 + \tau_2) - \mathrm{i}\omega_1, \end{cases} \tag{4.15}$$

and the $\vec{m}(t)$ solution for system of differential equations (4.6) for $\vec{M}_0 = (0, 0, \tau_0)$ can be expressed as

$$\vec{m}(t) = \begin{pmatrix} 0 \\ \tau_0 \sin(\omega_1 t) \\ \tau_0 \cos(\omega_1 t) \end{pmatrix}. \tag{4.16}$$

Figure 4.2 shows the error value between taking exact solution and approximation. This error was calculated as $\vec{m}(t) - \vec{m}_{ap}(t)$. $m(t)$ solution can be interpreted as a *rotation* around the x axis with an angular frequency $\omega_1 = \gamma B_0$.

The magnetization vector start to flip out of the z axis from its equilibrium position $M_0 = \tau_0 \vec{z}$ under the influence of the RF field ($\vec{\mathbf{B}}_1$). The angle between the magnetization vector and the z axis is a function of time and is defined as flip angle, $\theta = \omega_1 t$.

There are two flip angles commonly used in MRI $\theta = \frac{\pi}{2}$ and $\theta = \pi$ both can be obtained when we applied a RF magnetic field during $T_{RF} = \frac{\pi}{2\omega_1}$ and $T_{RF} = \frac{\pi}{\omega_1}$. Then, if we applied a high RF perturbation frequency ω_1, which is equal to γB_0, we will reduce the time to take lecture of the RF signal and the process become more efficient.

Consequently, we can calculate the global solution for the magnetisation vector as $M(t) = R(t)m(t)$ (see Definition 6), thus

$$\mathbf{M} = \begin{pmatrix} \cos(\omega_0 t) & \sin(\omega_0 t) & 0 \\ -\sin(\omega_0 t) & \cos(\omega_0 t) & 0 \\ 0 & 0 & 1 \end{pmatrix} \begin{pmatrix} 0 \\ \tau_0 \sin(\omega_1 t) \\ \tau_0 \sin(\omega_1 t) \end{pmatrix} = \begin{pmatrix} \tau_0 \sin(\omega_1 t) \sin(\omega_0 t) \\ \tau_0 \sin(\omega_1 t) \\ \tau_0 \sin(\omega_1 t) \end{pmatrix},$$

then

$$\mathbf{M} = \begin{pmatrix} \tau_0 \sin(\omega_1 t) \sin(\omega_0 t) \\ \tau_0 \sin(\omega_1 t) \cos(\omega_0 t) \\ \tau_0 \cos(\omega_1 t) \end{pmatrix}. \tag{4.17}$$

Figure 4.1 shows graphical interpretation for $\vec{m}$ vector into the RF process for an angle of $\theta = \frac{\pi}{2}$ and $\theta = \pi$.

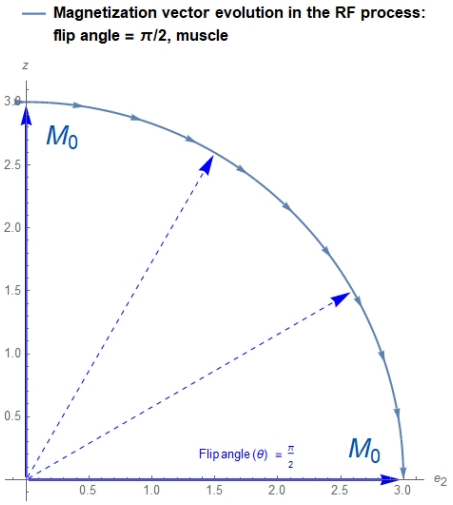

(a) $m_z(t)$,$m_{e_2}(t)$-muscle.

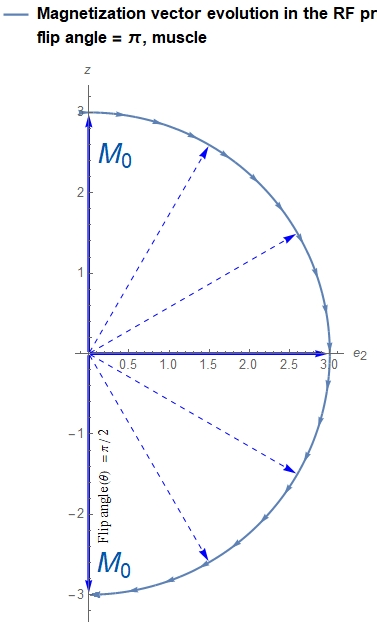

(b) $m_z(t)$,$m_{e_2}(t)$-muscle.

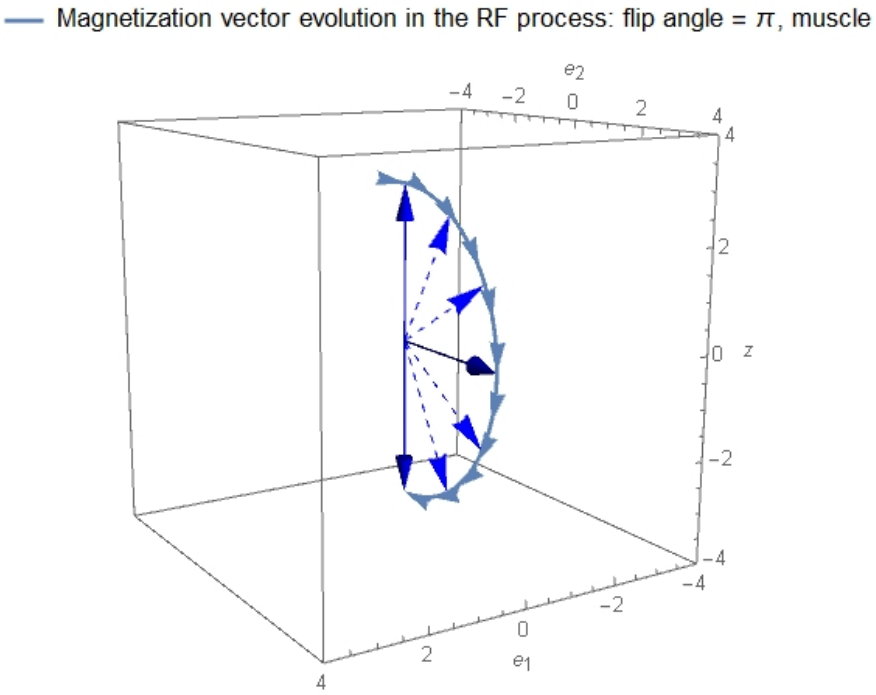

(c) $m_z(t)$,$m_{e_1}(t)$,$m_{e_2}(t)$-muscle.

Figure 4.1: Magnetization vector into the RF process. $\theta = \frac{\pi}{2}$ and $\theta = \pi$.

Figure 4.2 shows the $\vec{m}(t)$ vector into the RF process for a flip angle θ.

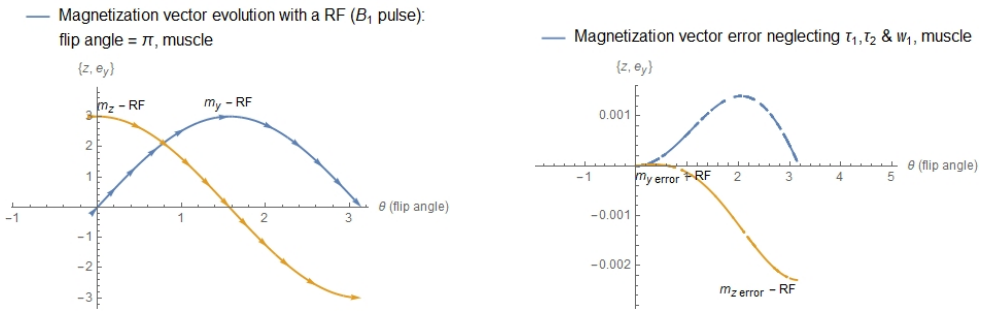

(a) $m_z(t)$,$m_{e_2}(t)$-muscle. (b) $m_z(t)$,$m_{e_2}(t)$-error.

Figure 4.2: Magnetization vector m_z and m_{e_2} into the RF process. $\theta = \frac{\pi}{2}$ and $\theta = \pi$.

Figure 4.3 shows $\vec{m}$ and error $(\vec{m}(t) - \vec{m}_{ap}(t))$ for $\theta = \frac{\pi}{2}$ and $\theta = \pi$.

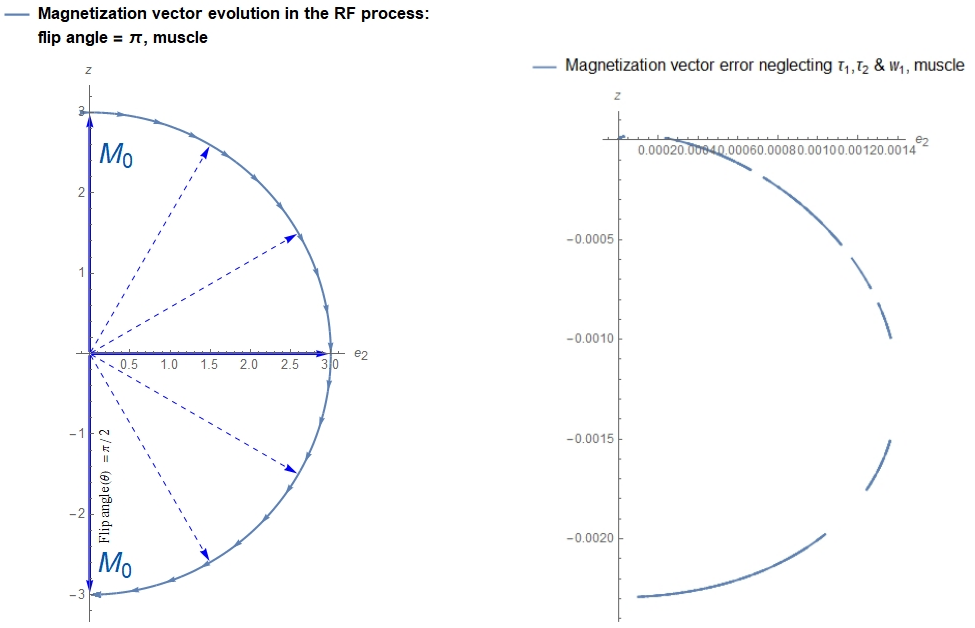

(a) $m_z(t)$,$m_{e_2}(t)$-muscle. (b) $m_z(t)$,$m_{e_2}(t)$-muscle.

Figure 4.3: Magnetization $m_z(t)$ and $m_{e_2}(t)$ and error $\vec{m} - \vec{m}_{ap}$ into the RF process.

Figure 4.4 shows magnetization $\vec{M}$ approximation into the RF process for an angle of $\theta = \frac{\pi}{2}$ and $\theta = \pi$ for different B_1 magnitudes.

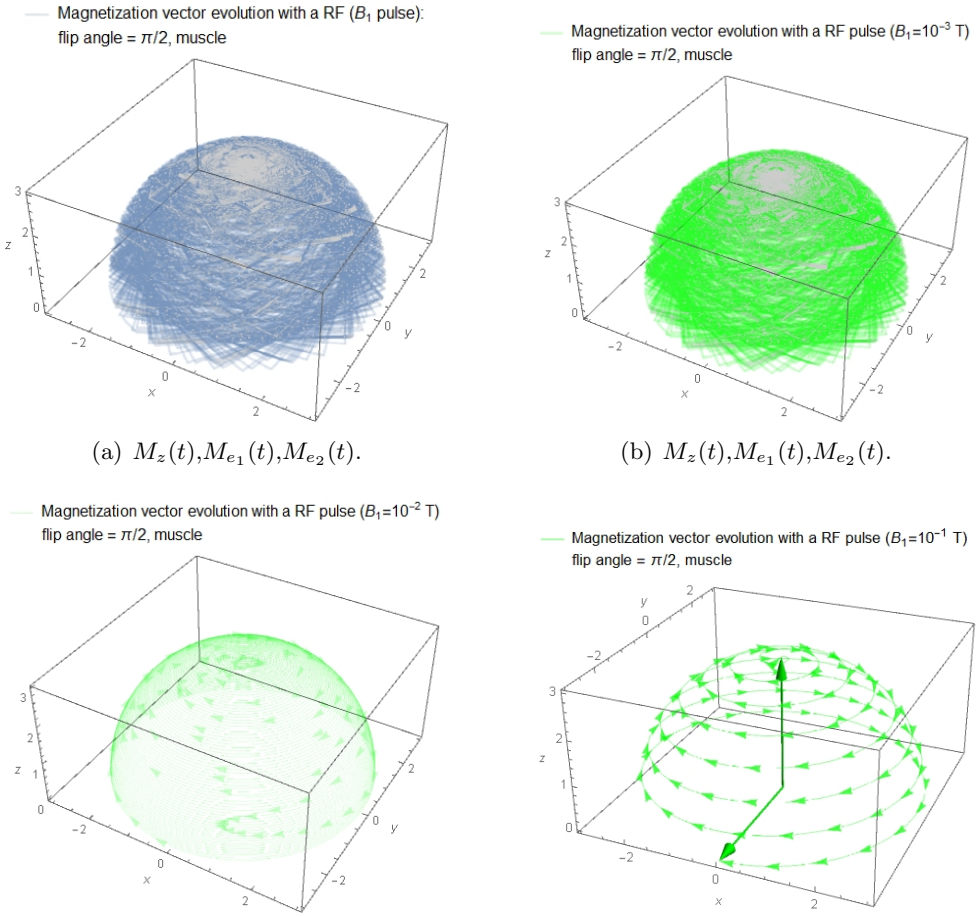

(a) $M_z(t)$,$M_{e_1}(t)$,$M_{e_2}(t)$.

(b) $M_z(t)$,$M_{e_1}(t)$,$M_{e_2}(t)$.

(c) $M_z(t)$,$M_{e_1}(t)$,$M_{e_2}(t)$.

(d) $M_z(t)$,$M_{e_1}(t)$,$M_{e_2}(t)$.

Figure 4.4: Magnetization vector $\vec{M}$ for different B_1 RF amplitude process.

Chapter 5

Recent research trends.

For solving an ODE system such as equation (2.1), multiple numerical methods have been proposed and are widely available in the literature. If the RF excitation field amplitude, phases and magnetic field gradients are constant and smooth, and there are not eddy currents fields nor inhomogeneities which are not present, the Bloch equations are a linear ODE system with constant coefficients. In this conditions different analytical solutions are available for solving Bloch equations for MR experiments [23, 24, 25].

In a previous studies several authors used explicit $4-5^{th}$ order adaptive Runge-Kutta (**RK45**) for Bloch equations simulations.

In contrast, non linear equations are complex problems and require much more efforts. S. Balac and L. Chupin [1] published a method for solving non linear differential Bloch equation with an analytical approach for non-homogeneous fields due to eddy currents. We expose this method in section 5.1.

But one of the greatest problems is to solve the magnetization transport phenomena. In order to study the effect of fluid flow in a MRI experiment, the transport of magnetizations due to flow field $u(t, \vec{r})$ must be taken into account and is modelled by the modified and well-posed Bloch equation:

$$\boxed{\frac{\partial \vec{M}}{\partial t} + (\vec{u} \cdot \nabla)\vec{M} = \gamma \vec{M} \times \vec{B} - \frac{M_x \vec{x} + M_y \vec{y}}{T_2} - \frac{(M_z + \tau_0)\vec{z}}{T_1}.} \tag{5.1}$$

The modified Bloch model was solved using multiple numerical strategies previously e.g., Jou et al. [30], first solved the flow field in a computational mesh using finite volume method (**FVM**) softwares and then studied the effect

of flow on magnetization using finite difference method (**FDM**).

As A. Hazra exposed in its doctoral programme [10], multiple utilities of numerical simulations have been combined to produce a few general purpose MRI simulators. Accurate simulation of this initial-value problem is still challenging for the following reasons: very tiny time steps, sufficiently fine spatial resolution, and non-smooth data (e.g. gradient field G). To overcome this difficulty, the execution speeds were improved using parallelization with message passing interface (**MPI**)[27] or graphic process unit (**GPU**) [28].

Jurczuk etal. [15] solved equation 5.1 by **splitting the transport and the MR** terms [29]. In their work, the magnetization transport was calculated using lattice-Boltzmann method (**LBM**) and the reaction part was calculated using operator splitting techniques.

A semi-analytical technique based on operator splitting [29] has the following advantages [10]:

- different numerical methods can be used to treat different sub-problems with optimal numerical methods for the each subproblems.
- it is easy to change numerical algorithms for different sub-problems in order to achieve improvements of the codes.
- different time-scales can be used to resolve different subproblems which helps in reducing computational load. In many cases, the splitting procedure leads to better parallel implementation.

However, these initial studies lack a proper analysis of the Bloch model for flowing objects. A. Hazra [10] proved the well-posedness of the modified Bloch model and the spatial semi-discretization with **Discontinuous Galerkin formulation**. The basic idea of this method is exposed in section 5.2.

5.1 Dealing with perturbation fields.

Under RF field perturbations the Bloch equation can not be reduced to a ODE system with constant coefficients in an appropriate frame and neither it is not possible to compute analytically. It means that for each voxel the Bloch equation needs to be solved using a numerical discretization scheme and it is then enough costly to obtain a good resolution image.

Therefore, under perturbations the matrix A is not constant and solving the differential system becomes inefficient. We want to stand out the fact that the more time we expend in solve the Bloch equation the more time we waste in interpreting artifacts and recover the scanner investment.

As we show in equation (2.2), it is possible to express the total magnetic field as $\vec{B} = \vec{B_0} + \vec{B_G} + \vec{B_1} + \vec{B'}$ and we can also split up perturbation fields, $\vec{B'}$, in four different perturbation fields depending on their origin behaviour:

$$\vec{B'} = \vec{B'_0} + \vec{B'_G} + \vec{B'_1} + \overrightarrow{B'_E}, \tag{5.2}$$

where notation is:

- $\vec{B'_0} = (B'_{0x}, B'_{0y}, B'_{0z})$, represents the magnetic field perturbations generated by the magnet, due to its physical inhomogeneities and depends basically on the production processes and its precise installation requirements.
- $\vec{B_G}' = (B'_{Gx}, B'_{Gy}, B'_{Gz})$, represents the magnetic field perturbations generated by the action of the coil gradients located inside the scanner.
- $\vec{B_1}' = (B'_{1x}, B'_{1y}, B'_{1z})$, represents the magnetic field perturbations generated by the RF pulses.
- $\vec{B'_E} = (B'_{Ex}, B'_{Ey}, B'_{Ez})$, represents the magnetic field perturbations generated by whatever external elements o physical phenomena located outside the magnet or the scan room. Usually, they are due to high variations of intensity on wires (e.g. when a TAG is located near the MRI room) or even with traffic of undergrounds or trains near the hospital.

Faraday's law (equation 1.15) states that the electromotive force $\epsilon(t)$ is also given by the rate of change of the magnetic flow.

Therefore, this $\epsilon(t)$ generates **eddy currents** which induce magnetic fields associated to them and perturb the initial magnetic fields created by the MRI. The conductive material in which eddy currents are induced may be any metallic component of the MRI scanner (other coils, shields, tubes, and housing), wires or devices within the patient.

Within the MRI scanner, eddy currents are induced any nearby conducting

media, which include inside the gradient coils themselves, the main magnet and shim coil windings, cryoshields, liquid helium vessel, and RF shields. Eddy currents create new magnetic fields which caused two undesired phenomena: unwanted time-varying gradients and shifts in the main magnetic field ($\vec{\mathbf{B}}_0$).

As per Faraday's Law, the magnitude of eddy currents depends on the rate of change of the inciting magnetic field. Thus fast imaging sequences (where gradients are pulsed on and off quickly and where RF pulses are on-off repeatedly) produce the largest and most severe eddy current problems.

Several techniques are available to minimize the effects of eddy currents :

1. design methods that interrupt potential current loops (e.g. use of slotted coils and shields into the scanner),
2. passive shields or coils installed into the scanner room to compensate external perturbation (e.g to compensate traffic signals);
3. active shielding of gradients (secondary coils outside to constrain magnetic flux changes induced by primary gradients);
4. pre-emphasis (modifying the input current to the gradients to account for expected eddy-current distortions); or
5. image post-processing (to correct for spatial non linearities and frequency/phase shifts due to eddy currents).

The first four techniques could be physically made by modifying the magnet, gradients or RF coils and the last one by solving the associated non-linear differential Bloch equation system which corrects the artifacts and shows the true images.

In this way S.Balac and L. Chupin [1] presented in 2007 an original method to compute solution $\vec{M}$ to the Bloch equation under RF field inhomogeneities (only for $\vec{B_1'}$ originated just by Eddy currents) at a given time T directly, without any discretisation of the time interval $[0, T]$. The method is based on a series expansion of the solution. Through those transform, the Bloch equation is changed of into an infinite ODE's system with constant coefficients.

We are going to review this method.

The RF field perturbation vector components generated by eddy currents due to a $\vec{B}_1$ RF signal with $\omega_1 = \gamma\|\vec{B}_1\|$ frequency is given in a general case by

$$\begin{aligned}\vec{B}_1'(r,t) = &((u_1(r)\cos(\omega_0 t) + v_1(r)\sin(\omega_0 t))\,\vec{x} + \\ &((u_2(r)\cos(\omega_0 t) + v_2(r)\sin(\omega_0 t))\,\vec{y} + \\ &((u_3(r)\cos(\omega_0 t) + v_3(r)\sin(\omega_0 t))\,\vec{z},\end{aligned} \tag{5.3}$$

where $u_i, v_i \quad i = 1,2,3$ are unknown values and ω_0 is the perturbation frequency which is the same as $\vec{B}_1$ because the eddy current effects has the same frequency as the magnetic field $\vec{B}_1$ has (see equations (4.11), (1.15), (1.16)).

According to Floquet theory [23], the fundamental solution $X(t)$ for the differential system (4.6) has the following expression:

$$X(t) = Q(t)e^{tF}, \tag{5.4}$$

where $Q(t)$ is a matrix with continuous and periodic (T_0) coefficients and F is a constant matrix. There are two ways of exploiting the Floquet structure of $X(t)$, the first one consist in performing a Fourier expansion of the fundamental solution, leading to an infinite system of linear differential equations with constant coefficient. When the constant coefficients have adequate properties, resolution of a truncated system furnishes an approximate solution. The second approach is of perturbative nature and deals with the Floquet form by expanding the two matrices Q and F as

$$Q(t) = \sum_{n=1}^{+\infty} Q_n(t), \quad F = \sum_{n=1}^{+\infty} F_n, \tag{5.5}$$

where every term F_n is chosen in order to ensure the matrix $Q_n(t)$ is periodic and in turn $Q_n(t)$ is fixed so as to guarantee the Floquet structure at any order of truncation. S. Balac and L. Chupin [1] proposed approach not directly using the Floquet form of a fundamental solution but exploiting some of the ideas of them. First, let us observe that the matrix $\tilde{A}(t)$ admits the following Fourier decomposition:

$$\tilde{A}(t) \underset{Fourier}{=} \sum_{k=-1}^{1} e^{2ik\omega_0 t} = A_{-2}e^{2i\omega_0 t} + A_0 + A_2 e^{2i\omega_0 t},$$

with

$$A_0 = \begin{pmatrix} -\tau_2 & 0 & -\omega_a^{(0)} \\ 0 & -\tau_2 & \omega_b^{(0)} \\ -\omega_a^{(0)} & \omega_b^{(0)} & -\tau_1 \end{pmatrix}; A_2 = \bar{A}_{-2} \begin{pmatrix} 0 & 0 & -\omega_a^{(2)} \\ 0 & 0 & \omega_b^{(2)} \\ \omega_a^{(2)} & -\omega_b^{(2)} & 0 \end{pmatrix};$$

and

$$\begin{array}{ll} \omega_a^{(0)} = \frac{1}{2}\gamma(u_2+v_1), & \omega_a^{(2)} = \frac{1}{4}\gamma(v_1-u_2+i(u_1+v_2)), \\ \omega_b^{(0)} = \frac{1}{2}\gamma(2B_1+u_1-v_2), & \omega_b^{(2)} = \frac{1}{4}\gamma(u_1+v_2+i(u_2+v_1)), \end{array}$$

and $A_2 = \bar{A}_{-2}$ is the conjugate matrix of A_2. As the solution $m(t)$ of (3.1,3.2) is not periodic it is not possible to compute it through its Fourier series expansion. Thus, we look for a formal solution of the the following type:

$$m(t) = \sum_{k\in\mathbb{Z}} m_k(t) e^{2ik\omega_0 t} \tag{5.6}$$

which looks like a Fourier series expansion but with non constant coefficients $\mathbf{m}_k(t)$. This decomposition is not unique since no condition is imposed on the functions $\mathbf{m}_k$. If we use the expansion (5.6) in the differential system (3.1,3.2) we obtain

$$\begin{aligned} &\sum_{k\in\mathbb{Z}} r_k(t) e^{2ik\omega_0 t} = 0, \\ &r_k(t) = \frac{\partial}{\partial t} m_k(t) - \sum_{j=-1}^{1} A_{2j} m_{k-j}(t) + 2ik\omega_0 m_k(t) - \delta_k b, \end{aligned} \tag{5.7}$$

with the sequence $(\delta_k)_k$ given by $\delta_0 = 1$ and $\delta_k = 0$ for $k \in \mathbb{Z}^*$. Contrary to a standard Fourier expansion, it can not be deduced that $r_k(t) = 0$ for all $k \in \mathbb{Z}$. Nevertheless, if we can solve all equations $r_k(t) = 0$ under appropiate initial conditions so that the series $\sum_{k\in\mathbb{Z}} m_k(t) e^{2ik\omega_0 t}$ converges then the series expansion $m(t)$ as given by (5.6) will be solution of the differential system (3.1). If $\sum_{k\in\mathbb{Z}} m_k(0) = M_0$ then $m(t)$ will be the solution of the differential system (3.1) under the initial condition $m(0) = M_0$ (3.2).

S. Balac and L. Chupin [1] introduced a suitable mathematical framework to proof theorem 1. Next, we will expose several theorem, lemma, corollary and proposition. You are be able to show their proofs in [1].

Theorem 1. *The following finite equation system*

$$\forall k \in \mathbb{Z} \begin{cases} \dfrac{\partial}{\partial t} m_k(t) = \sum\limits_{j=-1}^{1} A_{2j} m_{k-j}(t) + 2ik\omega_0 m_k(t) - \delta_k b, \\ \mathbf{m}_k(0) = \mathbf{M_0}, \end{cases} \tag{5.8}$$

admits a ***unique solution*** *and that for a given time t the sequence* $(m_k(t))_{k\in\mathbb{Z}}$ ***converges very quickly towards zero*** *when k tends to* $\pm\infty$.

The analysis of the behaviour of the solution to the sequence of differential equations (5.8) will justify the fact that an approximation of the solution to the Bloch equation can be computed by solving a truncated finite differential system deduced from (5.8) by taking $k \in \{-N, ..., N\}$.

Definition 7. *A given sequence $(\mathbf{u}_k)_{k\in\mathbb{Z}}$ of vectors in $\mathbb{C}^3$ can be seen as an infinite vector,denoted by $\mathcal{U}$ in the sequel, with the kth component given by $\mathbf{U}_k = \mathbf{u}_k \in \mathbb{C}^3$. It is denoted by $\ell^2(\mathbb{Z})$ the space summable series*

$$\ell^2(\mathbb{Z}) = \{\mathcal{U} \in (\mathbb{C}^3)^{\mathbb{Z}}; \quad \sum_{k\in\mathbb{Z}} |u_k|^2 < +\infty\}, \tag{5.9}$$

and by $\ell^1(\mathbb{Z})$ denotes the corresponding space of absolute convergent series where $|u_k|$ denotes the euclidean norm of u_k in $\mathbb{C}^3$.

Definition 8. *For any positive number p it is defined the following **space of weighted square summable series**:*

$$\ell^2_p(\mathbb{Z}) = \{\mathcal{U} \in \ell^2(\mathbb{Z}); \quad \sum_{k\in\mathbb{Z}} (k^{2p}+1)|u_k|^2 < +\infty\}.$$

This space is equipped with the scalar product $<,>_{\ell^2_p(\mathbb{Z})}$ and its associated norm $\|\mathcal{U}\|_{\ell^2_p(\mathbb{Z})}$ defined as follows: for $\mathcal{U}, \mathcal{V} \in \ell^2_p(\mathbb{Z})$

$$\langle \mathcal{U}, \mathcal{V}\rangle_{\ell^2_p(\mathbb{Z})} = \sum_{k\in\mathbb{Z}} (k^{2p}+1)(u_k \cdot v_k) \quad \textit{and} \quad \|\mathcal{U}\|^2_{\ell^2(\mathbb{Z})} = \langle \mathcal{U}, \mathcal{U}\rangle_{\ell^2(\mathbb{Z})}.$$

Definition 9. *It is also introduced the **space of fast decreasing series** defined by*

$$\ell^2_\infty(\mathbb{Z}) = \bigcap_{p\in\mathbb{N}} \ell^2_p(\mathbb{Z}).$$

Lemma 1. *The spaces $\ell^2_p(\mathbb{Z})$ have the following properties*

1. *$\ell^2_0(\mathbb{Z}) = \ell^2(\mathbb{Z})$ and $\|\mathcal{U}\|^2_{\ell^2_0(\mathbb{Z})} = \sqrt{2}\|\mathcal{U}\|^2_{\ell^2(\mathbb{Z})}$ for all $\mathcal{U} \in \ell^2_0(\mathbb{Z})$.*
2. *The inclusion $\ell^2_p(\mathbb{Z}) \subset \ell^2_q(\mathbb{Z})$ holds for all $(p, q) \in (\mathbb{R}^+)^2$ with $p \geq q$ and we have $\|\mathcal{U}\|^2_{\ell^2_q(\mathbb{Z})} \leq \|\mathcal{U}\|^2_{\ell^2_p(\mathbb{Z})}$ for all $\mathcal{U} \in \ell^2_p(\mathbb{Z})$.*
3. *The inclusion $\ell^2_p(\mathbb{Z}) \subset \ell^1(\mathbb{Z})$ holds for all $(p > 1)$ and we have $\|\mathcal{U}\|^2_{\ell^1(\mathbb{Z})} \leq \sqrt{1 + 2\zeta(2p)}\|\mathcal{U}\|^2_{\ell^2_p(\mathbb{Z})}$ for all $\mathcal{U} \in \ell^2_p(\mathbb{Z})$ where ζ is the Riemann function.*

4. *If S denote the shift operator on $\ell^2(\mathbb{Z})$ defined by $(\mathcal{SU})_k = u_{k-1}$ for all $k \in \mathbb{Z}$ then for all $p \in \mathbb{N}$ we have*

$$\|\mathcal{SU}\|^2_{\ell^2_p(\mathbb{Z})} \leq 2^p \|\mathcal{U}\|^2_{\ell^2_p(\mathbb{Z})} \quad \textit{and} \quad \|\mathcal{S}^{-1}\mathcal{U}\|^2_{\ell^2_p(\mathbb{Z})} \leq 2^p \|\mathcal{U}\|^2_{\ell^2_p(\mathbb{Z})}.$$

Proposition 1. *There exists a* ***unique solution*** $\mathcal{U} \in \mathcal{C}^\infty(\mathbb{Z}^+, \ell^2_\infty(\mathbb{Z}))$ *to the differential system*

$$\begin{cases} \dfrac{\partial}{\partial t}\mathcal{U}(t) = \mathcal{A}(t)\mathcal{U}(t) + \mathcal{B}, \\ \mathcal{U}(0) = \mathcal{M}(0), \end{cases} \tag{5.10}$$

where linear operator $\mathcal{A}(t)$ is time dependant and defined using the shift operator S and the identity $\mathcal{I}$ in $\ell^2(\mathbb{Z})$ as follow

$$\mathcal{A}(t) = \mathcal{A}_2 e^{2i\omega_0 t}\mathcal{S} + \mathcal{A}_0 + \mathcal{A}_{-2} e^{2i\omega_0 t}\mathcal{S}^{-1}.$$

Moreover, for all $p \in \mathbb{N}$ and for all $t \in \mathbb{R}^+$, the solution satisfies

$$\|\mathcal{U}(t)\|_{\ell^2_p(\mathbb{Z})} \leq e^{C_p(t)}|M_0| + (e^{C_p(t)} - 1)\frac{|b|}{C_p},$$

where $C_p = 2^{p+1}\|A_2\| + \|A_0\|$ is a constant.

Corollary 1. *There* ***exists a unique solution*** $(m_k)_{k\in\mathbb{Z}}$ *to the system of differential equations (5.8); it satisfies*

$$\forall t \in \mathbb{R}^+ + \forall p \in \mathbb{N} \quad (m_k(t))_{k\in\mathbb{Z}} \in \mathbb{Z},$$

i.e. $m_k(t)$ tends towards zero as k tends to $\pm\infty$ faster than any power of $1/k$.

Proposition 2. *About the asymptotic behaviour: the sequence of functions $(\mathcal{E}^{[N]})_{N\in\mathbb{N}}$ where $\mathcal{E}^{[N]} : t \in \mathbb{R}^+ \mapsto \mathcal{U}(t) - \mathcal{U}^{[N]}(t)$ belongs to $L^\infty_{loc}(\mathbb{R}^+; \ell^2_\infty(\mathbb{N}, \ell^2_\infty(\mathbb{Z})))$. This means that for any $t \in \mathbb{R}^+$, the sequence of complex vectors $(\mathcal{E}^{[N]}(t))_{N\in\mathbb{N}}$* ***tends towards zero faster*** *than any power of $1/N$. In other words, for all $t \in \mathbb{R}^+$ the sequence $\mathcal{U}^{[N]}(t)$* ***converges very quickly*** *to $\mathcal{U}(t)$ as N tends to infinity.*

Corollary 2. *We can see an overview of the accuracy and efficiency of the of the method:*

$$B_0 = 1T, B_1 = 10^{-3}T, M_0 = 1,$$
$$T_1 = 750ms, T_2 = 50ms \textit{ and } \theta = \tfrac{\pi}{2}.$$

WITHOUT PERTURBATIONS

Comparison of accuracy and CPU times for 16^3 executions [1].

	N=0	N=1	N=2	N=3	ode45
CPU seconds	3.82	9.17	17.56	29.53	69.21
Error %	0.0089	0.0089	0.0089	0.0089	0.01

WITH RF PERTURBATIONS

	N=0	N=1	N=2
Seconds	4.36	12.1	25.97
M_x	-0.**24326287**201152	-.**24326289**631217	-.**24326289**631192
M_y	0.**96630713**580637	0.**96630713**685089	0.**96630713**685049
M_z	0.**07993334**331631	0.**07993336**879906	0.**07993336**879932

Corollary 3. *The evolution of the magnetization vector m under the assumption that τ_1 and τ_2 can be neglected compared to ω_1 and the solution $\mathbf{m}^{[0]}$ to (5.8) under the initial condition $\vec{\mathbf{M}}_0 = M_0\vec{z}$ reads:*

$$m^{[0]} = \begin{pmatrix} -\frac{v_1+u_2}{b} M_0 \sin(\alpha t) \\ \frac{2B_1+u_1-v_2}{b} M_0 \sin(\alpha t) \\ M_0 \sin(\alpha t) \end{pmatrix}, \tag{5.11}$$

where $b = \sqrt{(2B_1 + u_1 - v_2)^2 + (v_1 + u_2)^2}$, $\alpha = \frac{1}{2}\gamma b$.

Figure 5.1 shows the comparison with and without considering the effect of the RF perturbation magnetic field.

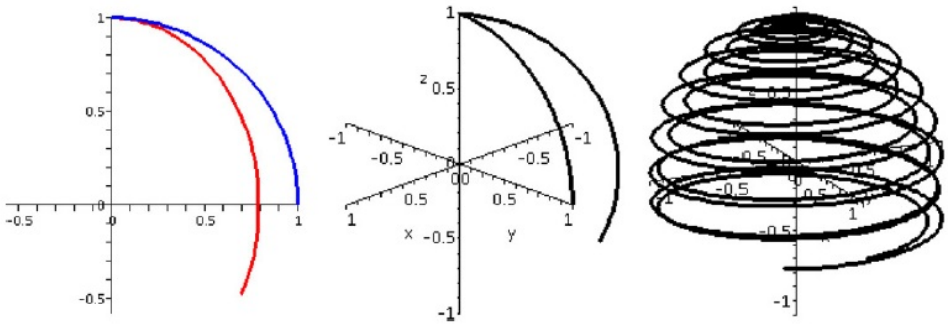

Figure 5.1: Comparison of the magnetisation vector evolution for a $\pi/2$ pulse with and without RF perturbation [1].

5.2 Well-posed Bloch equation under flow fields.

A. Hazra, G.Lube and H.G. Raumer [2] studied the modified Bloch problem as a model of MRI for flowing spins in an incompressible flow field. They established the well-posedness of the corresponding evolution problem and analyse its spatial semi-discretization using discontinuous Galerkin methods.

Due to signal demodulation, see equation (1.27), the signal acquired from the object in an MRI process is equivalent to an equation where magnetizations $M^{'}$ and the magnetic field

$$\begin{aligned} \vec{B}_{eff}(t) &= B_x(t)\vec{e}_1 + B_y(t)\vec{e}_2 + B_z(t)\vec{z}, \\ \vec{M}^{'}(t) &= {M'}_x(t)\vec{e}_1 + {M'}_y(t)\vec{e}_2 + M_z(t)\vec{z}, \\ B_z(t) &= G(t)\cdot r, \end{aligned} \tag{5.12}$$

are written in the rotation frame but with velocity $\vec{u}(t,r)$ kept in the laboratory frame. In order to study the effect of fluid flow in MRI, the transport of the magnetization due to flow field $\vec{u}(t,r)$ must be taken into account and equation 5.1 becomes:

$$\boxed{\frac{\partial \vec{M}^{'}}{\partial t} + (\vec{u}\cdot\nabla)\vec{M}^{'} = \gamma \vec{M}^{'} \times \vec{B}_{eff} - \frac{M_x^{'}\vec{e}_1 + M_y^{'}\vec{e}_2}{T_2} - \frac{(M_z+\tau_0)\vec{z}}{T_1}.} \tag{5.13}$$

For notational simplicity, authors usually omit the '. Hereafter magnetization $\vec{M}$ will always be expressed in the rotating frame and the velocity, $\vec{u}$ represents the velocity of the magnetic flow field in the laboratory frame. This equation assumes that no diffusion term exist as effect of diffusion is negligible.

A. Hazra, G. Lube and H.G. Raumer [2] define in their work the well-posedness of the Bloch equation, therefore problem (5.13) can be rewritten with appropriate boundary and initial condition. Let show the main ideas of their work.

Proposition 3. ***Well-posedness of the Bloch model.***
Let $\Omega \subset \mathbb{R}^3$ be the flow domain with piecewise smooth Lipschitz boundary Γ and outer normal $\mathbf{n}$. The compressible flow field $\mathbf{u}(t,r)$ introduces the splitting $\Gamma = \Gamma_- \cup \Gamma_+ \cup \Gamma_0$ where $\Gamma_- = \{\mathbf{r}\in\Gamma | \mathbf{u}\cdot\mathbf{n} < 0\}, \Gamma_+ = \{\mathbf{r}\in\Gamma|\mathbf{u}\cdot\mathbf{n}>0\}$ and $\Gamma_0 = \{\mathbf{r}\in\Gamma|\mathbf{u}\cdot\mathbf{n}=0\}$ represent the inflow boundary, outflow boundary and solid wall, respectively. We assume that inflow and outflow are separated, $dist(\Gamma_-,\Gamma_+) := min_{(P,Q)\in\Gamma_-\times\Gamma_+}|P-Q| > 0$,see figure (5.2). Then differential

system (5.13) can be written as

$$\begin{cases} \dfrac{\partial \mathbf{M}}{\partial t} + (\mathbf{u}\cdot\nabla)\mathbf{M} + \gamma\mathbf{B}\times\mathbf{M} + D\mathbf{M} &= \mathbf{f}, & (t,r)\in[0,T]\times\Omega, \\ \mathbf{M} &= \mathbf{M}_\Gamma, & (t,r)\in[0,T]\times\Gamma_-, \\ \mathbf{M} &= \mathbf{M}^0, & (t,r)\in\{0\}\times\Omega, \end{cases} \tag{5.14}$$

where $B_{eff} = B = (B_x, B_y, B_z)^T$, $D = diag(\tau_2, \tau_2, \tau_1)$ *and the constant source term* $f = (0, 0, \tau_1\tau_0)^T$.

Under this new variational model, A. Hazra, G.Lube and H.G. Raumer [2] analyse its spatial semi-discretization using **discontinuous Galerkin methods** and established the error estimates. An explicit **Runge-Kutta method** and an **operator splitting** between advection and magnetization can be applied. They made a numerical experiment for validating this approximation and **the computation can be strongly accelerated** via GPU computing.

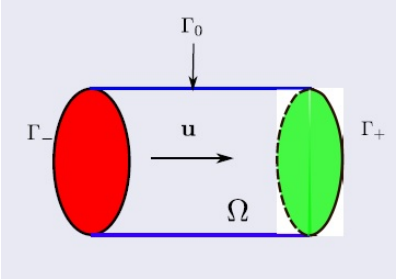

Figure 5.2: Leipzig Boundary condition assumptions [2].

Consider the space $\mathbf{H} := [L^2(\Omega)]^3$ with inner product $(\mathbf{u},\mathbf{v})_\mathbf{H} := \int_\Omega u\cdot v dr$, norm $\|\mathbf{v}\|_H := \sqrt{(v,v)}$ and defining the space

$$\mathbf{X} = \{N \in H : (u\cdot\nabla)N \in H\}, \tag{5.15}$$

with graph norm

$$\|N\|_X := \left(\|(u\cdot\nabla)N\|_H^2 + \|N\|_H^2\right)^{\frac{1}{2}}. \tag{5.16}$$

Multiplying 5.14 by arbitrary test function $N \in X$, integrating over Ω and imposing weakly it is possible to obtain

Definition 10. ***Variational form of the Bloch equation*** *[2].*
The variational formulation of the Bloch problem treat to find $\mathbf{M} : (0,T] \to X$ *s.t.*

$$\begin{cases} (\partial_t\mathbf{M},\mathbf{N})_\mathbf{H} + a(t;\mathbf{M},\mathbf{N}) &= l(\mathbf{N}), & \forall\mathbf{N}\in\mathbf{X}, \\ \mathbf{M}|_{t=0} &= \mathbf{M}^0, \end{cases}. \tag{5.17}$$

where (5.17) is a Friedrichs system (see [31], section 7). Unfortunately, theory is not applicable since some coefficients are time-dependent.Therefore we set for $0 < \epsilon \ll 1$ $X_\epsilon := [W^{1,2}(\Omega)]^3$

Definition 11. ***Considering an elliptic regularization*** *[2].*
Then the variational formulation of the Bloch problem treat to find $\mathbf{M}_\epsilon : (0,T] \to X_\epsilon$ *s.t.*

$$\left\{ \begin{array}{rcll} (\partial_t \mathbf{M}_\epsilon, \mathbf{N})_{\mathbf{H}} + a_\epsilon(t; \mathbf{M}_\epsilon, \mathbf{N}) & = & l(\mathbf{N}), & \forall \mathbf{N} \in \mathbf{X}_\epsilon, \\ \mathbf{M}_\epsilon|_{t=0} & = & \mathbf{M}^0, & \end{array} \right. \tag{5.18}$$

with

$$a_\epsilon(t; \mathbf{M}, \mathbf{N}) := a(t; \mathbf{M}, \mathbf{N}) + \epsilon(\nabla \mathbf{M}, \nabla \mathbf{N})_H \tag{5.19}$$

It's noted that variational formulation of the regularized Bloch problem incorporates do-nothing boundary conditions $\epsilon \nabla M_\epsilon \cdot n = 0$ on $\Gamma_0 \cup \Gamma_+$.

Theorem 2. ***Well posed problem.***
For all $\epsilon > 0$*, for given* $u \in [L^\infty(0,T; W^{1,\infty}(\Omega))]$ *with* $div\, u = 0$ *and* $B \in [L^\infty(0,T;H)]^3$*, there exists a unique solution* $M_\epsilon \in L^\infty(0,T;H) \cap L^2(0,T;X_\epsilon)$ *to problem (5.18). For* $t \in (0,T]$ *and with* $\sigma := \tau_1$*, the following a-priori estimate is valid*

$$\frac{1}{2}\|M_\epsilon(t)\|_H^2 + \int_0^t e^{\sigma(\tau - t)} \left[\epsilon \|\nabla M_\epsilon(\tau)\|_H^2 + \frac{1}{2} \int_\Gamma |(u \cdot n)| (M_\epsilon \cdot M_\epsilon)(s,\tau) ds \right] d\tau \\ \leq \frac{1}{2}\|M_\epsilon(0)\|_H^2 e^{-\sigma t} + \frac{1}{2\sigma} \int_0^t \|f(\tau)\|_H^2 e^{\sigma(\tau - t)} d\tau.$$

Finally, it is possible to pass to the limit $\epsilon \to +0$, i.e. to the Bloch model.

Theorem 3. ***Well posed problem.*** $\epsilon \to +0$.
The variational Bloch model equation (5.17) admits a unique solution $M \in L^\infty(0,T;H) \cap L^2(0,T;X)$*. The kinetic energy of the magetic field is bounded by:*

$$\frac{1}{2}\|M(t)\|_H^2 + \int_0^t e^{\sigma(\tau - t)} \left[\int_\Gamma |(u \cdot n)| (M \cdot M)(s,\tau) ds \right] d\tau \\ \leq \frac{1}{2}\|M(0)\|_H^2 e^{-\sigma t} + \frac{1}{2\sigma} \int_0^t \|f(\tau)\|_H^2 e^{\sigma(\tau - t)} d\tau.$$

the result of Theorem 2 and a-priori estimate of last Theorem 3 remains valid for case $u = 0$, i.e. Bloch equations for spacially stationary objects.

The next step authors suggest is the use of discontinuous Galerkin finite element method (**dG-FEM**) for a spatial discretization of the problem. In this way it's necessary to formulate the problem.

Notation. ***Discontinuous Galerkin formulation.***

- *admissible mesh* $\mathcal{T}_h := \{\Omega_i\}_{i=1}^I$ *into complex simplicial subdomains* $\{\Omega_i\}$ *(see figure (5.3)).*

- *discontinuous FE space:*

$$[\mathbb{P}_k(\mathcal{T}_h)]^d := \left\{ N_h \in H; N_h|_{\Omega_i} \in [\mathbb{P}_k(\Omega_i)]^d \quad \forall \Omega_i,\, I = 1, 2, \cdots, I \right\},$$

  where $\mathbb{P}_k$ *denotes the set of polynomials of degree* $k \in \mathbb{N}$

- $X_h = [\mathbb{P}_k(\mathcal{T}_h)]^d \cap X$

- *for adjacent subdomains* Ω_i, Ω_j *with interface* $E = \Gamma_{ij} = \bar{\Omega}_i \cap \bar{\Omega}_j$ *and unit normal vector* n_{ij} *define the average and jump of* $N_h \in X$ *across* Γ_{ij} *by*

$$\begin{array}{rl} \langle N_h \rangle_{\Gamma_{ij}}(r) & := \frac{1}{2}(N_h|_{\Omega_i}(r) + N_h|_{\Omega_j}(r)), \\ [N_h]_{\Gamma_{ij}}(r) & := N_h|_{\Omega_i}(r) - N_h|_{\Omega_j}(r), \end{array} \tag{5.20}$$

- *Let* $\mathcal{F}_h^i$ *be the set of all the interior interfaces* $E \subseteq \Omega$ *and define the upwind form*

$$S_h(t; M, N) := \sum_{E \in \mathcal{F}_h^i} \int_E \left(-(u \cdot n_E)[M] \cdot \langle N \rangle + \frac{1}{2}|u \cdot n_E|[M] \cdot [N] \right) ds.$$

- *gradient jumps over the interior faces are penalized*

$$p_\epsilon(M, N) := \tilde{\epsilon} \sum_{E \in \mathcal{F}_h^i} h_E^2 \int_E |u \cdot n_E| [\nabla M]_E \colon [\nabla N]_E \, ds, \quad \tilde{\epsilon} \geq 0.$$

- *all the involving terms together*

$$a_\epsilon^{upw}(t; \mathbf{M}, \mathbf{N}) := p_\epsilon(\mathbf{M}, \mathbf{N}) + a(t; \mathbf{M}, \mathbf{N}) + S_h(t; \mathbf{M}, \mathbf{N}). \tag{5.21}$$

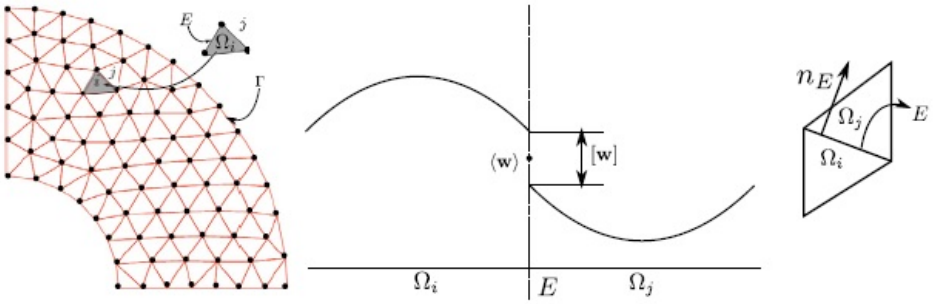

Figure 5.3: Left: 2D-simplicial mesh. Right: 1D-example of average and jump operators. [2].

Thus, the transformed equation (5.18) shows

Corollary 4. ***upwind dG-FEM.***
Then the upwind dG-FEM reads: find $M_h : (0,T] \to X_h$.

$$(\partial_t \mathbf{M}_h, \mathbf{N}_h)_{\mathbf{H}} + a_\epsilon^{upw}(t; \mathbf{M}_h, \mathbf{N}_h) = l(\mathbf{N}_h), \quad \forall \mathbf{N}_h \in \mathbf{X}_h, \tag{5.22}$$

Definition 12. *Let us define the norm* $\|N_h\|_U$ *via*

$$\|N_h\|_U^2 := \tilde{\epsilon} \sum_{E \in \mathcal{F}_h^i} h_E^2 \int_E |u \cdot n_E| \|[\nabla N_h]_E\|_{L^2(E)}^2 + \frac{1}{2} \int_\Gamma |u \cdot n| |N_h|^2 ds + \frac{1}{2} \sum_{E \in \mathcal{F}_h^i} \int_E |u \cdot n_E| [N_h]_E^2 ds. \tag{5.23}$$

Theorem 4. *The* ***semi-discrete problem*** *(Corollary (4))* ***is well-posed*** *and* ***admits the a-priori estimate.***

$$\frac{1}{2}\|M_h(t)\|_H^2 + \int_0^t e^{\sigma(\tau - t)} |||M_h(\tau)|||_U^2 d\tau \leq \frac{1}{2}\|M_h(0)\|_H^2 e^{-\sigma t} + \frac{1}{2\sigma} \int_0^t e^{\sigma(\tau - t)} \|f(\tau)\|_H^2 d\tau. \tag{5.24}$$

The existence and uniqueness proof follows the lines of the proof of Theorem 3 and application of the Gronwall lemma yields the a-priori estimate. See [2] for a complete guidance.

Theorem 5. ***Spatial discretization error*** $M_H - \pi_h M$ *with* L^2*-ortogonal projection* $M \to \pi_h M \in X$.

$$\begin{aligned}&\frac{1}{2}\|M - M_h(t)\|_H^2 + \frac{1}{2}\int_0^t e^{\sigma(\tau-t)}|||(M-M_h)(\tau)|||_U^2 d\tau \\ \leq\ &\frac{1}{2}\|(M-M_h)(0)\|_H^2 e^{-\sigma t} + \int_0^t e^{\sigma(\tau-t)}(|||(M-\pi_h M)(\tau)|||_{U,b}^2 \\ &+\delta\|(M-\pi_h M)(\tau)\|_H + p_\epsilon(M,M)(\tau))d\tau \end{aligned} \tag{5.25}$$

with $\delta := \gamma\|B\|_{L^\infty} + \|D\|_{L^\infty}$ *and*

$$|||I_h|||_{U,b}^2 := max\left\{1; \|u\|_{L^\infty(0,T;W^{1,\infty}(\Omega))}\right\}|||I_h|||_U^2 + \sum_{T\in\tau_h}\|u\|_{L^\infty(\delta T)}\|I_h\|_{L^2(\partial T)}^2.$$

For smooth solution $M \in L^\infty(0,T;[W^{k+1,2}(\Omega)]^3)$*, the last term is of order* $\mathcal{O}(h^{2k+1})$.

For finish the article, authors [2] alluded to a temporal discretization, so the starting point is the **spatially discretize** and find $M_h : (0,T] \to V_h$ s.t $\forall N_h \in X_h$

$$\begin{cases} (\partial_t M_h(t), N_h)_H + a_\epsilon^{upw}(t; M_h(t), N_h) = l(N_h), \\ M_h(0) = M_{h0}. \end{cases} \tag{5.26}$$

But equation 5.26 have still several problems to deal with:

a) Multiscale character: magnetization much faster than advection.

b) Restricted temporal smoothness of data, in particular $\vec{G} = G_x\vec{x} + G_y\vec{y} + G_z\vec{z}$.

To solve these problems we can applied the fully coupled approximation or the operator splitting approach.

Definition 13. ***Fully coupled approximation.***
Define a discrete operator $A_\epsilon^{upw} : X + X_h \to X_h$ *via* $(A_\epsilon^{upw}(t)v, w)_H := a_\epsilon^{upw}(t; v; w)$.
Let L *be a functional (constant in time) on* X_h *with* $L = l(w)$.
We denote $M_h^n = M_h(t^n)$*, etc..*
Low-order ***explicit Runge-Kutta*** *sheme on* $0 = t^0 < t^1 < t^2 < \ldots t^N$ *with time steps* $\tau_n := t^{n+1} - t^n$*,* $n = 0, 1, \ldots, N-1$*. Therefore,*

$$M_h^{n,1} = M_h^n - \tau_n A_\epsilon^{upw} M_h^n + \tau_n L, \tag{5.27}$$

$$M_h^{n+1,1} = \frac{1}{2}(M_h^n + M_h^{n,1}) - \frac{1}{2}\tau_n A_\epsilon^{upw} M_h^{n,1} + \frac{1}{2}\tau_n L. \tag{5.28}$$

RK2-analysis provides in case of smooth data in time, an error of order $\mathcal{O}(\tau_n^2 + h^{k+\frac{1}{2}})$ *with polynomial degree* k *of spatial discretization.*

Definition 14. ***Operator splitting.***
We can write semi-discrete problem (equation (5.26)) formally as a ODE-system

$$\frac{dM_h(t)}{dt} = F_{adv}(t, M_h(t)) + F_{mag}(t, M_h(t)), \tag{5.29}$$

with

$$F_{adv}(t, M) := -\nabla \cdot (uM),$$
$$F_{mag} := \gamma B \times M + DM - f.$$

The simplest sequential operator splitting on $t^n \leq t \leq t^{n+1}$ *gives*

$$\frac{dM_h^*(t)}{dt} = \quad F_{adv}(t, M_h^*(t)), \quad M_h^*(t) = M_h(t^n), \tag{5.30}$$
$$\frac{dM_h^{**}(t)}{dt} = \quad F_{mag}(t, M_h^{**}(t)), \quad M_h^{**}(t) = M_h^*(t^n). \tag{5.31}$$

An inspection of 5.30 shows for the splitting error at $t = t^n$

$$\epsilon_S = \frac{1}{2}\tau_n^2[\frac{\partial F_{adv}}{\partial M}F_{mag} - \frac{\partial F_{mag}}{\partial M}F_{adv}] + \mathcal{O}(\tau_n^3). \tag{5.32}$$

The commutation error $[F_{adv}, F_{mag}] = \frac{\partial F_{adv}}{\partial M}F_{mag} - \frac{\partial F_{mag}}{\partial M}F_{adv}$ *can be written as*

$$[F_{adv}, F_{mag}] = (\nabla \cdot u)[F_{mag}(t, M_h(t)) - \frac{\partial F_{mag}}{\partial t}(t, M_h)M_h(t)] + (u \cdot \nabla_r)F_{mag}(t, M_h).$$

Error vanished if either F_{mag} *is independent of* r *and* $div\, u = 0$ *or* F_{mag} *is independent of* r *and linear in* M_h *(this is not our case).*
See that it is possible to apply a symmetric or Strang-Marchuk splitting which reduces the splitting error to $\mathcal{O}(\tau_n^2)$.

Chapter 6

Introducing R.D.E.s into Bloch model.

The aim of this chapter and second part of this work is to introduce the uncertainty into the basic Bloch model and into the MRI process (equation 2.1). As we already know, Bloch model was created under physical processes, in special inside the magnetic and chemical spin-interactions. On one hand, we have seen longitudinal $\mathbf{T_1}$ and transverse $\mathbf{T_2}$ magnetization times (see section 2.2,) which have a strong relationship into Bloch equation due to the interactions between nuclei and the environment of molecules, thus these magnitudes have certain randomness due to the collision and interactions existing inside tissues. In fact, the existence of $T_2 - start$ ($\mathbf{T_2^*}$) (see 2.3) invites us to introduce an uncertainty into the relaxation process to $\mathbf{T_2}$.

On the other hand magnetic magnitudes such as $\vec{\mathbf{B}}_0, \vec{\mathbf{B}}_1, \vec{\mathbf{B}}_G, \vec{\mathbf{B}}'$ not only depend on a physical process but e.g. in the non-homogeneity constructions of: room, magnets, gradients or coils, thus they have associated an internal variability and it is possible to calculate mean and deviation in the manufacture processes, after commissioning or at the end of the equip assembly process.

Magnetization vector ($\vec{\mathbf{M}}$) and initial value problem (**IVP**) ($\vec{\mathbf{M}}_0$) is consequently produced by randomized magnitudes.

Bloch equations in relaxation and RF-process have been exposed and solved analytically in chapter 3 and chapter 4 respectively.

Therefore, we are able to transform Bloch equations into a system of ran-

dom differential equation (RDEs).

Bloch equation in the relaxation process:

$$\begin{aligned} M_x(t) = &\quad M_0 e^{(-\frac{t}{T_2})} \sin(\gamma B_0 t), && (6.1)\\ M_y(t) = &\quad M_0 e^{(-\frac{t}{T_2})} \cos(\gamma B_0 t), && (6.2)\\ M_{xy}(t) = &\quad M_0 e^{(-\frac{t}{T_2})}, && (6.3)\\ M_z(t) = &\quad \tau_0 (1 - e^{(-\frac{t}{T_1})}). && (6.4) \end{aligned}$$

Bloch equation in the RF process. Rotation frame:

$$\begin{aligned} m_y(t) = &\quad \tau_0 \sin(\gamma B_1 t), && (6.5)\\ m_z(t) = &\quad \tau_0 \cos(\gamma B_1 t). && (6.6) \end{aligned}$$

Bloch equation in the RF process. Laboratory frame:

$$\begin{aligned} M_x(t) = &\quad \tau_0 \sin(\gamma B_1 t) \sin(\gamma B_0 t), && (6.7)\\ M_y(t) = &\quad \tau_0 \sin(\gamma B_1 t) \cos(\gamma B_0 t), && (6.8)\\ M_{xy}(t) = &\quad \tau_0 \sin(\gamma B_1 t), && (6.9)\\ M_z(t) = &\quad \tau_0 \cos(\gamma B_1 t). && (6.10) \end{aligned}$$

From now on, the data M_0, $\tau_0 = M_0$, B_0, T_1, T_2 and B_1 are assumed to be continuous random variables (RVs) defined on common probability space $(\Omega, \mathcal{F}, \mathbb{P})$, whose domain are assumed to be:

$$\begin{aligned} D_{M_0} &= \{m_0 = M_0(\omega), \omega \in \Omega : m_{0,1} \leq m_0 \leq m_{0,2},\}, m_{0,1}, m_{0,2} \in \mathbb{R},\\ D_{B_0} &= \{b_0 = B_0(\omega), \omega \in \Omega : b_{0,1} \leq b_0 \leq b_{0,2},\}, b_{0,1}, b_{0,2} \in \mathbb{R},\\ D_{B_1} &= \{b_1 = B_1(\omega), \omega \in \Omega : b_{1,1} \leq b_1 \leq b_{1,2},\}, b_{1,1}, b_{1,2} \in \mathbb{R}, \qquad (6.11)\\ D_{T_1} &= \{t_1 = T_1(\omega), \omega \in \Omega : t_{1,1} \leq t_1 \leq t_{1,2},\}, t_{1,1}, t_{1,2} \in \mathbb{R}^+,\\ D_{T_2} &= \{t_2 = T_2(\omega), \omega \in \Omega : t_{2,1} \leq t_2 \leq t_{2,2},\}, t_{2,1}, t_{2,2} \in \mathbb{R}^+. \end{aligned}$$

Hereinafter, we will omit the ω sample dependence when written domains of

continuous RVs. As we have shown in section 2.1 interval of domains are,

$$\begin{aligned} -\infty < m_{0,1} < m_{0,2} &< \infty, \\ -\infty < b_{0,1} < b_{0,2} &< \infty, \\ -\infty < b_{1,1} < b_{1,2} &< \infty, \\ 0 < t_{1,1}, t_{1,2} &< \infty, \\ 0 < t_{2,1}, t_{2,2} &< \infty. \end{aligned}$$

Do not confuse m_0 RV with m_y, m_z magnetization values in the rotation time.

R.D.E. Notation:
We denote probabilistic density functions (PDFs) and random vectors as,

- $f_{M_0}(m_0)$, $f_{B_0}(b_0)$, $f_{B_1}(b_1)$, $f_{T_1}(t_1)$ and $f_{T_2}(t_2)$ the probabilistic density function PDFs of the continuous RVs M_0, B_0, B_1, T_1 and T_2, respectively.

- $f_{M_0,T_2}(m_0, t_2)$ and $f_{M_0,T_1}(m_0, t_1)$ will denote the joint PDFs of the random vectors (M_0, T_2) and (M_0, T_1), respectively. Domains of these two dimensional PDFs can be written directly as product of the sets $D_{M_0} \cdot D_{T_2}$ and $D_{M_0} \cdot D_{T_1}$, respectively.

- $f_{M_x}(m_x)$, $f_{M_y}(m_y)$, $f_{M_xy}(m_{xy})$, $f_{M_z}(m_z)$, the 1-PDF of the unknown solutions for Bloch equations (6.1)-(6.4) and (6.7)-(6.10) into the laboratory frame.

- $f_{m_y}(n_y)$, $f_{m_z}(n_z)$, the 1-PDF of the unknown solutions for Bloch equations (6.5) and (6.6) into the rotational frame.

In order to simplify graphical notation in Mathematica software in plots we will be denoted:

- $M_{xy(M_0)}$, as the 1-PDF of the stochastic process (SP) defined by $M_{xy}(t)$ with M_0 as a random variable (equation 6.3),

- $M_{y(T_2)}$, as the 1-PDF of the stochastic process (SP) defined by $M_y(t)$ with T_2 as a random variable (equation 6.2),

- $m_{z(\tau_0)}$ as the 1-PDF of the stochastic process (SP) defined by $m_z(t)$ with τ_0 as a random variable (equation 6.6),

- $M_{xy(M_0,T_2)}$, as the joint PDF of the stochastic process (SP) defined by $M_{xy}(t)$ with (M_0, T_2) as a random vector (equation 6.3),

- in general $SP_{X(RV_1)}$ will be denoted the 1-PDF of the stochastic, process $SP_X(t)$, with RV_1 as a random variable.
- in general $SP_{X(RV_1,RV_2)}$ will be denoted the 1-PDF of the stochastic process, $SP_X(t)$, with (RV_1, RV_2) as a random vector.

Note that obtaining the first probability density function (1-PDF) of the solutions (equations 6.1 to 6.10) is more desirable since, from it, we can compute the previous statistical functions as simple particular cases and it provides a comprehensive probabilistic characterization of the solution for each fixed time t^*.

To introduce and solve a system of differential equations in this work, we are going to use the Random Variable Transformation (**RVT**) technique. This method states as follows in its general form (see [19]). Thereafter we will calculate and plot all **1-pdf** random variables of Bloch equation and so on we will obtain means and variability through theirs variances.

Theorem 6. ***Multidimensional RVT method.***
Let us consider $X = (X_1, \ldots, X_m)$ and $Y = (Y_1, \ldots, Y_m)$ two m-dimensional absolutely continuous random vectors defined on a complete probability space $(\Omega; \mathcal{A}; \mathbb{P})$.
Let $\mathbf{r} : \mathbb{R}^m \to \mathbb{R}^m$ be a one-to-one deterministic transformation of $\mathbf{X}$ into $\mathbf{Y}$, i.e., $\mathbf{Y} = \mathbf{r}(\mathbf{X})$. Assume that $\mathbf{r}$ is continuous in $\mathbf{X}$ and has continuous partial derivatives with respect to X. Then, if $\mathbf{f_X}(\mathbf{x})$ denotes the joint probability density function of vector $\mathbf{X}$, and $\mathbf{s} = \mathbf{r}^{-1} = (s_1(y_1, \ldots, y_m), \ldots, s_m(y_1, \ldots, y_m))$ represents the inverse mapping of $\mathbf{r} = (r_1(x_1, \ldots, x_m), \ldots, r_m(x_1, \ldots, x_m))$, the joint probability density function of vector $\mathbf{Y}$ is given by

$$f_Y(y) = f_X(s(y))\,|J_m|\,, \quad D_Y = \{y : y_1 \leq y \leq y_2\}\,, \tag{6.12}$$

where $|J_m|$, which is assumed to be different from zero, denotes the absolute value of the Jacobian defined by the determinant

$$J_m = det \begin{pmatrix} \frac{\partial s_1(y_1,\ldots,y_m)}{\partial y_1} & \cdots & \frac{\partial s_m(y_1,\ldots,y_m)}{\partial y_1} \\ \vdots & \ddots & \vdots \\ \frac{\partial s_1(y_1,\ldots,y_m)}{\partial y_m} & \cdots & \frac{\partial s_m(y_1,\ldots,y_m)}{\partial y_m} \end{pmatrix}, \tag{6.13}$$

Therefore, RVT is a probability technique that allows us to calculate the PDF $f_Y(y)$ of a RV, Y, resulting after the transformation of another RV, say

X, whose PDF, $f_X(x)$ is known.

We consider several cases of study in this work. Relaxation equations (6.1), (6.2) are similar because of ω_0 variable represents the magnetic rotating vector around z-axe, thus we only solve for one of them. In the same way we operate with RF process equations (6.7) and (6.8).

C. Casabán, J.C. Cortés, J.-V. Romero, and M.-D. Roselló ([20]) established the first probability density function to the solution of several linear random initial value problems of ODE. Equations (6.3) and (6.4) of relaxation process can be solved using this result (see [20], Table 1: cases I.1, I.2 and I.3).

Theorem 7. ***RVT technique in the simplest scalar formulation.***
If X is a continuous RV lying on the domain or support $D_X = \{x : x_1 \leq x \leq x_2\}$, whose PDF is $f_X(x) > 0$ and $Y = r(X)$ being $r : D_X \subseteq \mathbb{R} \to \mathbb{R}$ a monotone mapping on D_X, then

$$f_Y(y) = f_X(s(y)) \left| \frac{\partial s(y)}{\partial y} \right|, \quad D_Y = y : y_1 \leq y \leq y_2, \tag{6.14}$$

where $s(y) = x$ is the inverse function of r on D_X, which is assumed to have a continuous derivative on D_y and $|\frac{ds(y)}{dy}|$ denotes the modulus of the derivative of $s(y)$. In the particular case that r increases (decreases) on D_X, the domain $D_Y of Y = r(X)$ is determined by $D_y = \{y : y_1 = r(x_1) \leq y \leq r(x_2) = y_2\} (D_y = \{y : y_1 = r(x_2) \leq y \leq r(x_1) = y_2\})$.

Theorem 8. ***RVT technique in the two-dimensional version.***
Let $X = (X_1, X_2)$ be a two-dimensional RV with joint PDF $f_{X_1,X,2}$.Let

$$\begin{aligned} y_1 &= r_1(x_1, x_2), \\ y_2 &= r_2(x_1, x_2), \end{aligned} \tag{6.15}$$

be a one-to-one deterministic map from $\mathbb{R}^2$ to $\mathbb{R}^2$; that is, there exists its inverse transformation:

$$\begin{aligned} x_1 &= s_1(y_1, y_2), \\ x_2 &= s_2(y_1, y_2), \end{aligned} \tag{6.16}$$

on the range of the previous map (6.15). Let one assume that both maps (r_1, r_2) and (s_1, s_2) are continuous. Let further assume that be following partial derivatives

$$\frac{\partial x_1}{\partial y_1}, \quad \frac{\partial x_1}{\partial y_2}, \quad \frac{\partial x_2}{\partial y_1}, \quad \frac{\partial x_2}{\partial y_2}, \tag{6.17}$$

exist and are continuous and the Jacobian J_2 of the inverse map satisfies

$$J_2 = det \begin{pmatrix} \frac{\partial x_1}{\partial y_1} & \frac{\partial x_2)}{\partial y_1} \\ \frac{\partial x_2}{\partial y_1} & \frac{\partial x_2)}{\partial y_2} \end{pmatrix} \neq 0, \tag{6.18}$$

on the range of the transformation 6.15. Then, the joint PDF $f_{Y_1,Y_2}(y_1, y_2)$ of the two-dimensional RV, $Y = (Y_1, Y_2) = (r_1(X_1, X_2), r_2(X_1, X_2))$ is given by

$$f_{Y_1,Y_2}(y_1, y_2) = f_{X_1,X_2}(s_1(y_1, y_2), s_2(y_1, y_2))|J_2|. \tag{6.19}$$

If we applied Theorem 8 in the particular case that transformation r_1 only depends on variable x_1 and r_2 only depends on variable x_2. As it will be seen latter, this result can be applied to someone of Bloch equations (6.1)-(6.4).

Proposition 4. ***RVT technique in the two-dimensional version. Single dependence.***
Let $X = (X_1, X_2)$ be a two-dimensional RV with joint PDF f_{X_1,X_2}. Let

$$\begin{aligned} y_1 &= r_1(x_1), \\ y_2 &= r_2(x_2), \end{aligned} \tag{6.20}$$

be a one-to-one deterministic map from $\mathbb{R}^2$ to $\mathbb{R}^2$; that is, there exists its inverse transformation:

$$\begin{aligned} x_1 &= s_1(y_1), \\ x_2 &= s_2(y_2), \end{aligned} \tag{6.21}$$

on the range of the previous map (6.20). Let one assume that both maps (r_1, r_2) and (s_1, s_2) are continuous and satisfy

$$\frac{\partial x_1}{\partial y_1} \cdot \frac{\partial x_2}{\partial y_2} \neq 0, \tag{6.22}$$

on the range of the map (6.20) and (6.21). Then the joint PDF $f_{Y_1,Y_2}(y_1, y_2)$ of the two-dimensional RV, $Y = (Y_1, Y_2) = (r_1(X_1), r_2(X_2))$ is given by

$$f_{Y_1,Y_2}(y_1, y_2) = f_{X_1,X_2}(s_1(y_1), s_2(y_2)) \left| \frac{\partial x_1}{\partial y_1} \cdot \frac{\partial x_2}{\partial y_2} \right|. \tag{6.23}$$

Proposition 5. ***RVT technique: product of two-continuous RVs.***
Let (X_1, X_2) be a continuous random vector with joint PDF $f_{X_1,X_2}(x_1, x_2)$

with respective domains $D_{X_1} = \{x_1 \neq 0 : x_{1,1} \leq x_1 \leq x_{1,2}\}$ *and* $D_{X_2} = \{x_2 : x_{2,1} \leq x_2 \leq x_{2,2}\}$. *Then the PDF* $f_{Y_1}(y_1)$ *of their product* $Y_1 = X_1 X_2$ *is given by*

$$f_{Y_1}(y_1) = \int_{x_{1,1}}^{x_{1,2}} f_{X_1,X_2}\left(x_1, \frac{y_1}{x_1}\right) \frac{1}{|x_1|} dx_1. \tag{6.24}$$

Equivalently, if $D_{X_1} = \{x_1 : x_{1,1} \leq x_1 \leq x_{1,2}\}$ *and* $D_{X_2} = \{x_2 \neq 0 : x_{2,1} \leq x_2 \leq x_{2,2}\}$ *then*

$$f_{Y_1}(y_1) = \int_{x_{2,1}}^{x_{2,2}} f_{X_1,X_2}\left(\frac{y_1}{x_2}, x_2\right) \frac{1}{|x_2|} dx_2. \tag{6.25}$$

If X_1 *and* X_2 *are independent continuous RVs with PDF's* $f_{X_1}(x_1)$ *and* $f_{x_2}(x_2)$, *respectively, then (6.24) and (6.25) become*

$$f_{Y_1}(y_1) = \int_{x_{1,1}}^{x_{1,2}} f_{X_1}(x_1) f_{X_2}\left(\frac{y_1}{x_1}\right) \frac{1}{|x_1|} dx_1, \tag{6.26}$$

$$f_{Y_1}(y_1) = \int_{x_{1,1}}^{x_{1,2}} f_{X_1}\left(\frac{y_1}{x_2}\right) f_{X_2}(x_2) \frac{1}{|x_2|} dx_2. \tag{6.27}$$

Once we have calculated the 1-PDF of the solutions through a random variable or a random vector, we are be able to characterize them by means, variance and moments of higher order with respect to the origin.

Definition 15. *Expectation, variance and moment of order n with respect to the origin of a RV, respectively.*

$$\mu_X = \mathbb{E}[X] = \int_{D_X} x f_X(x) dx, \tag{6.28}$$

$$\sigma_X^2 = \mathbb{V}[X] = \mathbb{E}[(X - \mu_X)^2] = \int_{D_X} (x - \mu_X)^2 f_X(x) dx, \tag{6.29}$$

$$\alpha_n = E[X^n] = \int_{D_X} x^n f_X(x) dx. \tag{6.30}$$

$\mathbb{E}[X]$, $\mathbb{E}[X^n]$ and $\mathbb{V}[X]$ have been calculated and plotted in chapter 7 and chapter 8 for each Bloch equation solutions (6.1) to (6.10) with Mathematica software. In this way, the so-called König theorem $\mathbb{V}[X] = \mathbb{E}[X^2] - \mathbb{E}[X]^2$, has been applied to calculate $\mathbb{V}[X]$.

Chapter 7

R.D.E.S. into relaxation process.

This chapter shows the 1-PDF formulation for each equation involved in the relaxation process. After that we show the results graphically the plots generated via Mathematica software. For some RVs it was necessary a numerical integration to calculate the expectation and the variance. '*NIntegrate*' function with a high '*MinRecursion*' value option was applied and several specific exclusions domains was required to avoid errors. As well it was required to reduce the '*PlotPoints*' value below 30 units in some RVs. '*Method*' option was set in automatic state.

7.1 M_0 r.v. initial condition.

Thus, we will assume $\mathbf{M_0}$ be a random variable and the system of Ordinary Differential Equation (**O.D.E.**) (equation 4.1), becomes a system of Random Ordinary Differential Equation (**R.O.D.E.**).

Let assume $\mathbf{M_0} \sim N[\mu_0, \sigma_{M_0}]$, (see chapter 6), therefore the probability density function of M_0 RV, is defined as:

$$f_{M_0}(m_0) = \frac{1}{\sqrt{2\pi\sigma_{M_0}^2}} e^{-\frac{1}{2}\left(\frac{m_0 - \mu_{M_0}}{\sigma_{M_0}}\right)^2}.$$

In order to show and present the results achieved we will consider $\mu_{M_0} = M_0$

as the deterministic value proposed in the initial value problem (IVP) and σ_{M_0} value as a dispersion of the mean μ_{M_0} value, thus $\sigma_{M_0} = 0.1\mu_{M_0}$.

7.1.1 Calculating the 1-PDF $M_x(m_x)$.

We can calculate the $M_x(m_x)$ 1-PDF using Theorem 7, with $X = M_0$, $Y = M_x$, $r(x) = M_x$, $s(y) = m_0 = \dfrac{m_x e^{\tau_2 t}}{\sin(\gamma B_0 t)}$,

$$f_{M_x(m_x)} = f_{M_0}(s(m_x)) \left| \frac{\partial m_0}{\partial m_x} \right|.$$

$$\begin{aligned}
f_{M_x(m_x)} &= \frac{1}{\sqrt{2\pi\sigma_{M_0}^2}} e^{-\frac{1}{2}\left(\frac{\frac{m_x e^{t\tau_2}}{\sin(\gamma B_0 t)} - \mu_{M_0}}{\sigma_{M_0}} \right)^2} \left| \frac{e^{t\tau_2}}{\sin(\gamma B_0 t)} \right|, && (7.1)\\
\mathbb{E}[M_x] &= \int_{D_{M_x}} m_x f_{M_x}(m_x) dm_x, && (7.2)\\
\mathbb{V}[M_x] &= \int_{D_{M_x}} (m_x - \mu_{M_x})^2 f_{M_x}(m_x) dm_x. && (7.3)
\end{aligned}$$

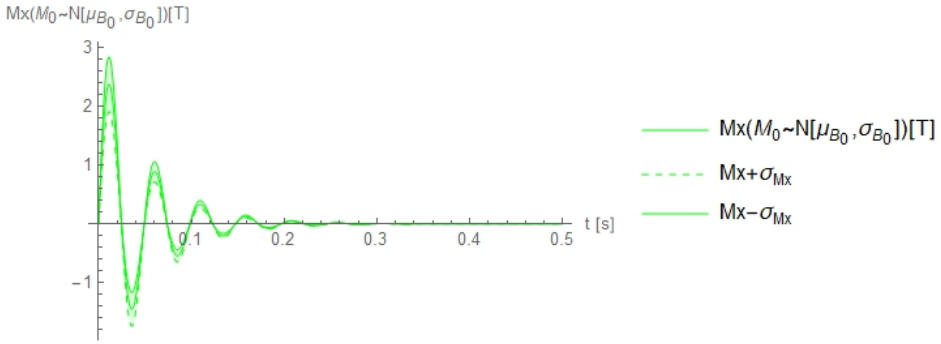

(a) 1-PDF $M_x(m_x, t)$ with M_0 RV Muscle.

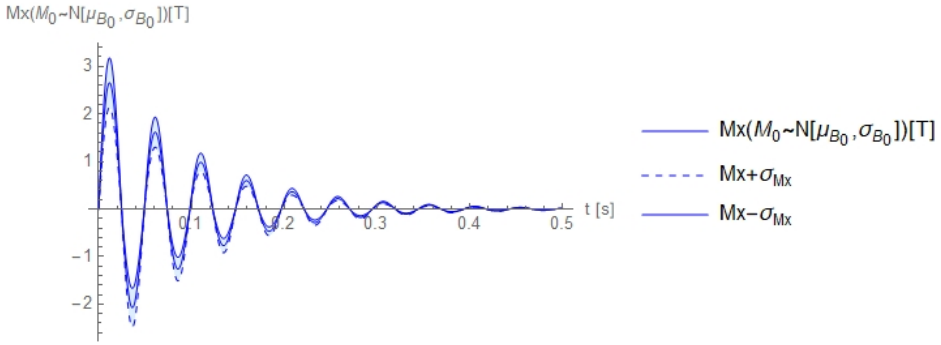

(b) 1-PDF $M_x(m_x, t)$ with M_0 RV Gray matter.

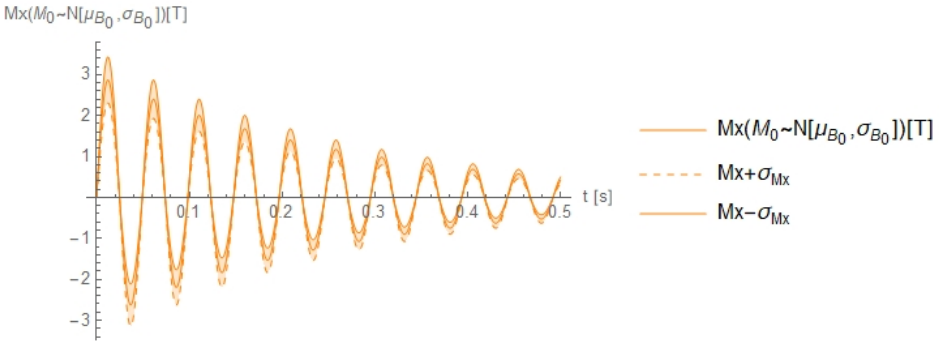

(c) 1-PDF $M_x(m_x, t)$ with M_0 RV Blood.

Figure 7.1: 1-PDF $M_x(m_x)$ with M_0 RV Relaxation process.

7.1.2 Calculating the 1-PDF $M_y(m_y)$.

We can calculate the $M_y(m_y)$ 1-PDF using Theorem 7, with $X = M_0$, $Y = M_y$, $r(x) = M_y$, $s(y) = m_0 = \dfrac{m_y e^{\tau_2 t}}{\cos(\gamma B_0 t)}$, $\quad f_{M_y(m_y)} = f_{M_0}(s(m_y)) \left| \dfrac{\partial m_0}{\partial m_y} \right|$.

$$
\begin{aligned}
f_{M_y(m_y)} &= \frac{1}{\sqrt{2\pi\sigma_{M_0}^2}} e^{-\frac{1}{2}\left(\frac{\frac{m_y e^{t\tau_2}}{\cos(\gamma B_0 t)} - \mu_{M_0}}{\sigma_{M_0}} \right)^2} \left| \frac{e^{t\tau_2}}{\cos(\gamma B_0 t)} \right|, && (7.4)\\
\mathbb{E}[M_y] &= \int_{D_{M_y}} m_y f_{M_y}(m_y) dm_y, && (7.5)\\
\mathbb{V}[M_y] &= \int_{D_{M_y}} (m_y - \mu_{M_y})^2 f_{M_y}(m_y) dm_y. && (7.6)
\end{aligned}
$$

Note that $f_{M_y(m_y)}$ are graphically equivalent to $f_{M_x(m_x)}$ with a $\frac{\pi}{2}$ phase difference.

7.1.3 Calculating the 1-PDF $M_{xy}(m_{xy})$.

We can calculate the $M_{xy}(m_{xy})$ 1-PDF using Theorem 7, with $X = M_0$, $Y = M_{xy}$, $r(x) = M_{xy}$, $s(y) = m_0 = m_{xy} e^{\tau_2 t}$

$$
f_{M_{xy}(m_{xy})} = f_{M_0}(m_0 = s(m_{xy})) \left| \frac{\partial(m_0)}{\partial m_{xy}} \right|.
$$

$$
\begin{aligned}
f_{M_{XY}(m_{xy})} &= \frac{1}{\sqrt{2\pi\sigma_{M_0}^2}} e^{-\frac{1}{2}\left(\frac{m_{xy} e^{t\tau_2} - \mu_{M_0}}{\sigma_{M_0}} \right)^2} \left| e^{t\tau_2} \right|, && (7.7)\\
\mathbb{E}[M_{xy}] &= \int_{D_{M_{xy}}} m_{xy} f_{M_{xy}}(m_{xy}) dm_{xy}, && (7.8)\\
\mathbb{V}[M_{xy}] &= \int_{D_{M_{xy}}} (m_{xy} - \mu_{M_{xy}})^2 f_{M_{xy}}(m_{xy}) dm_{xy}. && (7.9)
\end{aligned}
$$

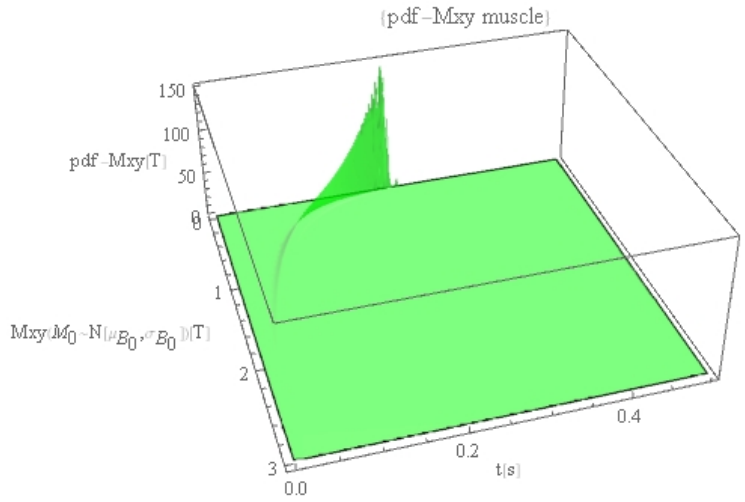

(a) 1-PDF $M_{xy}(m_{xy}, t)$ with M_0 RV Muscle.

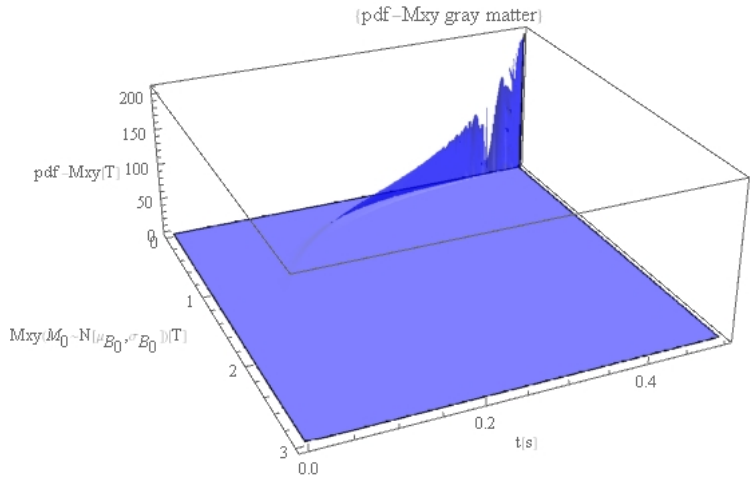

(b) 1-PDF $M_{xy}(m_{xy}, t)$ with M_0 RV Gray matter.

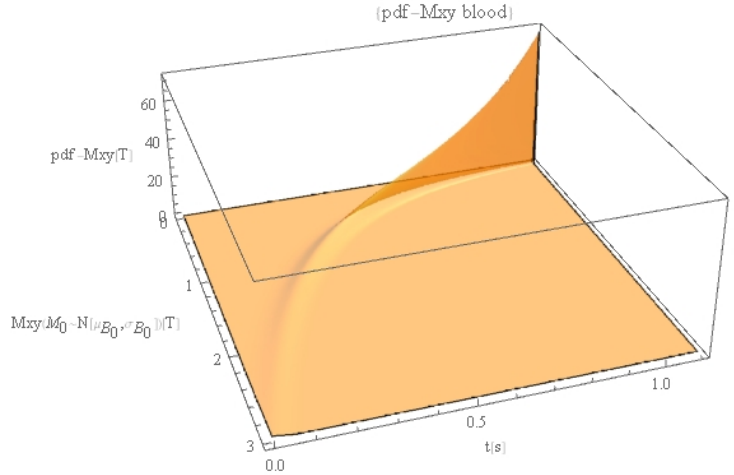

(c) 1-PDF $M_{xy}(m_{xy}, t)$ with M_0 RV Blood.

Figure 7.2: 1-PDF of M_{xy} transversal magnetization into the relaxation process for several tissues.

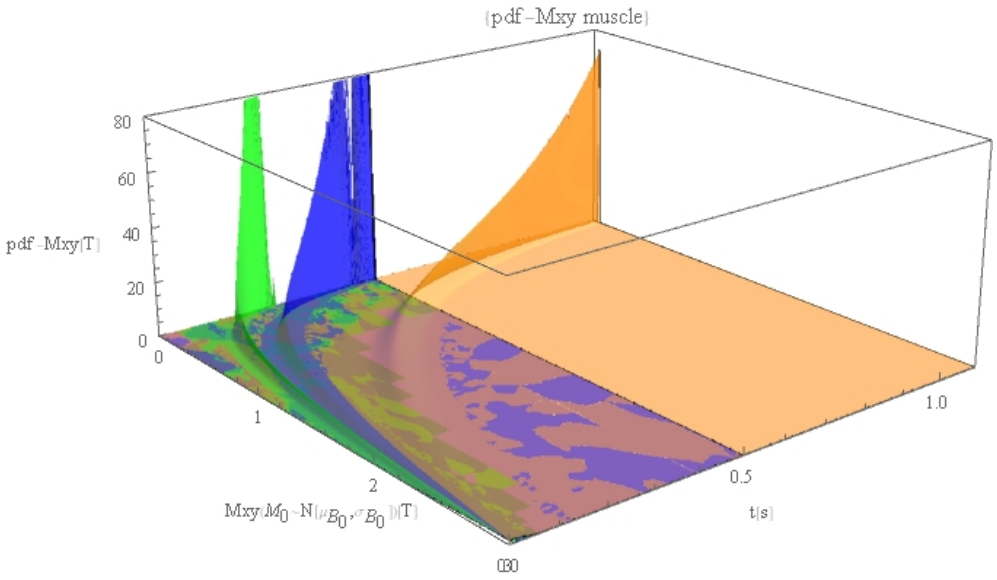

Figure 7.3: 1-PDF $M_{xy}(m_{xy}, t)$ transversal magnetization into the relaxation process for muscle, gray matter and blood.

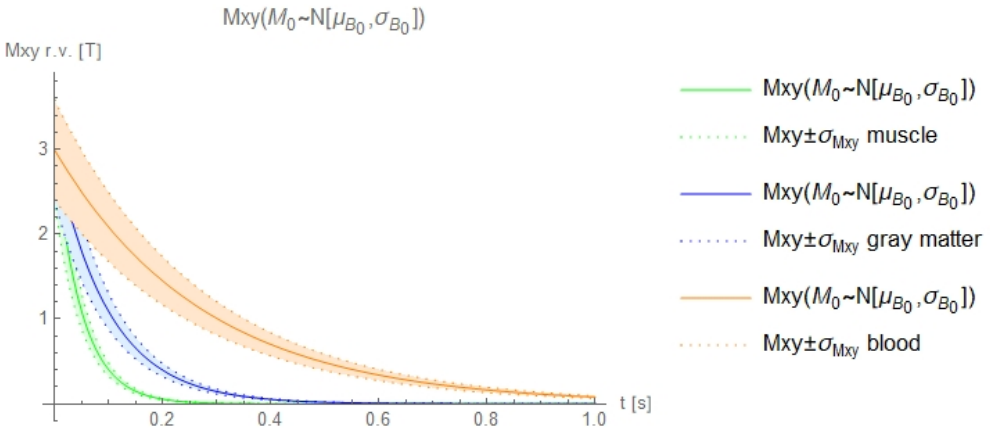

Figure 7.4: $M_{xy}(m_{xy})$ RV mean and variance.

7.1.4 Calculating the 1-PDF $M_z(m_z)$.

We can calculate the $M_z(m_z)$ 1-PDF using Theorem 7, with $X = M_0$, $Y = M_z$, $r(x) = M_z$, $s(y) = m_0 = \dfrac{m_z}{1 - e^{-\tau_1 t}}$,

$$f_{M_z(m_z)} = f_{M_0}(m_0 = s(m_z)) \left| \frac{\partial(m_0)}{\partial m_{xy}} \right|.$$

$$\begin{aligned} f_{M_z(m_z)} &= \frac{1}{\sqrt{2\pi\sigma_{M_0}^2}} e^{-\frac{1}{2}\left(\frac{\frac{m_z}{(1-e^{-\tau_1 t})} - \mu_{M_0}}{\sigma_{M_0}} \right)^2} \left| \frac{1}{1 - e^{-\tau_1 t}} \right|, && (7.10) \\ \mathbb{E}[M_z] &= \int_{D_{M_z}} m_z f_{M_z}(m_z) dm_z, && (7.11) \\ \mathbb{V}[M_z] &= \int_{D_{M_z}} (m_z - \mu_{M_z})^2 f_{M_z}(m_z) dm_z. && (7.12) \end{aligned}$$

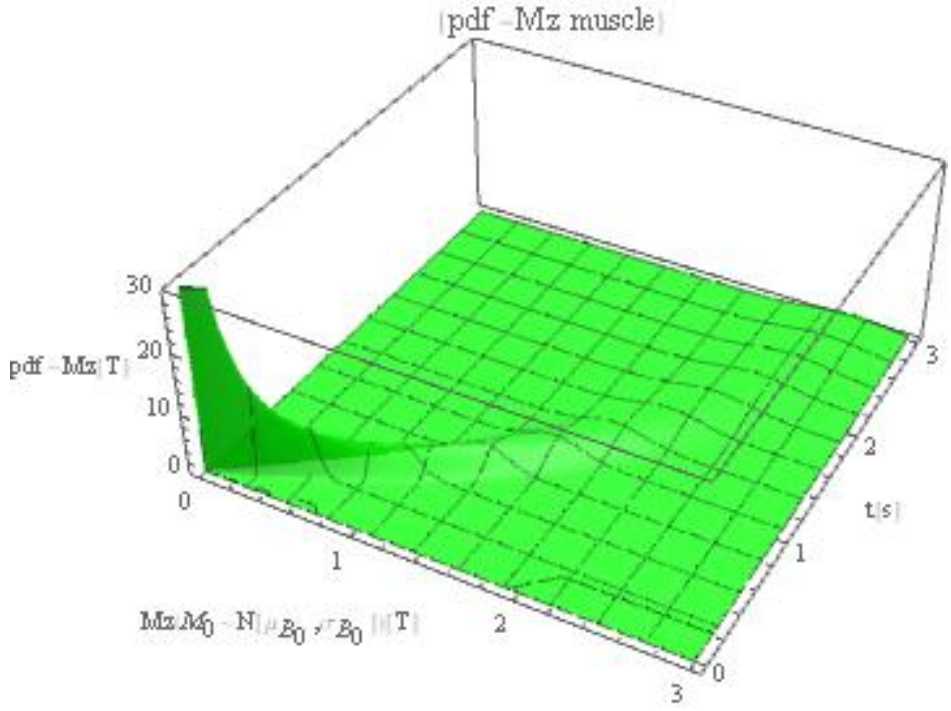

(a) 1-PDF $M_z(m_z, t)$ muscle.

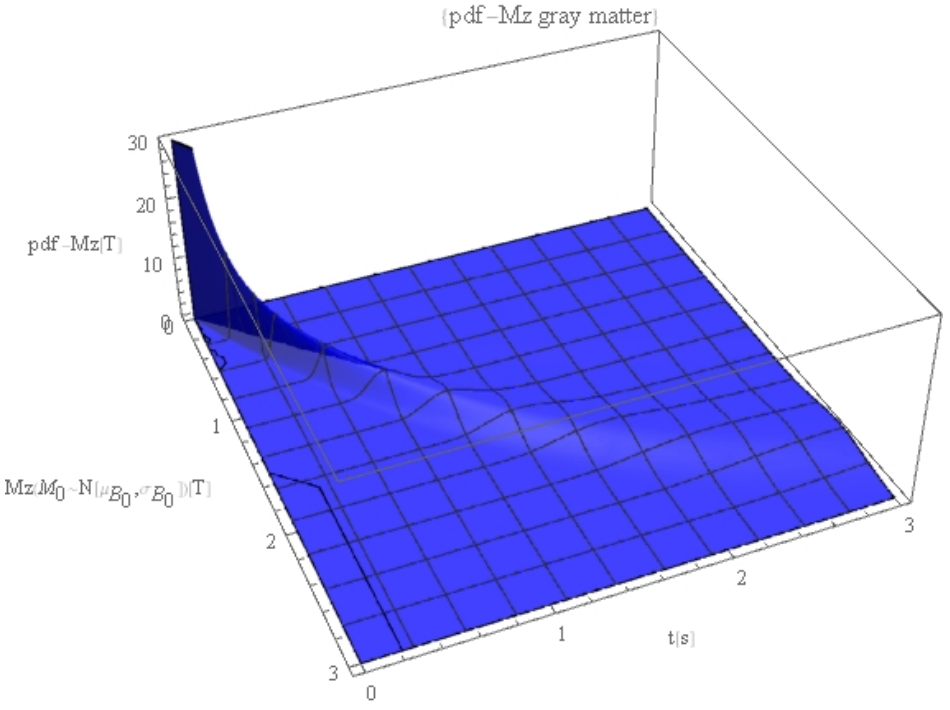

(b) 1-PDF $M_z(m_z, t)$ gray matter.

Figure 7.5: 1-PDF $M_z(m_z, t)$ into the relaxation process.

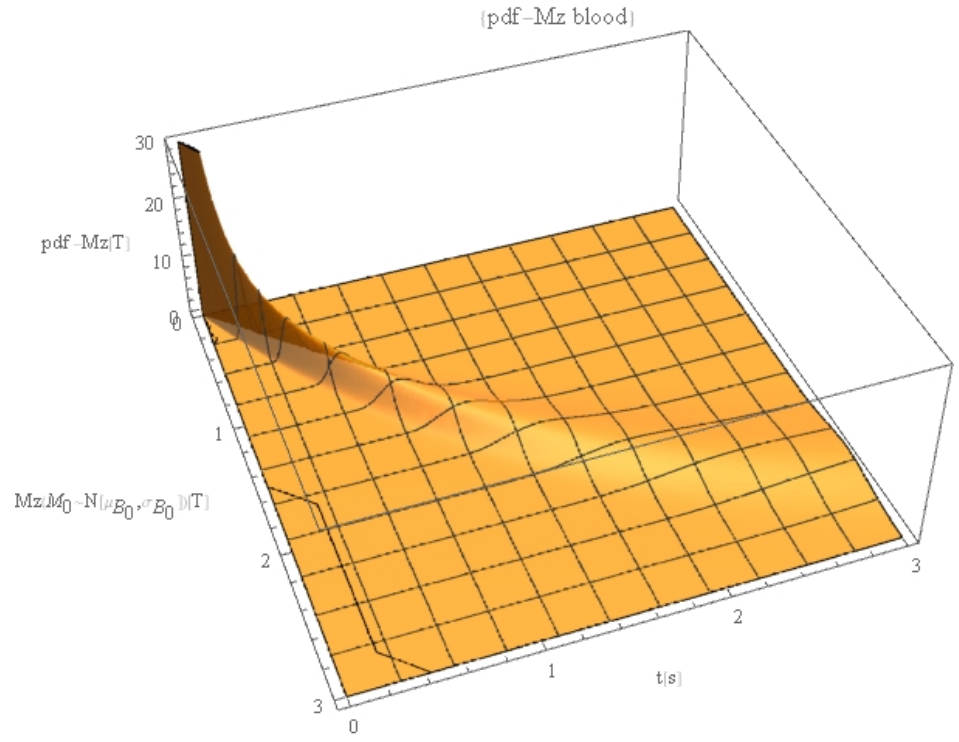

(a) 1-PDF $M_z(m_z, t)$ of blood.

Figure 7.6: 1-PDF for $M_z(m_z, t)$ into the relaxation process.

And we can calculate the mean and the variance. The results are shown in Figure 7.7.

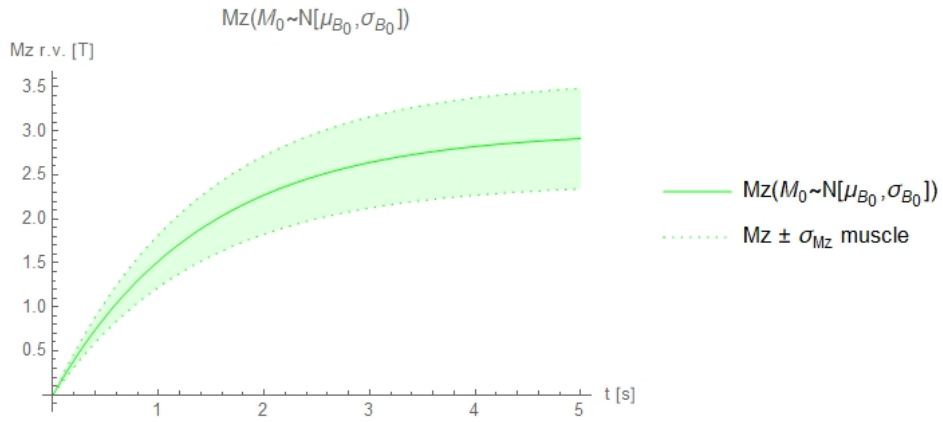

(a) $\mathbb{E}[M_z(m_z)]$ $\pm 1.96\sigma_{M_z}$, muscle.

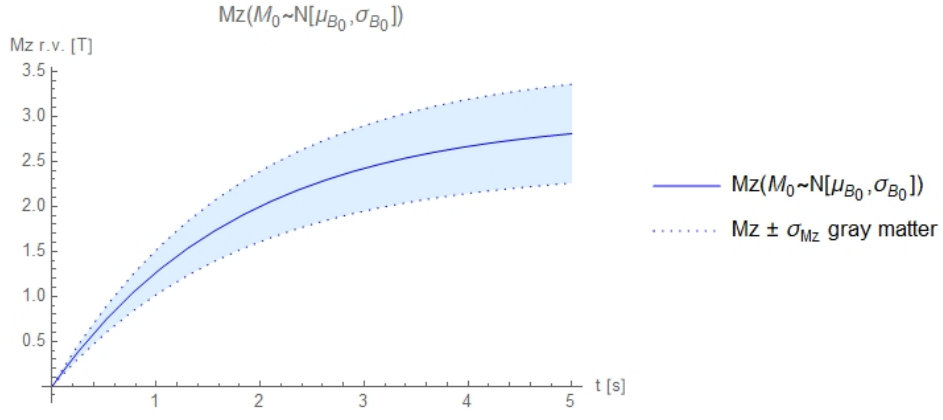

(b) $\mathbb{E}[M_z(m_z)]$ $\pm 1.96\sigma_{M_z}$, gray matter.

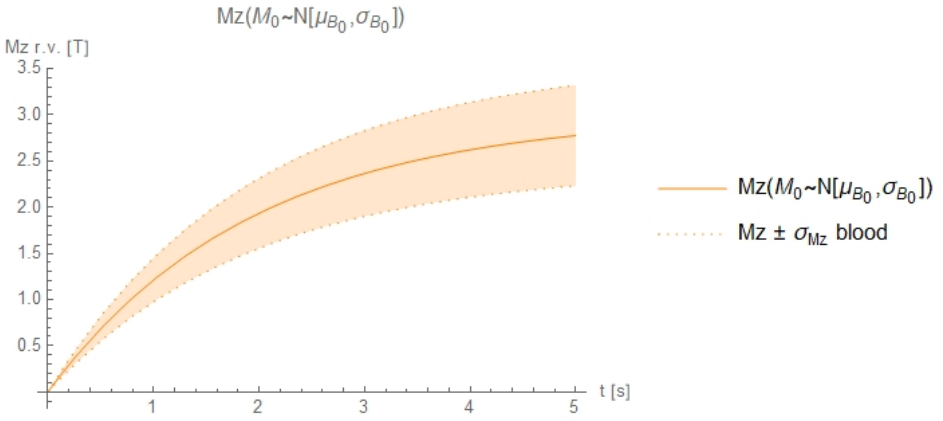

(c) $\mathbb{E}[M_z(m_z)]$ $\pm 1.96\sigma_{M_z}$, blood.

Figure 7.7: Mean and variance of $M_z(m_z, t)$ for different tissues.

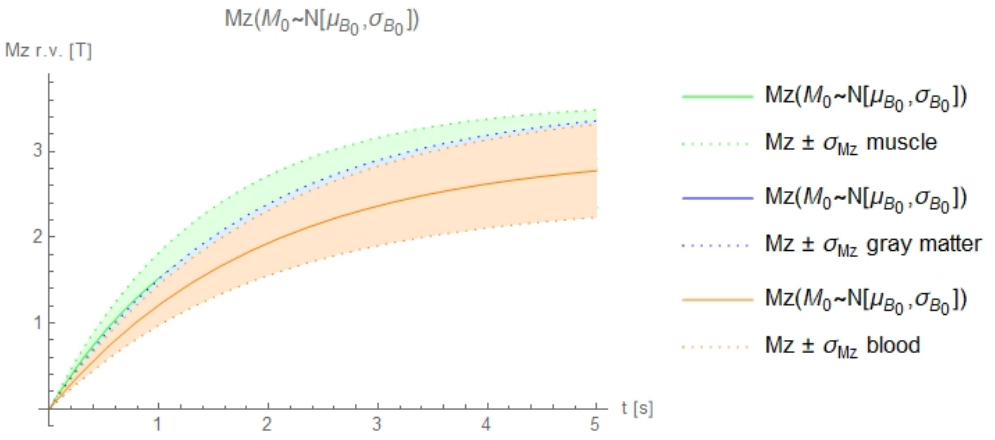

Figure 7.8: Mean and variance of $M_z(m_z, t)$ for all tissues.

7.1.5 $1 - PDF M_{xy}(m_{xy})$ and $M_z(m_z)$.

Figure 7.9 shows the 1-PDF of the transversal and longitudinal magnetization vector $\vec{M}$ altogether, into the relaxation process for different tissues.

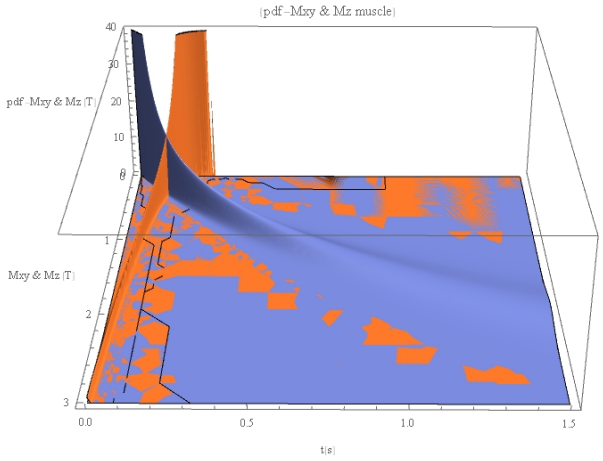

(a) 1-PDF $M_z(m_z, t)$ and 1-PDF $M_{xy}(m_{xy}, t)$ muscle.

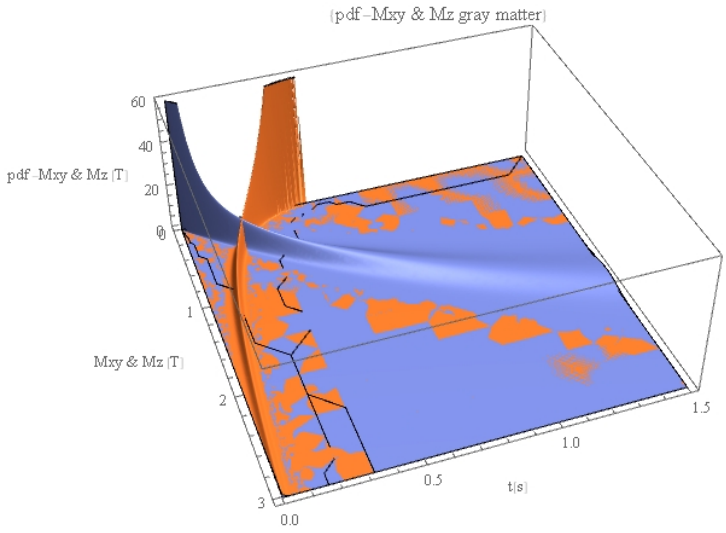

(b) 1-PDF $M_z(m_z, t)$ and 1-PDF $M_{xy}(m_{xy}, t)$ gray matter.

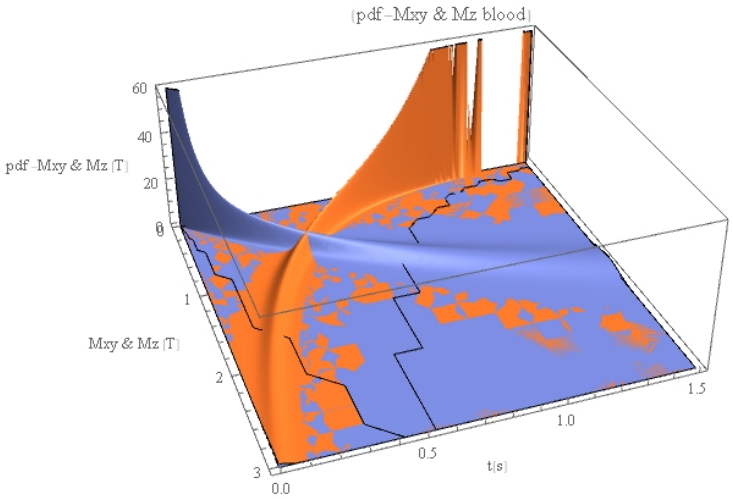

(c) 1-PDF $M_z(m_z, t)$ and 1-PDF $M_{xy}(m_{xy}, t)$ blood.

Figure 7.9: 1-PDF $M_{xy}(m_{xy}, t)$ and $M_z(m_z, t)$ into the relaxation process.

7.2 B_0 r.v. magnetic flux density.

As in section 7.1 we will assume $\mathbf{M}_0$ be a random variable and the system of Ordinary Differential Equation (**O.D.E.**) (equation 4.1), becomes a system of Random Ordinary Differential Equation (**R.O.D.E.**).

Let assume $\mathbf{B}_0 \sim N[\mu_{B_0}, \sigma_{B_0}]$, (see chapter 6), therefore the probability density function of B_0 RV, is defined as:

$$f_{B_0}(b_0) = \frac{1}{\sqrt{2\pi\sigma_{B_0}^2}} e^{-\frac{1}{2}\left(\frac{b_0 - \mu_{B_0}}{\sigma_{B_0}}\right)^2},$$

In order to show and present the results achieved we will consider $\mu_{B_0} = B_0$ as the deterministic value proposed in the initial value problem (IVP) and σ_{B_0} value as a dispersion of the mean μ_{M_0} value, thus $\sigma_{B_0} = 0.1\mu_{B_0}$.

7.2.1 Calculating the 1-PDF $M_x(m_x)$.

We can calculate the $M_x(m_x)$ 1-PDF using Theorem 7, with $X = B_0$, $Y = M_x$, $r(x) = M_x$, $s(y) = b_0 = \dfrac{\arcsin(\frac{m_x}{M_0}e^{\tau_2 t})}{\gamma t}$,

$$f_{M_x(m_x)} = f_{B_0}(s(m_x)) \left| \frac{\partial b_0}{\partial m_x} \right|.$$

$$\begin{aligned}
f_{M_x}(m_x) &= \frac{1}{\sqrt{2\pi\sigma_{B_0}^2}} e^{-\frac{1}{2}\left(\frac{\frac{1}{\gamma t}\arcsin\left(\frac{m_x}{M_0}e^{t\tau_2}\right) - \mu_{B_0}}{\sigma_{B_0}}\right)^2} \left| \frac{e^{t\tau_2}}{\gamma t M_0 \sqrt{1 - \left(\frac{m_x}{M_0}e^{t\tau_2}\right)^2}} \right|, \\
\mathbb{E}[M_x] &= \int_{D_{M_x}} m_x f_{M_x}(m_x) dm_x, \qquad (7.13) \\
\mathbb{V}[M_x] &= \int_{D_{M_x}} (m_x - \mu_{M_x})^2 f_{M_x}(m_x) dm_x.
\end{aligned}$$

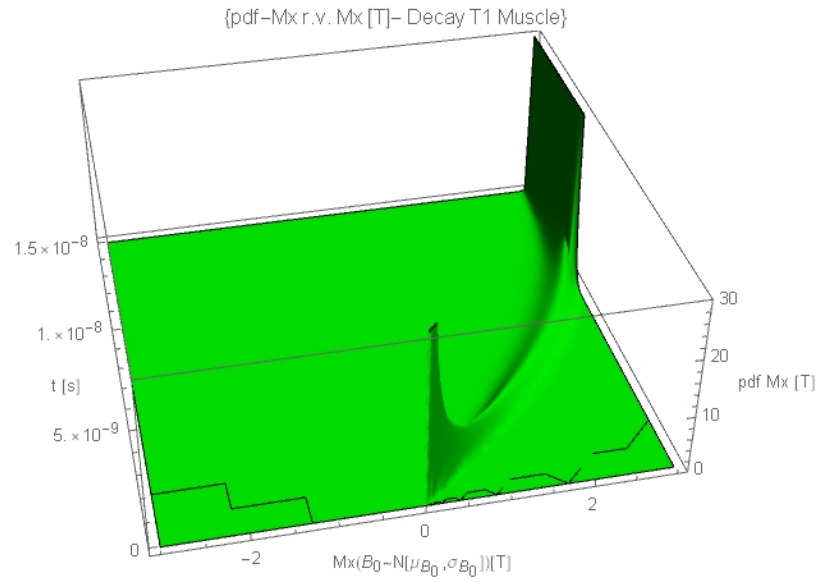

Figure 7.10: 1-PDF $M_x(m_x, t)$ muscle, during the first cycle.

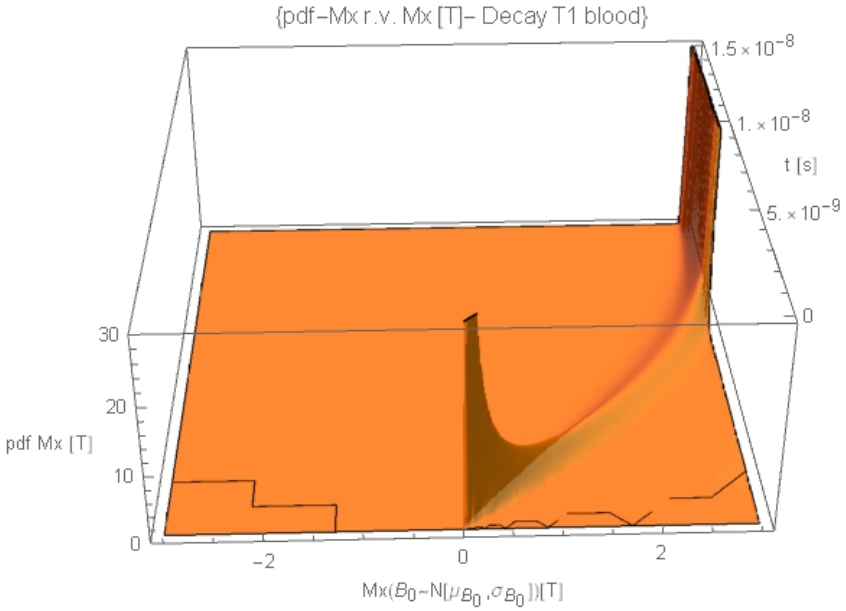

Figure 7.11: 1-PDF $M_x(m_x, t)$ blood, during the first cycle.

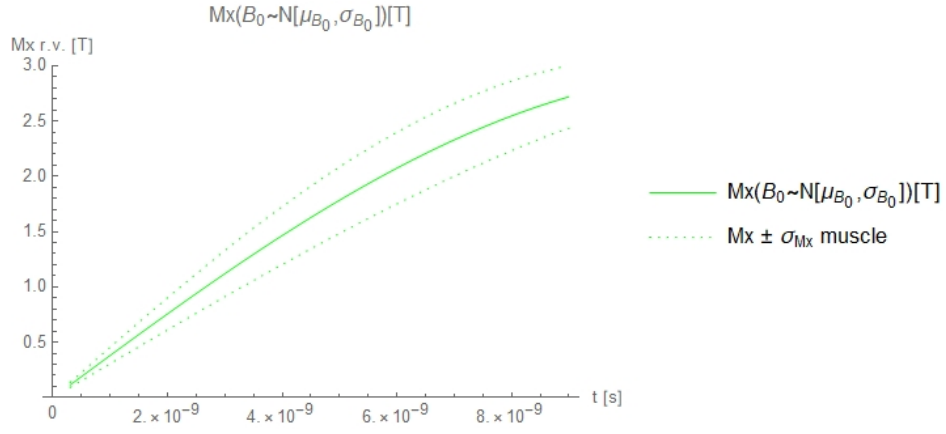

(a) $\mathbb{E}[M_x] \pm 1.96\sigma_{M_x}$ muscle.

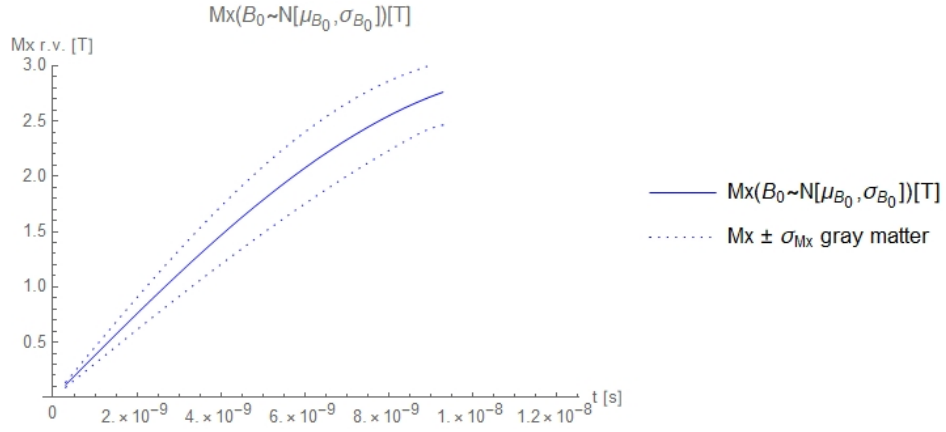

(b) $\mathbb{E}[M_x] \pm 1.96\sigma_{M_x}$ gray matter.

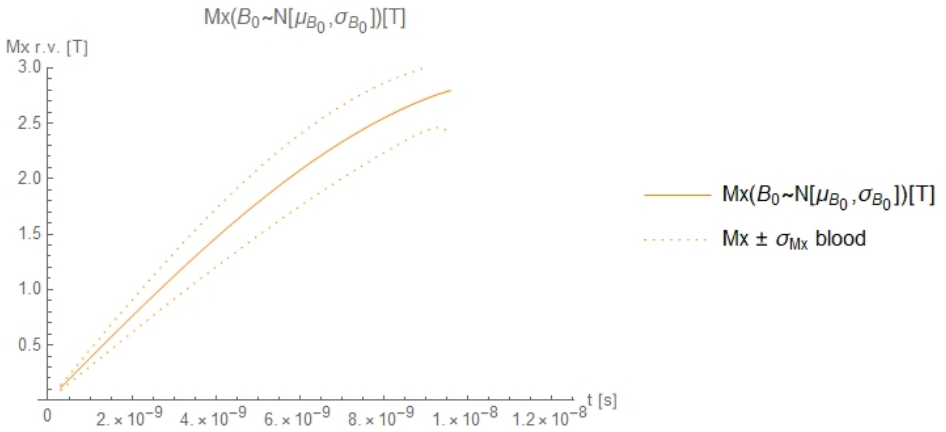

(c) $\mathbb{E}[M_{x(B_0)}(t)] \pm 1.96\sigma_{M_{x(B_0)}(t)}$ blood.

Figure 7.12: 1-PDF $M_x(m_x, t)$ in the relaxation process.

7.2.2 Calculating the $M_y(m_y)(t)$ RV

We can calculate the $M_y(m_y)$ 1-PDF using Theorem 7, with $X = B_0$, $Y = M_y$, $r(x) = M_y$, $s(y) = b_0 = \dfrac{\arccos(\frac{m_y}{M_0}e^{\tau_2 t})}{\gamma t}$,

$$f_{M_y}(m_y) = f_{B_0}(s(m_y)) \left| \frac{\partial b_0}{\partial m_y} \right|.$$

$$\begin{aligned}
\mathbf{f_{M_y}} &= \frac{1}{\sqrt{2\pi\sigma_{B_0}}} e^{-\frac{1}{2}\left(\frac{\frac{1}{\gamma t}\arccos\left(\frac{m_y}{M_0}e^{t\tau_2}\right) - \mu_{B_0}}{\sigma_{B_0}} \right)^2} \left| \frac{-e^{t\tau_2}}{\gamma t M_0 \sqrt{1 - \left(\frac{m_y}{M_0}e^{t\tau_2}\right)^2}} \right|, \\
\mathbb{E}[M_y] &= \int_{D_{M_y}} m_x f_{M_y}(m_y) dm_y, \qquad (7.14) \\
\mathbb{V}[M_y] &= \int_{D_{M_y}} (m_y - \mu_{M_y})^2 f_{M_y}(m_y) dm_y.
\end{aligned}$$

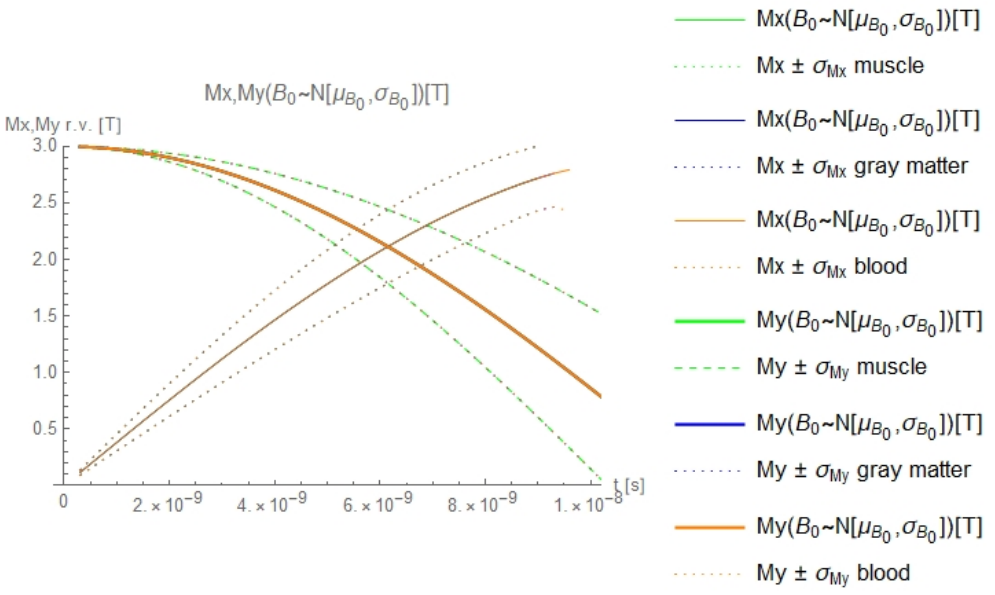

Figure 7.13: $\mathbb{E}[M_x(m_x,t)] \pm 1.96\sigma_{M_x}$,$\mathbb{E}[M_y(m_y,t)] \pm 1.96\sigma_{M_y}$ in the relaxation process.

7.3 T_1 and T_2 r.v. times.

Thus, we will assume $\mathbf{M_0}$ be a random variable and the system of Ordinary Differential Equation (**O.D.E.**) (4.1), becomes a systema of Random Ordinary Differential Equation (**R.O.D.E.**).
Let assume $\mathbf{T_2} \sim U[T_2 - \epsilon_2, T_2 + \epsilon_2]$, (see chapter 6), therefore the probability density function of M_xy RV, is defined as:

$$\mathbf{f_{T_2}} = \frac{1}{2\epsilon_2},$$

and let assume $\mathbf{T_1} \sim U[T_1 - \epsilon_1, T_1 + \epsilon_1]$, (see chapter 6), therefore the probability density function of M_xy RV, is defined as:

$$\mathbf{f_{T_1}} = \frac{1}{2\epsilon_1}.$$

Thus, we will assume $\mathbf{T_1}$ and $\mathbf{T_2}$ be random variables and the system of Ordinary Differential Equation (**O.D.E.**) (4.1), becomes a system of Random

Ordinary Differential Equation (**R.O.D.E.**) and we are able to consider $\mathbf{T}_1 \sim U[T_1 - \epsilon_1, T_1 + \epsilon_1]$ RV in the analytical solution of Bloch equation.

7.3.1 Calculating the 1-PDF $M_{xy}(m_{xy})$.

Let assume $\mathbf{T}_2 \sim U[T_2 - \epsilon_2, T_2 + \epsilon_2]$, therefore its PDF is defined as:

$$f_{T_2} = \frac{1}{2\epsilon_2},$$

where ϵ_2 is and experimental value obtained for different B_0 magnet values and can be shown in Table 2.2. And we can calculate the 1-PDF as

$$\begin{aligned} f_{M_{xy}(m_{xy})} &= \frac{1}{2\epsilon_2}\left|\frac{t}{m_{xy}\log^2\frac{m_{xy}}{M_0}}\right|, \\ \mathbb{E}[M_{xy}] &= \int_{D_{M_{xy}}} m_{xy} f_{M_{xy}}(m_{xy}) dm_{xy}, \\ \mathbb{V}[M_{xy}] &= \int_{D_{M_{xy}}} (m_{xy} - \mu_{M_{xy}})^2 f_{M_{xy}}(m_{xy}) dm_y. \end{aligned} \tag{7.15}$$

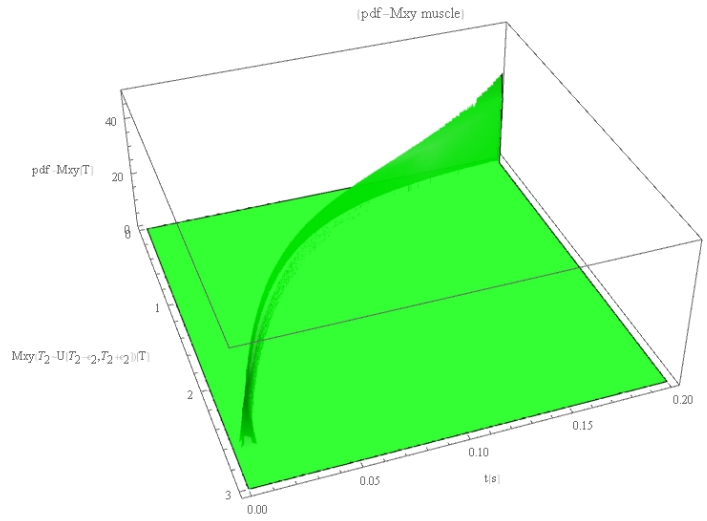

(a) 1-PDF for $M_{xy}(m_{xy})$ muscle.

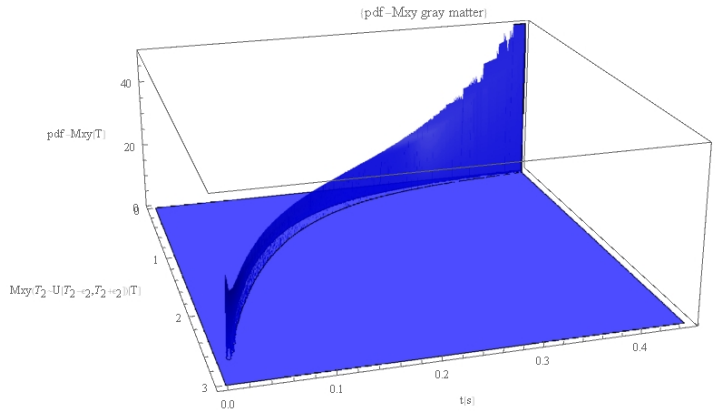

(b) 1-PDF for $M_{xy}(m_{xy})$ gray matter.

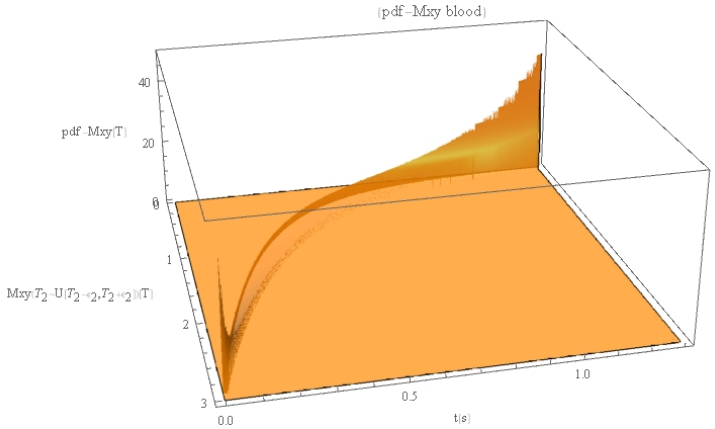

(c) 1-PDF for $M_{xy}(m_{xy})$ blood.

Figure 7.14: 1-PDF $M_{xy}(m_{xy}, t)$ into the relaxation process.

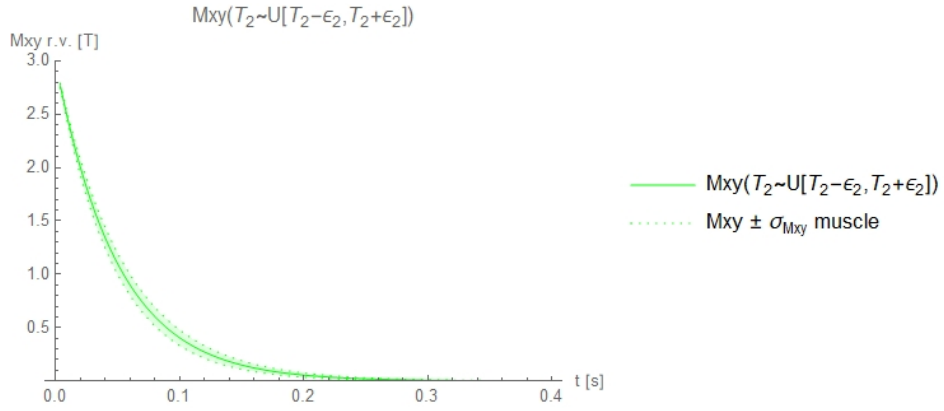

(a) $\mathbb{E}[M_{xy}] \pm 1.96 \cdot \sigma_{M_{xy}}$ muscle.

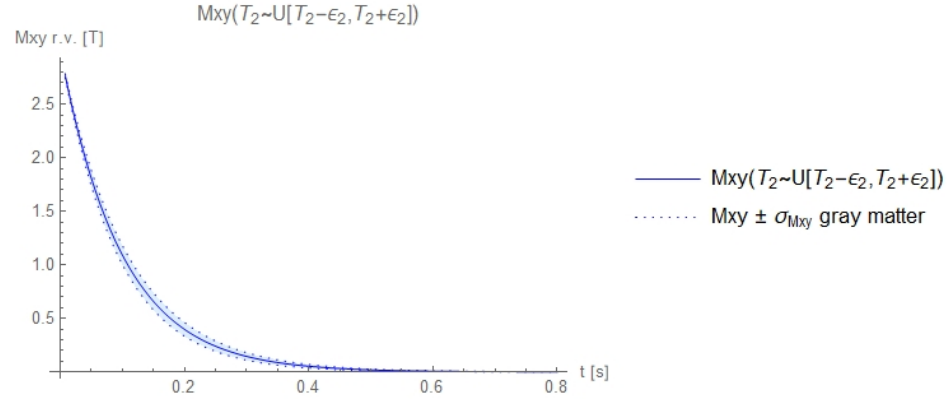

(b) $\mathbb{E}[M_{xy}] \pm 1.96 \cdot \sigma_{M_{xy}}$ gray matter.

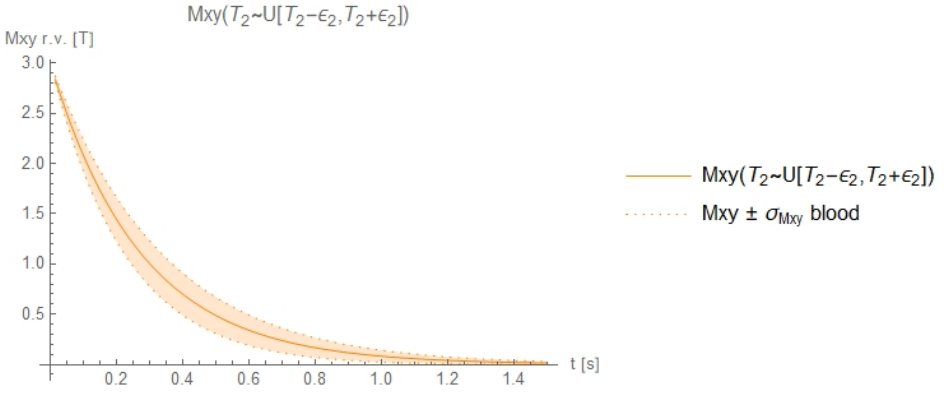

(c) $\mathbb{E}[M_{xy}] \pm 1.96 \cdot \sigma_{M_{xy}}$ blood.

Figure 7.15: $\mathbb{E}[M_{xy}] \pm 1.96 \cdot \sigma_{M_{xy}}$ into the relaxation process.

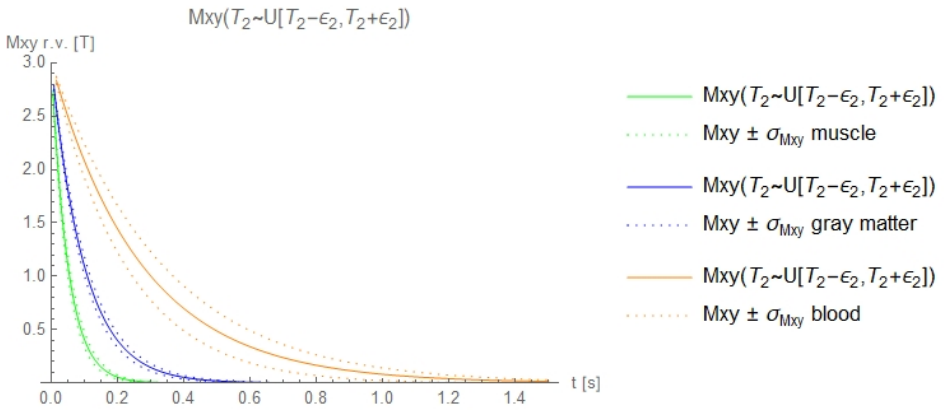

Figure 7.16: $E[M_{xy}]\pm 1.96\cdot\sigma_{M_{xy}}$ for different tissues into the relaxation process.

7.3.2 Calculating the 1-PDF $M_z(m_z)$.

Let assume $\mathbf{T}_1 \sim U[T_1 - \epsilon_1, T_1 + \epsilon_1]$, therefore its PDF is defined as:

$$f_{T_1} = \frac{1}{2\epsilon_1},$$

where ϵ_1 is and experimental value obtained for different B_0 magnet values and it can be shown in Table 2.2. So we can calculate the 1-PDF as

$$\begin{aligned} f_{M_z}(m_z) &= \frac{1}{2\epsilon_1}\left|\frac{t}{(\tau_0 - m_z)\log^2\left(\frac{\tau_0 - m_z}{M_0}\right)}\right|, \\ \mathbb{E}[M_z] &= \int_{D_{M_z}} m_z f_{M_z}(m_z) dm_z, \\ \mathbb{V}[M_z] &= \int_{D_{M_z}} (m_z - \mu_{M_z})^2 f_{M_z}(m_z) dm_z. \end{aligned} \tag{7.16}$$

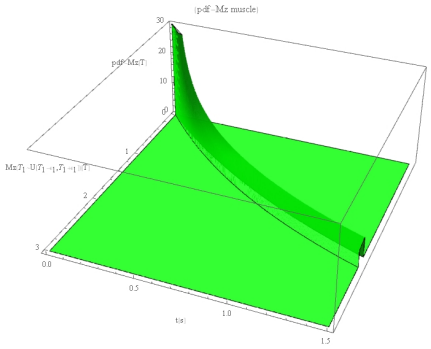

(a) 1-PDF for $M_z(m_z)$ muscle.

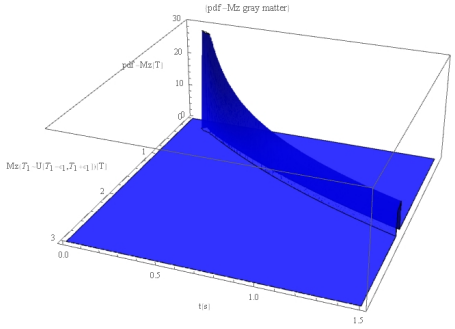

(b) 1-PDF for $M_z(m_z)$ gray matter.

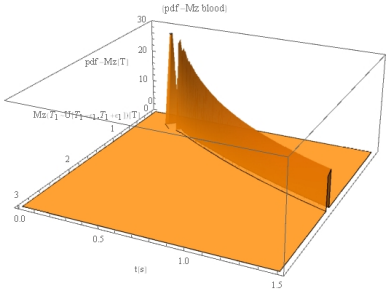

(c) 1-PDF for $M_z(m_z)$ blood.

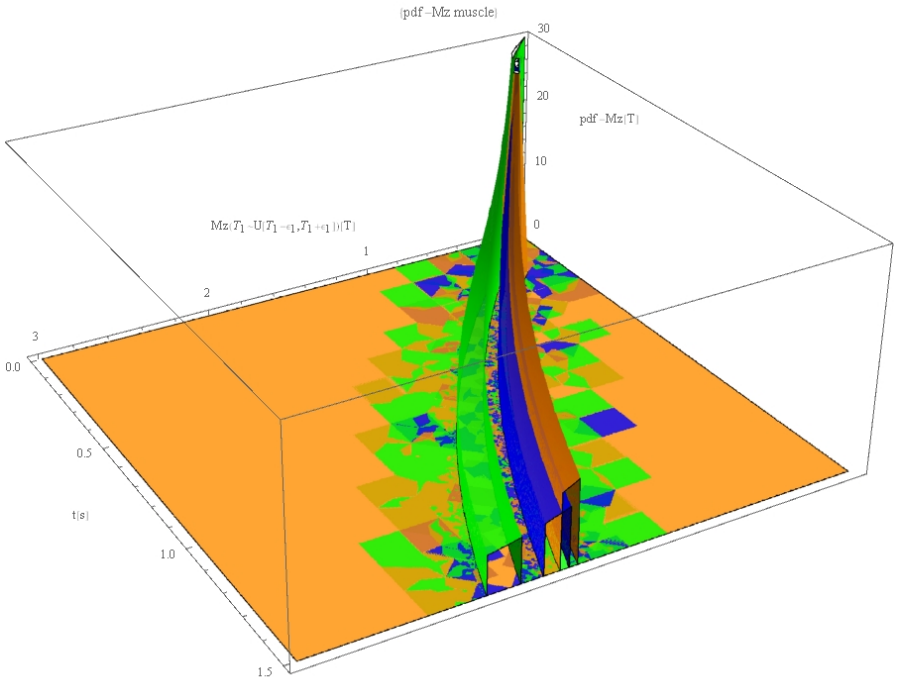

(d) 1-PDF for $M_z(m_z)$ all tissues.

Figure 7.17: 1-PDF $M_z(m_z, t)$ for longitudinal magnetization vector into the relaxation process.

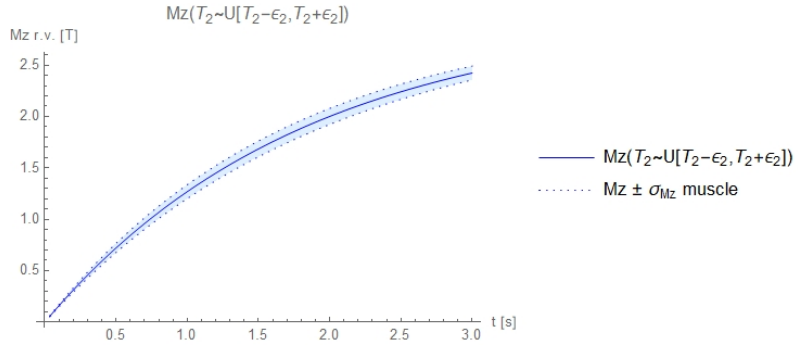

(a) $\mathbb{E}[M_z] \pm 1.96 \cdot \sigma_{M_z}$ gray matter.

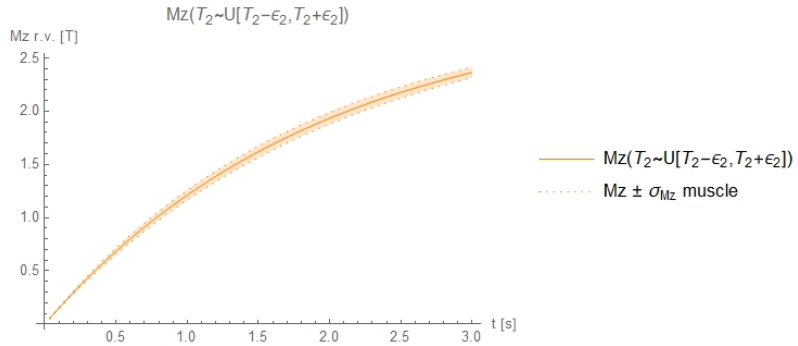

(b) $\mathbb{E}[M_{xy}] \pm 1.96 \cdot \sigma_{M_{xy}}$ blood.

Figure 7.18: $\mathbb{E}[M_z] \pm 1.96 \cdot \sigma_{M_z}$ of the longitudinal magnetization vector into the relaxation process.

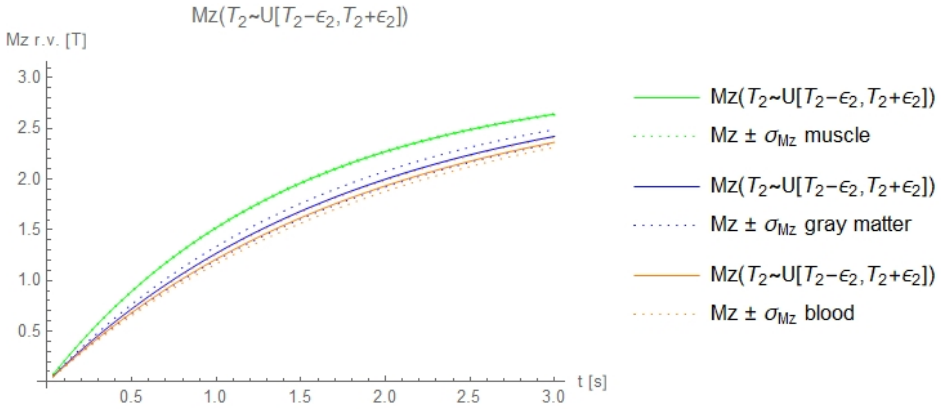

Figure 7.19: $\mathbb{E}[M_z] \pm 1.96 \cdot \sigma_{M_z}$ for different tissues into the relaxation process.

Chapter 8

Introducing R.D.E.s in the RF process.

This section shows the 1-PDF formulation for each equations involved in the radio-frequency process both in the rotation and laboratory frames. After that we show the results graphically the plots generated via Mathematica software. In some RVs it was necessary a numerical integration to calculate the expectation and the variance. '*NIntegrate*' function with a high '*MinRecursion*' value option was applied and several specific exclusions domains was required to avoid errors. As well it was required to reduce the '*PlotPoints*' value below 30 units in some RVs. '*Method*' option was set in automatic state.

8.1 τ_0 r.v. initial magnetization condition.

Thus, we will assume $\tau_0 = M_0$ be a random variable and the system of differential equation (**D.E.**) (4.1), becomes a system of random differential equation (**R.D.E.**).
Let $\tau_0 = M_0 \sim N[\mu_{M_0}, \sigma_{M_0}]$, (see chapter 6), therefore the probability density function (p.d.f.) of τ_0 RV of the Bloch equation into the RF process is defined as

$$f_{M_0}(m_0) = \frac{1}{\sqrt{2\pi\sigma_{M_0}^2}} e^{-\frac{1}{2}\left(\frac{m_0 - \mu_{M_0}}{\sigma_{M_0}}\right)^2},$$

In order to show and present the achieved results we will consider $\mu_{M_0} = M_0$ as the deterministic value proposed in the initial value problem (IVP) and σ_{M_0}

value as a dispersion of the mean μ_{M_0} value, thus $\sigma_{M_0} = 0.1\mu_{M_0}$.

8.1.1 Calculating the 1-PDF $m_y(n_y)$.

We can calculate the $m_y(n_y)$ 1-PDF using Theorem 7, with $X = M_0$, $Y = m_y$, $r(x) = m_y$, $s(y) = m_0 = \dfrac{n_y}{\sin(\gamma B_1 t)}$,

$$f_{m_y(n_y)} = f_{M_0}(s(n_y)) \left| \frac{\partial m_0}{\partial n_y} \right|.$$

$$\begin{aligned}
f_{m_y}(n_y) &= \frac{1}{\sqrt{2\pi\sigma_{M_0}^2}} e^{-\frac{1}{2}\left(\frac{\frac{n_y}{\sin(\gamma B_1 t)} - \mu_{M_0}}{\sigma_{M_0}} \right)^2} \left| \frac{1}{\sin(\gamma B_1 t)} \right|, \\
\mathbb{E}[m_y] &= \int_{D_{m_y}} n_y f_{m_y}(n_y) dn_y, \\
\mathbb{V}[m_y] &= \int_{D_{m_y}} (n_y - \mu_{m_y})^2 f_{m_y}(n_y) dn_y.
\end{aligned} \tag{8.1}$$

Figure 8.1 shows 1-PDF $f_{m_y}(n_y)$ magnetization vector in the rotating frame into the RF process for a flip angle of $\theta = \pi$. Figures 8.2 and 8.3 show the mean and the variability of m_y.

8.1.2 Calculating the 1-PDF $m_z(n_z)$.

We can calculate the $m_z(n_z)$ 1-PDF using Theorem 7, with $X = M_0$, $Y = m_z$, $r(x) = m_z$, $s(y) = m_0 = \dfrac{n_z}{\cos(\gamma B_1 t)}$,

$$f_{m_z(n_z)} = f_{M_0}(s(n_z)) \left| \frac{\partial m_0}{\partial n_z} \right|.$$

$$\begin{aligned}
f_{m_z}(n_y) &= \frac{1}{\sqrt{2\pi\sigma_{M_0}^2}} e^{-\frac{1}{2}\left(\frac{\frac{n_z}{\cos(\gamma B_1 t)} - \mu_{M_0}}{\sigma_{M_0}} \right)^2} \left| \frac{1}{\cos(\gamma B_1 t)} \right|, \\
\mathbb{E}[m_z] &= \int_{D_{m_z}} n_z f_{m_z}(n_z) dn_x, \\
\mathbb{V}[m_z] &= \int_{D_{m_z}} (n_z - \mu_{m_z})^2 f_{m_z}(n_z) dn_z.
\end{aligned} \tag{8.2}$$

Figure 8.1 shows 1-PDF magnetization vector in the rotating frame into the RF process for a flip angle of $\theta = \pi$.

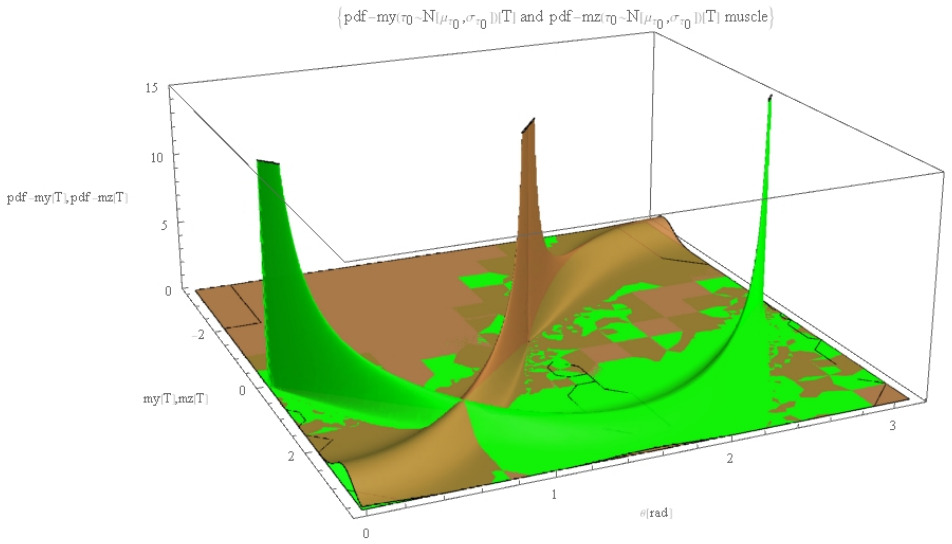

(a) $m_y(t)$,$m_z(t)$.

Figure 8.1: 1-PDF $m_y(n_y)$ and 1-PDF $m_z(n_z)$ in the rotating frame $\tau_0 \sim N[\mu_{\tau_0}, \sigma_{\tau_0}]$. Flip angle $(\theta) = \pi$.

Figures 8.2 and 8.3 show magnetization vector in the rotating frame into the RF process for a flip angle of $\theta = \pi$.

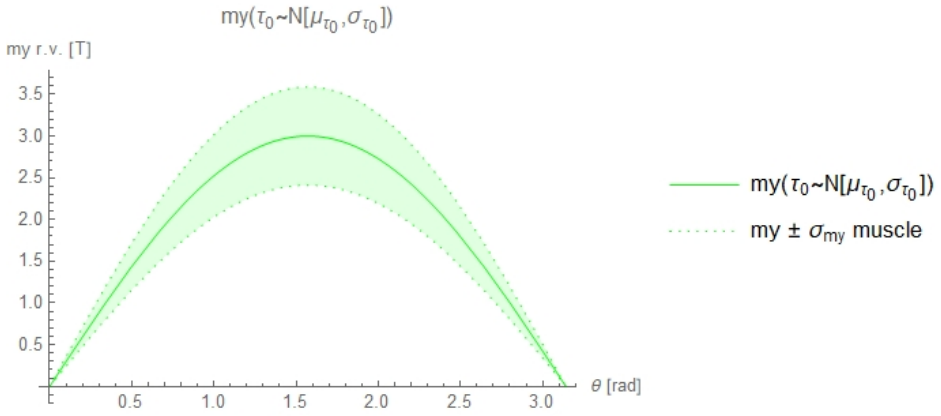

(a) $m_y(t)$,θ.

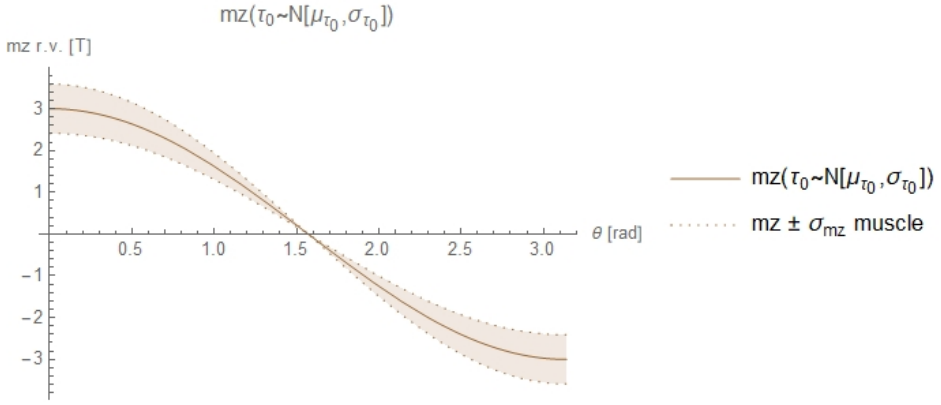

(b) $m_z(t)$,θ.

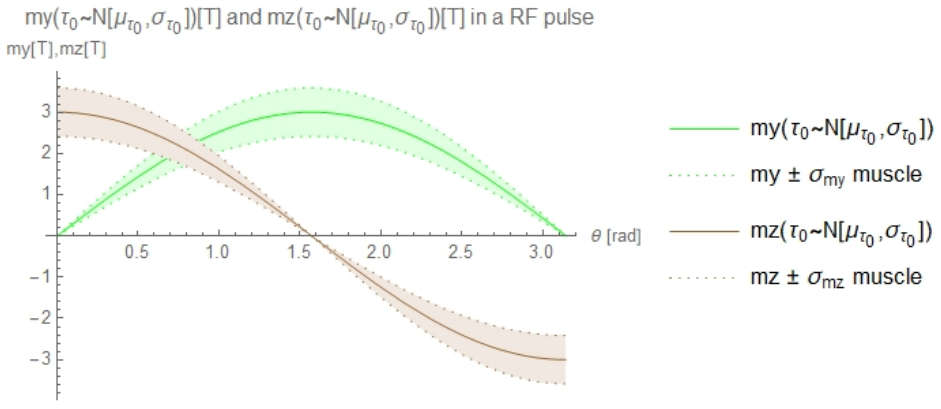

(c) $m_z(t)$,$m_y(t)$,θ.

Figure 8.2: $\mathbb{E}[m_y] \pm 1.96 \cdot \sigma_{m_y}$ and $\mathbb{E}[m_z] \pm 1.96 \cdot \sigma_{m_z}$ into the RF process.

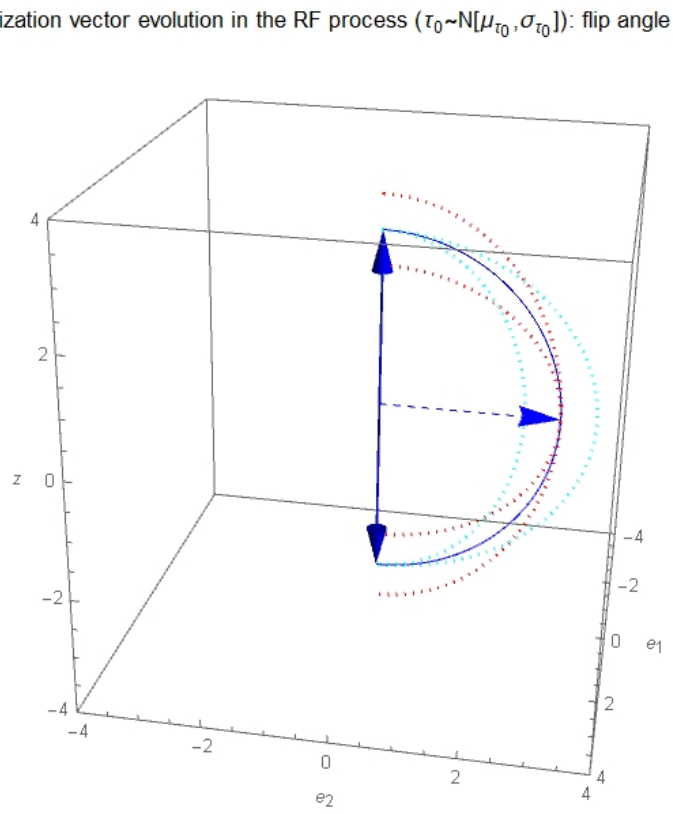

(a) $m_x(t)$,$m_y(t)$,$m_z(t)$.

Figure 8.3: Mean and variability of the magnetization vector $(0, \mathbb{E}[m_y] \pm 1.96 \cdot \sigma_{m_y}, \mathbb{E}[m_z] \pm 1.96 \cdot \sigma_{m_z})$ in the rotating frame.

8.1.3 Calculating the 1-PDF $M_x(m_x)$.

We can calculate the $M_x(m_x)$ 1-PDF using Theorem 7, with $X = M_0$, $Y = M_x$, $r(x) = m_x$, $s(y) = m_0 = \dfrac{m_x}{\sin(\gamma B_1 t)\sin(\gamma B_0 t)}$,

$$f_{M_x(m_x)} = f_{M_0}(s(m_x)) \left| \frac{\partial m_0}{\partial m_x} \right|.$$

$$
\begin{aligned}
f_{M_x}(m_x) &= \frac{1}{\sqrt{2\pi\sigma_{M_0}^2}} e^{-\frac{1}{2}\left(\frac{\frac{m_x}{\sin(\gamma B_1 t)\sin(\gamma B_0 t)} - \mu_{M_0}}{\sigma_{M_0}}\right)^2} \left|\frac{1}{\sin(\gamma B_1 t)\sin(\gamma B_0 t)}\right|, \\
\mathbb{E}[M_x] &= \int_{D_{M_x}} m_x f_{M_x}(m_x) dm_x, \qquad (8.3) \\
\mathbb{V}[M_x] &= \int_{D_{M_x}} (m_x - \mu_{M_x})^2 f_{M_x}(m_x) dm_x.
\end{aligned}
$$

Figure 8.4 shows 1-PDF $M_x(m_x)$ of the magnetization vector in the laboratory frame into the RF process for a flip angle of $\theta = \pi$.

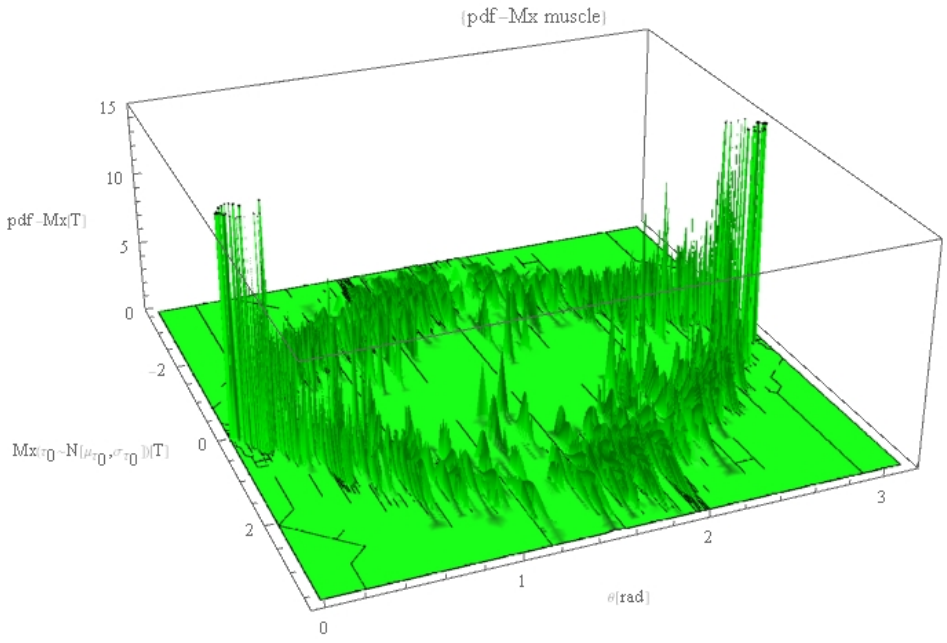

Figure 8.4: 1-PDF $M_x(m_x, t)$ in the laboratory frame.

8.1.4 Calculating the 1-PDF $M_y(m_y)$.

We can calculate the $M_y(m_y)$ 1-PDF using Theorem 7, with $X = M_0$, $Y = M_y$, $r(x) = m_y$, $s(y) = m_0 = \dfrac{m_y}{\sin(\gamma B_1 t)\cos(\gamma B_0 t)}$,

$$f_{M_y(m_y)} = f_{M_0}(s(m_y)) \left| \frac{\partial m_0}{\partial m_y} \right|.$$

$$\begin{aligned}
f_{M_y}(m_y) &= \frac{1}{\sqrt{2\pi\sigma_{M_0}^2}} e^{-\frac{1}{2}\left(\frac{\frac{m_y}{\sin(\gamma B_1 t)\cos(\gamma B_0 t)} - \mu_{M_0}}{\sigma_{M_0}} \right)^2} \left| \frac{1}{\sin(\gamma B_1 t)\cos(\gamma B_0 t)} \right|, \\
\mathbb{E}[M_y] &= \int_{D_{M_y}} m_y f_{M_y}(m_y) dm_y, \\
\mathbb{V}[M_y] &= \int_{D_{M_y}} (m_y - \mu_{M_y})^2 f_{M_y}(m_y) dm_y.
\end{aligned} \tag{8.4}$$

Note that $f_{M_y}(m_y)$ is graphically equivalent to $f_{M_x}(m_x)$ only with a $\frac{\pi}{2}$ phase difference in ω_0.

Figure 8.5 shows mean and variability $M_x(m_x), M_y(m_y)$ RVs in the laboratory frame into the RF process for a flip angle of $\theta = \pi$.

8.1.5 Calculating the 1-PDF $M_z(m_z)$.

We can calculate the $M_z(m_z)$ 1-PDF using Theorem 7, with $X = M_0$, $Y = M_z$, $r(x) = m_z$, $s(y) = m_0 = \dfrac{m_z}{\cos(\gamma B_1 t)}$,

$$f_{M_z(m_z)} = f_{M_0}(s(m_z)) \left| \frac{\partial m_0}{\partial m_z} \right|.$$

$$\begin{aligned}
f_{M_z}(m_z) &= \frac{1}{\sqrt{2\pi\sigma_{M_0}^2}} e^{-\frac{1}{2}\left(\frac{\frac{m_z}{\cos(\gamma B_1 t)} - \mu_{M_0}}{\sigma_{M_0}} \right)^2} \left| \frac{1}{\cos(\gamma B_1 t)} \right|, \\
\mathbb{E}[M_z] &= \int_{D_{M_z}} m_z f_{M_z}(m_z) dm_z, \\
\mathbb{V}[M_z] &= \int_{D_{M_z}} (m_z - \mu_{M_z})^2 f_{M_z}(m_z) dm_z.
\end{aligned} \tag{8.5}$$

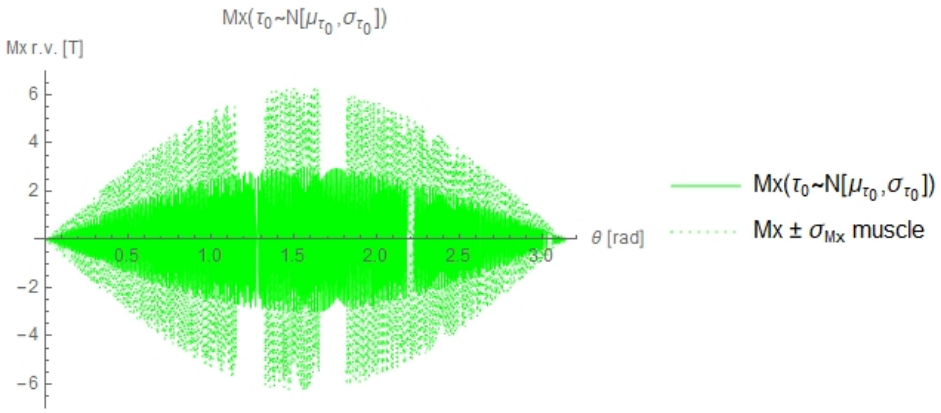

(a) $M_x(t)$,θ.

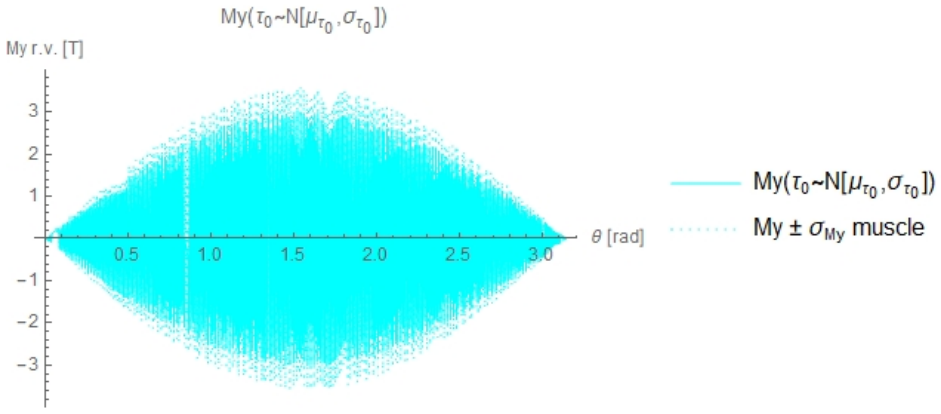

(b) $M_y(t)$,θ.

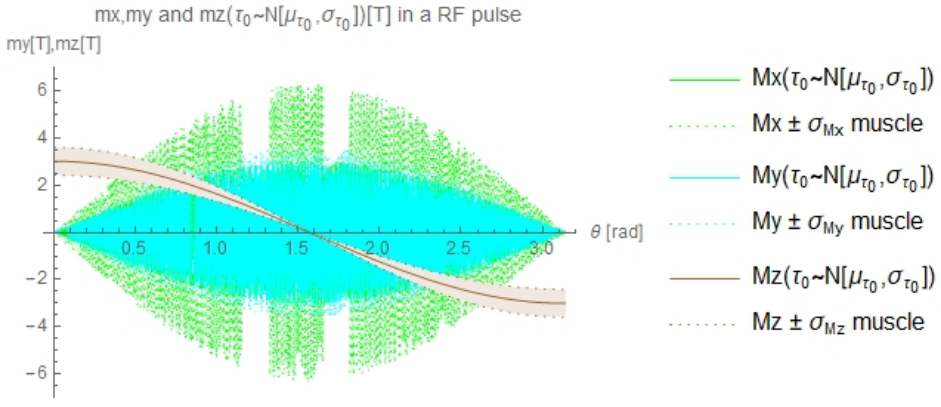

(c) $M_x(t)$,$M_y(t)$,$M_z(t)$,θ.

Figure 8.5: $\mathbb{E}[M_x(m_x)]$ $\pm 1.96\sigma_{M_x}$, $\mathbb{E}[M_y(m_y)]$ $\pm 1.96\sigma_{M_y}$ and $\mathbb{E}[M_z(m_z)]$ $\pm 1.96\sigma_{M_z}$ in the laboratory frame for $\tau_0 \sim N[\mu_{\tau_0}, \sigma_{\tau_0}]$.

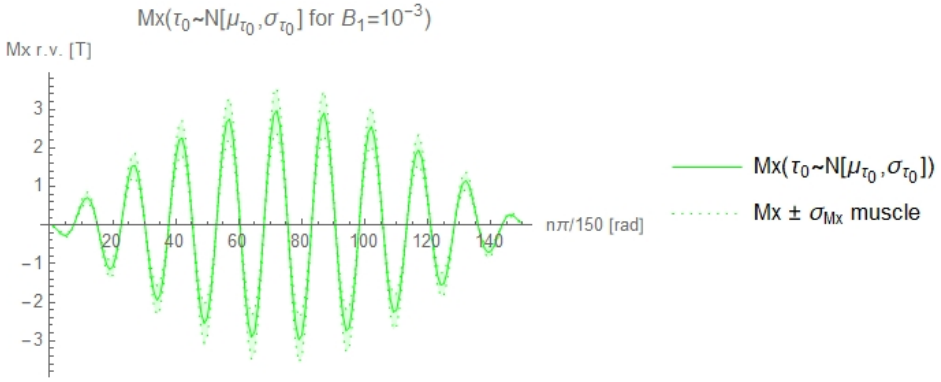

(a) $\mathbb{E}[M_x(m_x)] \pm 1.96\sigma_{M_x}$, $B_1 = 10^{-3}T$.

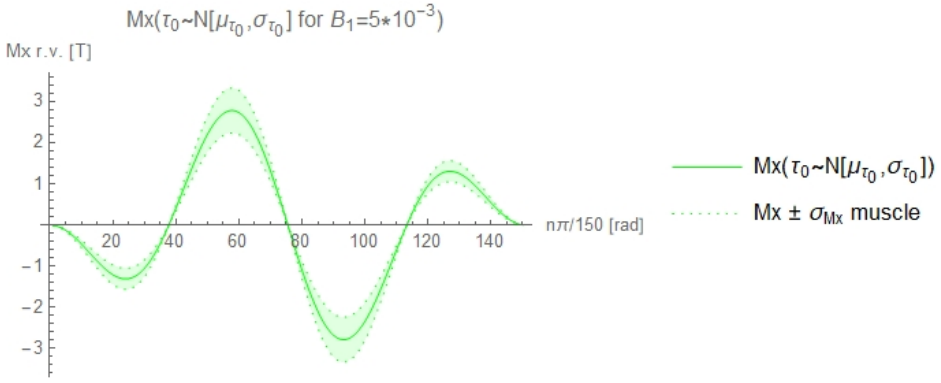

(b) $\mathbb{E}[M_x(m_x)] \pm 1.96\sigma_{M_x}$, $B_1^* = 5 \cdot B_1$.

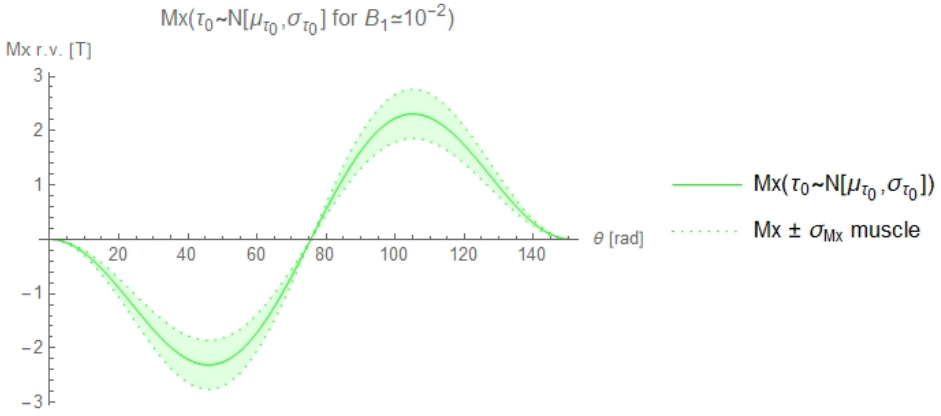

(c) $\mathbb{E}[M_x(m_x)] \pm 1.96\sigma_{M_x}$, $B_1^{**} = 10 \cdot B_1$.

Figure 8.6: $\mathbb{E}[M_x(m_x)] \pm 1.96\sigma_{M_x}$ in the laboratory frame for different B_1 RF pulse amplitude.

8.2 B_1 r.v. generated RF pulse.

Thus, we will assume B_1 be a random variable and the system differential equation (**D.E.**) (4.1), becomes a system of random differential equation (**R.D.E.**). Let $B_1 \sim N[\mu_{B_1}, \sigma_{B_1}]$, (see chapter 6), therefore the probability density function (p.d.f.) of B_1 RV of the Bloch equation into the RF process is defined as,

$$f_{B_1}(b_1) = \frac{1}{\sqrt{2\pi\sigma_{B_1}^2}} e^{-\frac{1}{2}\left(\frac{b_1 - \mu_{B_1}}{\sigma_{B_1}}\right)^2},$$

In order to show and present the achieved results we will consider $\mu_{B_1} = B_1$ as the deterministic value proposed for the generated pulse and σ_{B_1} value as a dispersion of the mean μ_{B_1} value, thus $\sigma_{B_1} = 0.1\mu_{B_1}$.

8.2.1 Calculating the 1-PDF $m_y(n_y)$.

We can calculate the $m_y(n_y)$ 1-PDF using Theorem 7, with $X = B_1$, $Y = m_y$, $r(x) = m_y$, $s(y) = b_1 = \dfrac{\arcsin\frac{n_y}{\tau_0}}{\gamma t}$,

$$f_{m_y(n_y)} = f_{B_1}(s(n_y)) \left|\frac{\partial b_1}{\partial n_y}\right|.$$

$$\begin{aligned}
f_{m_y}(n_y) &= \frac{1}{\sqrt{2\pi\sigma_{B_1}^2}} e^{-\frac{1}{2}\left(\frac{\frac{\arcsin\frac{n_y}{\tau_0}}{\gamma t} - \mu_{B_1}}{\sigma_{B_1}}\right)^2} \left|\frac{1}{\gamma t\sqrt{\tau_0^2 - n_y^2}}\right|, \\
\mathbb{E}[m_y] &= \int_{D_{m_y}} n_y f_{m_y}(n_y) dn_y, \\
\mathbb{V}[m_y] &= \int_{D_{m_y}} (n_y - \mu_{m_y})^2 f_{m_y}(n_y) dn_y.
\end{aligned} \tag{8.6}$$

8.2.2 Calculating the 1-PDF $m_z(n_z)$.

We can calculate the $m_z(n_z)$ 1-PDF using Theorem 7, with $X = B_1$, $Y = m_z$, $r(x) = m_z$, $s(y) = b_1 = \dfrac{\arccos\frac{n_z}{\tau_0}}{\gamma t}$,

$$f_{m_z(n_z)} = f_{B_1}(s(n_y)) \left|\frac{\partial b_1}{\partial n_z}\right|.$$

$$
\begin{aligned}
f_{m_z}(n_z) &= \frac{1}{\sqrt{2\pi\sigma_{B_1}^2}} e^{-\frac{1}{2}\left(\frac{\frac{\arccos\frac{n_y}{\tau_0}}{\gamma t}-\mu_{B_1}}{\sigma_{B_1}}\right)^2} \left|\frac{-1}{\gamma t\sqrt{\tau_0^2-n_y^2}}\right|, \\
\mathbb{E}[m_z] &= \int_{D_{m_z}} n_z f_{m_z}(n_z) dn_z, \\
\mathbb{V}[m_z] &= \int_{D_{m_z}} (n_z-\mu_{m_z})^2 f_{m_z}(n_z) dn_z.
\end{aligned} \tag{8.7}
$$

8.2.3 Calculating the 1-PDF $M_x(m_x)$.

We can calculate the $M_x(m_x)$ 1-PDF using Theorem 7, with $X = B_1$, $Y = M_x$, $r(x) = m_x$, $s(y) = b_1 = \dfrac{\arcsin\left(\frac{m_x}{\tau_0\sin(\omega_0 t)}\right)}{\gamma t}$,

$$
f_{M_x(m_x)} = f_{B_1}(s(m_x))\left|\frac{\partial b_1}{\partial m_x}\right|.
$$

$$
\begin{aligned}
f_{M_x}(m_x) &= \frac{1}{\sqrt{2\pi\sigma_{B_1}^2}} e^{-\frac{1}{2}\left(\frac{\arcsin\left(\frac{m_x}{\tau_0\sin(\omega_0 t)}\right)-\gamma t\mu_{B_1}}{\gamma t\sigma_{B_1}}\right)^2} \left|\frac{1}{\gamma t\sqrt{\tau_0^2\sin\omega_0 t^2-m_x^2}}\right|, \\
\mathbb{E}[M_x] &= \int_{D_{M_x}} m_x f_{M_x}(m_x) dm_x, \\
\mathbb{V}[M_x] &= \int_{D_{M_x}} (m_x-\mu_{M_x})^2 f_{M_x}(m_x) dm_x.
\end{aligned} \tag{8.8}
$$

Figure 8.7 shows magnetization RV, $M_x(m_x)$, in the laboratory frame into the RF process for different B_1 RF amplitude values an angle of $\theta = \pi$.

8.2.4 Calculating the 1-PDF $M_y(m_y)$.

We can calculate the $M_y(m_y)$ 1-PDF using theorem 7, with $X = B_1$, $Y = M_y$, $r(x) = m_y$, $s(y) = b_1 = \dfrac{\arcsin\left(\frac{m_x}{\tau_0\cos(\omega_0 t)}\right)}{\gamma t}$,

$$
f_{M_y(m_y)} = f_{B_1}(s(m_y))\left|\frac{\partial b_1}{\partial m_y}\right|.
$$

$$
\begin{aligned}
f_{M_y}(m_y) &= \frac{1}{\sqrt{2\pi\sigma_{B_1}^2}} e^{-\frac{1}{2}\left(\frac{\arcsin\left(\frac{m_y}{\tau_0\cos(\omega_0 t)}\right)-\gamma t\mu_{B_1}}{\gamma t\sigma_{B_1}}\right)^2} \left|\frac{1}{\gamma t\sqrt{\tau_0^2\sin\omega_0 t^2 - m_y^2}}\right|, \\
\mathbb{E}[M_y] &= \int_{D_{M_y}} m_y f_{M_y}(m_y) dm_y, \qquad (8.9) \\
\mathbb{V}[M_y] &= \int_{D_{M_y}} (m_y - \mu_{M_y})^2 f_{M_y}(m_y) dm_y.
\end{aligned}
$$

Figure 8.7 shows magnetization RV, $M_y(m_y)$, in the laboratory frame into the RF process for different B_1 RF amplitude values an angle of $\theta = \pi$.

8.2.5 Calculating the 1-PDF $M_z(m_z)$.

In the laboratory frame $M_z(m_z)$ is identical to $m_z(n_z)$ in the rotation frame by definition.

Figure 8.7 shows 1-PDF $f_{M_z}(m_z)$ magnetization vector in the rotating frame into the RF process for a flip angle of $\theta = \pi$.

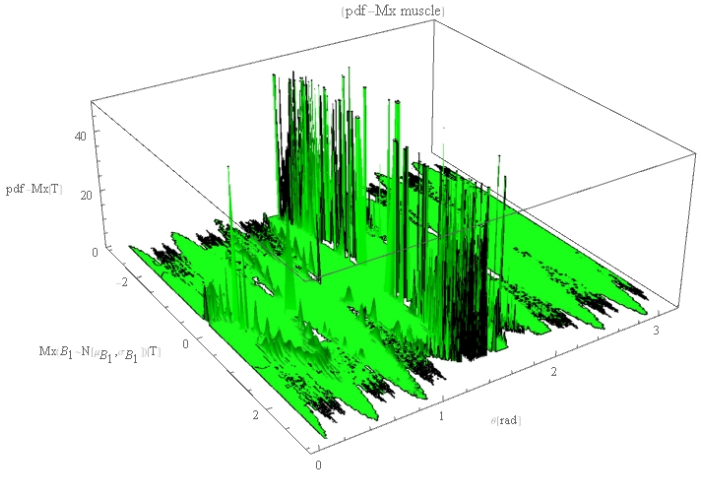

(a) 1-PDF $M_x(m_x, \theta)$.

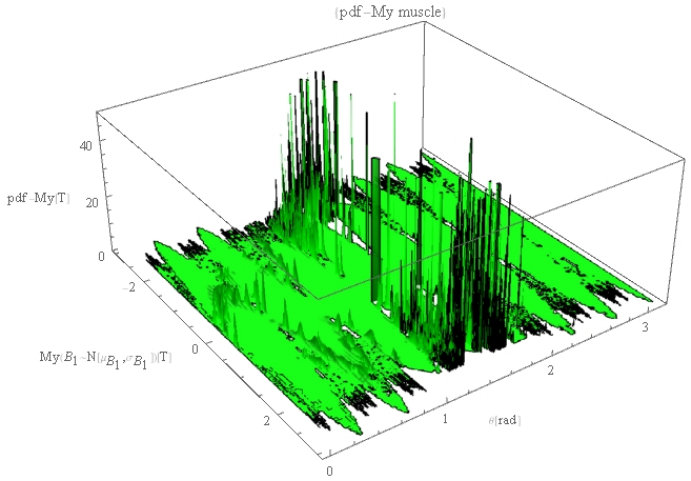

(b) $M_y(m_y, \theta)$.

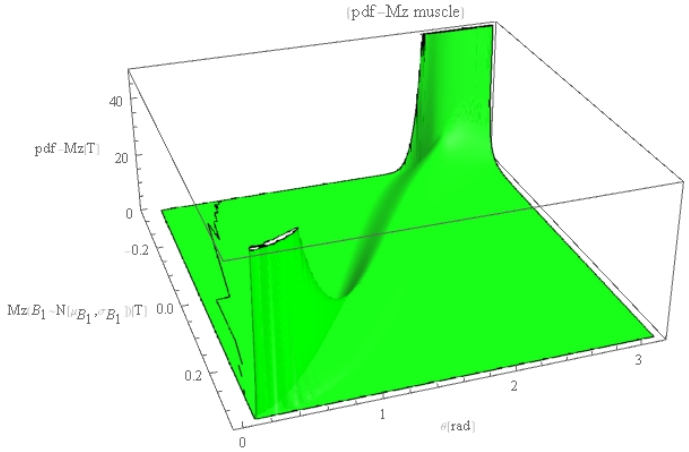

(c) $M_z(m_z, \theta)$.

Figure 8.7: $1 - PDF$ of $M_x(m_x), M_y(m_y), M_z(m_z)$ in the RF process. Laboratory frame.

8.3 B_0 r.v. magnetic flux density.

Thus, we will assume B_0 be a random variable and the system of differential equation (**D.E.**) (4.1), becomes a system of random differential equation (**R.D.E.**).

Let $B_0 \sim N[\mu_{B_0}, \sigma_{B_0}]$, (see chapter 6), therefore the probability density function (PDF) of B_0 RV of the Bloch equation into the RF process is defined as,

$$f_{B_0}(b_0) = \frac{1}{\sqrt{2\pi\sigma_{B_0}^2}} e^{-\frac{1}{2}\left(\frac{b_0 - \mu_{B_0}}{\sigma_{B_0}}\right)^2},$$

In order to show and present the achieved results we will consider $\mu_{B_0} = B_0$ as the deterministic value proposed for the generated pulse and σ_{B_0} value as a dispersion of the mean μ_{B_0} value, thus $\sigma_{B_0} = 0.1\mu_{B_0}$.

8.3.1 Calculating the 1-PDF $M_x(m_x)$.

We can calculate the $M_x(m_x)$ 1-PDF using Theorem 7, with $X = B_0$, $Y = M_x$, $r(x) = m_x$, $s(y) = b_0 = \dfrac{\arcsin\left(\frac{m_x}{\tau_0 \sin(\omega_1 t)}\right)}{\gamma t}$,

$$f_{M_x(m_x)} = f_{B_0}(s(m_x)) \left|\frac{\partial b_0}{\partial m_x}\right|.$$

$$\begin{aligned}
f_{M_x}(m_x) &= \frac{1}{\sqrt{2\pi\sigma_{B_0}^2}} e^{-\frac{1}{2}\left(\frac{\arcsin\left(\frac{m_x}{\tau_0 \sin(\omega_1 t)}\right) - \gamma t \mu_{B_0}}{\gamma t \sigma_{B_0}}\right)^2} \left|\frac{1}{\gamma t \sqrt{\tau_0^2 \sin\omega_1 t^2 - m_x^2}}\right|, \\
\mathbb{E}[M_x] &= \int_{D_{M_x}} m_x f_{M_x}(m_x) dm_x, \qquad (8.10) \\
\mathbb{V}[M_x] &= \int_{D_{M_x}} (m_x - \mu_{M_x})^2 f_{M_x}(m_x) dm_x.
\end{aligned}$$

8.3.2 Calculating the 1-PDF $M_y(m_y)$.

We can calculate the $M_y(m_y)$ 1-PDF using Theorem 7, with $X = B_0$, $Y = M_y$, $r(x) = m_y$, $s(y) = b_0 = \dfrac{\arccos\left(\frac{m_y}{\tau_0 \sin(\omega_1 t)}\right)}{\gamma t}$,

$$f_{M_y(m_y)} = f_{B_0}(s(m_y)) \left| \frac{\partial b_0}{\partial m_y} \right|.$$

$$\begin{aligned}
f_{M_y}(m_y) &= \frac{1}{\sqrt{2\pi\sigma_{B_0}^2}} e^{-\frac{1}{2}\left(\frac{\arccos\left(\frac{m_y}{\tau_0 \sin(\omega_1 t)}\right) - \gamma t \mu_{B_1}}{\gamma t \sigma_{B_1}} \right)^2} \left| \frac{-1}{\gamma t \sqrt{\tau_0^2 \sin \omega_1 t^2 - m_y^2}} \right|, \\
\mathbb{E}[M_y] &= \int_{D_{M_y}} m_y f_{M_y}(m_y) dm_y, \qquad (8.11) \\
\mathbb{V}[M_y] &= \int_{D_{M_y}} (m_y - \mu_{M_y})^2 f_{M_y}(m_y) dm_y.
\end{aligned}$$

Chapter 9

Conclusions

Bloch equation based on **MRI** simulators were developed for optimizing MR sequences, artifact detection, testing image reconstruction techniques, design of specialized RF pulses and also for educational purposes. The hardware computational technologies have advanced during the last decades but despite **mathematical modelling are necessary** to accelerate and make accurate simulations and imaging processes.

MRI is nowadays a very rapid process which is done in **real-time**. Neverdeless, there are still unsolved problems in understanding how the **quantitative o dynamic alteration of magnetic field are involved**. Researchers carry on with the aim of accelerate it, making more and more efficent the **MRI** process. Numerical simulation for solving the Bloch model can help in a better understanding of such **dynamic processes** are affected inside our body and organism. As well it is necessary to know about artifacts in real-time and also for improving the quality images.

Apart from the controlled experiments with precise input data, numerical simulators can also be used to simulate various limiting experimental conditions which are either improbable or difficult to reproduce in experiments.

The cost of a MRI diagnostic test is around 150€ and time-processes are between 10-20 minutes each one depending on the complexity of the test. There are more and more medical request for these technology in order to interpret and improve a diagnostic, therefore the time reduction process is a great value for saving money. Do not forget the future perspectives around the MRI which remains as a **non-invasive technique**.

All thinks considered, mathematician have the opportunity to contribute and research in this field for the following decades.

In this way we decided to **introduce variability into the MRI** and calculate the 1-PDF of all Bloch equations, both into the relaxation time and into the RF pulse process, thus we can contribute to design components such as coils, pulses, gradients and other parts of the integrated MR based on predicting contrast, resolution or determining SNR.

Accurate simulation of the initial value problem (IVP) is a challenging due to the very tiny steps, the fine spatial resolution, the gradient field shapes (non-smooth gradients) or the originated perturbations fields this is a great reason to consider the IVP with uncertainties. Perturbations and minor physical effects in a very short time increases randomness.

Furthermore, if we consider T_2 as a random variable (see Sections 2.2 and 2.3), it could be considered as a mixture of tissues. Figure 9.1 shows variability into M_{xy} considering T_2 as random variable.

As we showed T_1 and T_2 relaxation times are experimental values (see sections 2.1, 2.2 and 2.3), which have internal variability for some physical and chemical properties. Therefore, we can suppose to be random variables.

As well, it would be interesting to consider the variability of the random variables involving the Bloch model to achieve better results in the **TE** and **TR** selection parameters, predicting the contrast, resolution and SNR. See Figure 9.3.

Introducing variability into the RF pulse process inform us about IVP of the magnetization vector and its error position. In chapter 8 (remember figures 8.2 and 8.3 where we shown magnetization vector variability) we have introduced this variability into the flip angle which determine the initial position of the relaxation time. Bear in mind this is a very short process and impact directly in the TR and TE times selection.

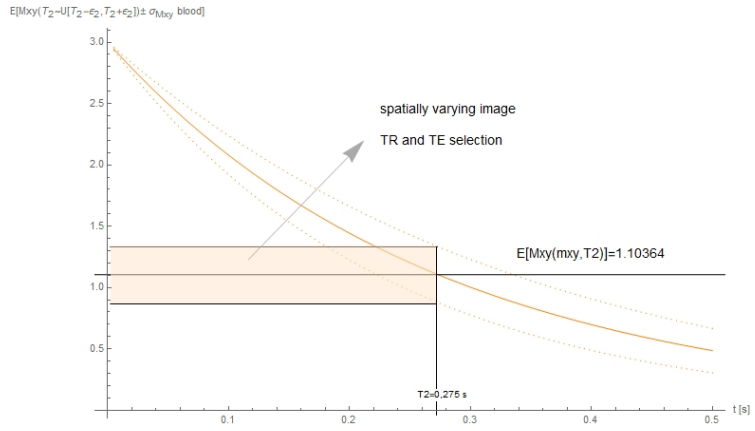

(a) $\mathbb{E}(M_{xy}(m_{xy}) \pm \sigma_{T_2})$ blood.

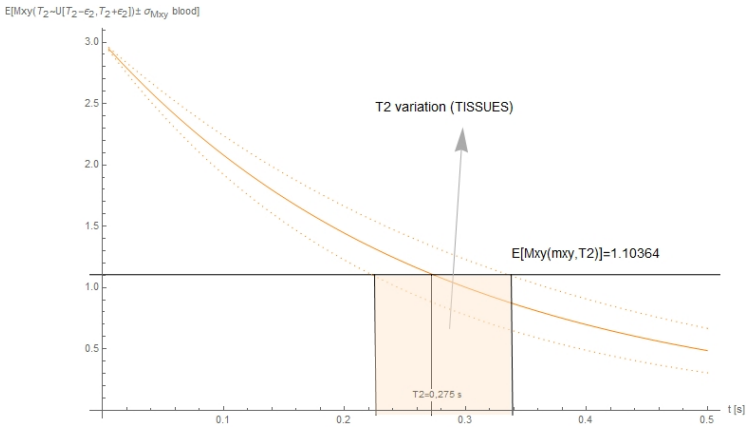

(b) $\mathbb{E}(M_{xy}(m_{xy}) \pm \sigma_{T_2})$ blood.

Figure 9.1: Variation of contrast, T_2 and spatially varying image.

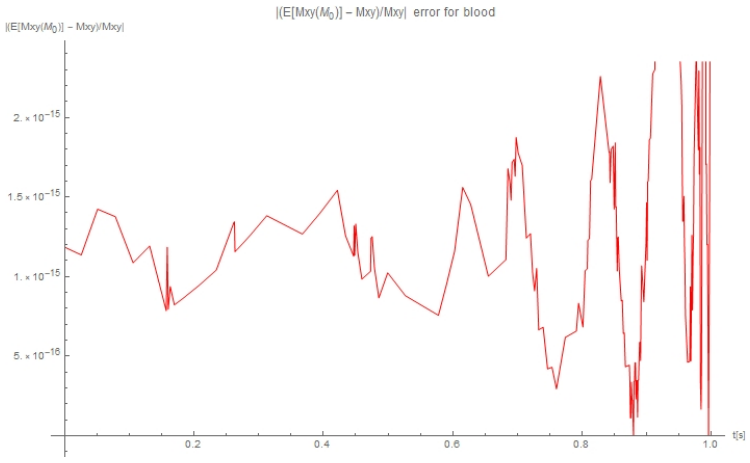

(a) $|\frac{\mathbb{E}(M_{xy})-M_{xy}}{M_{xy}}|$ error for M_0 initial condition rv. Blood tissue.

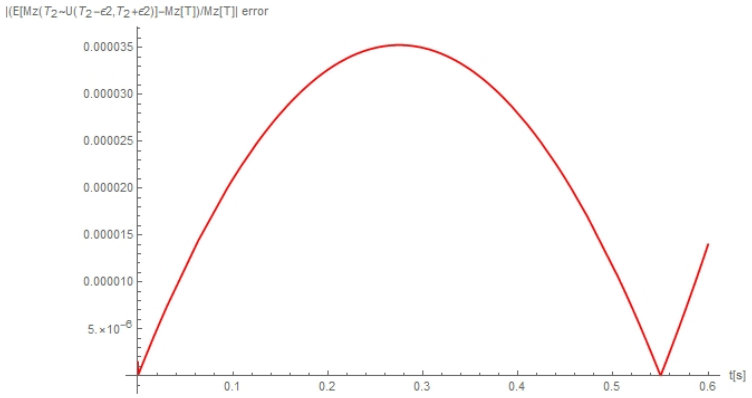

(b) $|\frac{\mathbb{E}(M_{xy})-M_{xy}}{M_{xy}}|$ error for T_2

Figure 9.2: $M_{xy}(m_{xy})$ error for M_0 and T_2 rv.

As we show in Figure 9.2, the error between means and deterministic values from Bloch equation can be neglected.

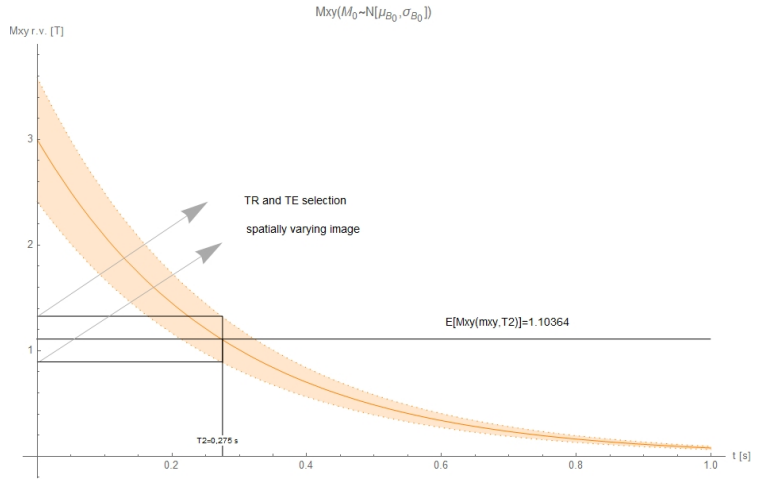

(a) $\mathbb{E}(M_{xy}) \pm \sigma_{xy}$, M_0 rv. Blood tissue. Contrast affection.

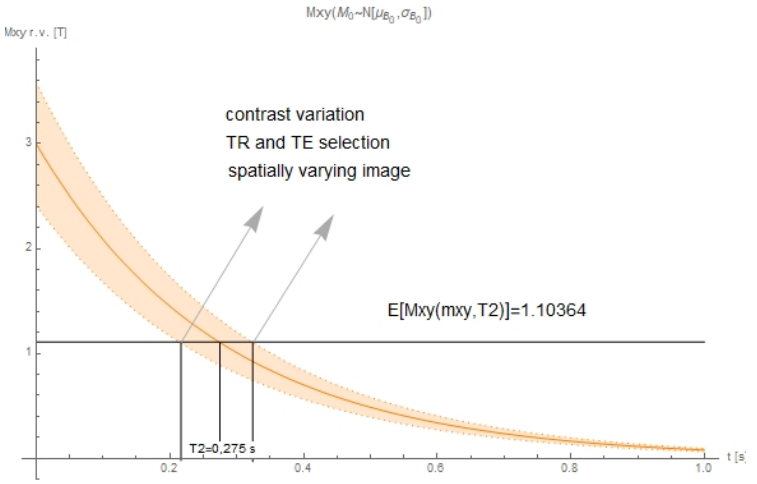

(b) $\mathbb{E}(M_{xy}) \pm \sigma_{xy}$, M_0 rv. Blood tissue. TR, TE and spatially variation image.

Figure 9.3: $M_{xy}(m_{xy})$ error for M_0 rv.

Figure 9.4 shows the spin density weighted which affect to the SNR and the selection of TR and TE times.

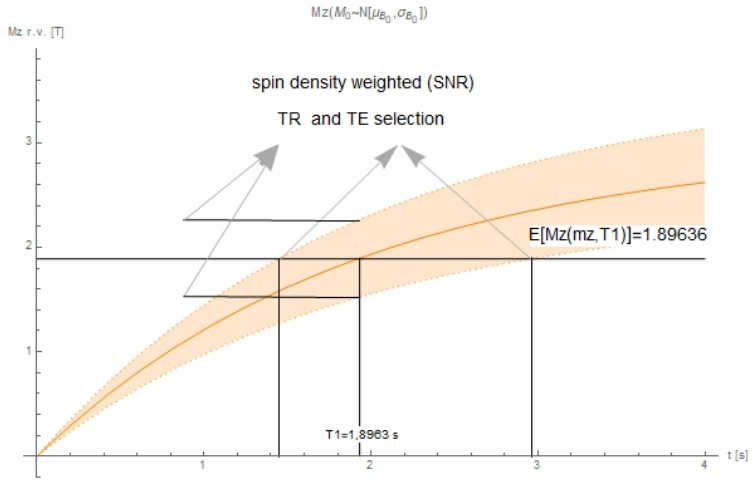

(a) $\mathbb{E}(M_z) \pm \sigma_{M_z}$, M_0 rv. Blood tissue. SNR and contrast affection.

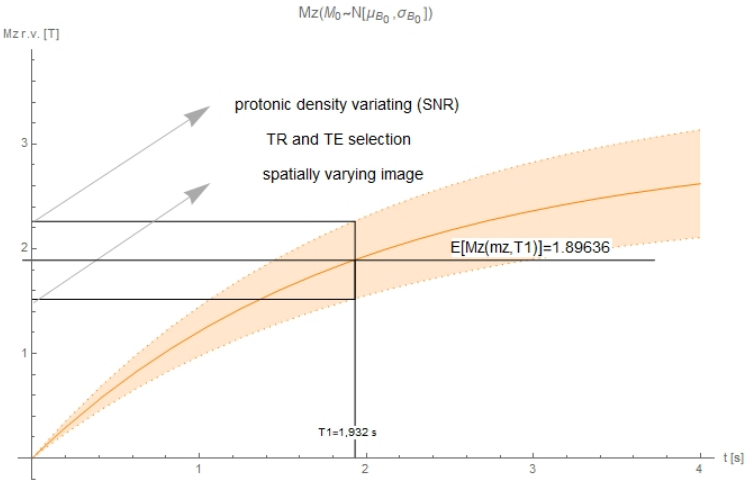

(b) $\mathbb{E}(M_z) \pm \sigma_{M_z}$, M_0 rv. Blood tissue. TR, TE and spatially variation image.

Figure 9.4: $\mathbb{E}(M_z) \pm \sigma_{M_z}$, M_0 rv. Blood tissue.

Dealing with the RF process we can show in Figures 8.2 and 8.3 that initial condition M_0 treated as a random variable will affect in the flip angle position, θ, and so on into the consequent IVP, M_0 of the relaxation process.

Beyond this, Figure 8.6 shows the consequent persistent rise of variation if we increase the B_1 RF pulse amplitude.

To finish this work we attach all 1-PDF of random Bloch equations in order to provide an easy location and understanding.

Table 9.1: $f_{M_x}(m_x)$. Relaxation process.

RV	$M_x(m_x)$ **1-PDF Relaxation process**
$\mathbf{M_0}$	$f_{M_x(m_x)} = \dfrac{1}{\sqrt{2\pi\sigma_{M_0}^2}} e^{-\frac{1}{2}\left(\frac{\frac{m_x e^{t\tau_2}}{\sin(\gamma B_0 t)} - \mu_{M_0}}{\sigma_{M_0}}\right)^2} \left\lvert \dfrac{e^{t\tau_2}}{\sin(\gamma B_0 t)} \right\rvert$
$\mathbf{B_0}$	$f_{M_x}(m_x) = \dfrac{1}{\sqrt{2\pi\sigma_{B_0}^2}} e^{-\frac{1}{2}\left(\frac{\frac{1}{\gamma t}\arcsin\left(\frac{m_x}{M_0}e^{t\tau_2}\right) - \mu_{B_0}}{\sigma_{B_0}}\right)^2} \left\lvert \dfrac{e^{t\tau_2}}{\gamma t M_0 \sqrt{1-\left(\frac{m_x}{M_0}e^{t\tau_2}\right)^2}} \right\rvert$

Table 9.2: $f_{M_y}(m_y)$. Relaxation process.

RV	$M_y(m_y)$ **1-PDF Relaxation process**
$\mathbf{M_0}$	$f_{M_y(m_y)} = \dfrac{1}{\sqrt{2\pi\sigma_{M_0}^2}} e^{-\frac{1}{2}\left(\frac{\frac{m_y e^{t\tau_2}}{\cos(\gamma B_0 t)} - \mu_{M_0}}{\sigma_{M_0}}\right)^2} \left\lvert \dfrac{e^{t\tau_2}}{\cos(\gamma B_0 t)} \right\rvert$
$\mathbf{B_0}$	$f_{M_y} = \dfrac{1}{\sqrt{2\pi\sigma_{B_0}}} e^{-\frac{1}{2}\left(\frac{\frac{1}{\gamma t}\arccos\left(\frac{m_y}{M_0}e^{t\tau_2}\right) - \mu_{B_0}}{\sigma_{B_0}}\right)^2} \left\lvert \dfrac{-e^{t\tau_2}}{\gamma t M_0 \sqrt{1-\left(\frac{m_y}{M_0}e^{t\tau_2}\right)^2}} \right\rvert$

Table 9.3: $f_{M_{xy}}(m_{xy})$. Relaxation process.

RV	$M_{xy}(m_{xy})$ **1-PDF Relaxation process**
$\mathbf{M_0}$	$f_{M_{XY}(m_{xy})} = \frac{1}{\sqrt{2\pi\sigma^2_{M_0}}} e^{-\frac{1}{2}\left(\frac{M_{xy}e^{t\tau_2} - \mu_{M_0}}{\sigma_{M_0}}\right)^2} \left\|e^{t\tau_2}\right\|$
$\mathbf{T_2} \sim U[T_2 - \epsilon_2, T_2 + \epsilon_2]$	$f_{M_{xy}(m_{xy})} = \frac{1}{2\epsilon_2} \left\|\frac{t}{m_{xy}\log^2 \frac{m_{xy}}{M_0}}\right\|$

Table 9.4: $f_{M_z}(m_z)$. Relaxation process.

RV	$M_z(m_z)$ **1-PDF Relaxation process**
$\tau_\mathbf{0}$	$f_{M_z(m_z)} = \frac{1}{\sqrt{2\pi\sigma^2_{M_0}}} e^{-\frac{1}{2}\left(\frac{\frac{m_z}{(1-e^{-\tau_1 t})} - \mu_{M_0}}{\sigma_{M_0}}\right)^2} \left\|\frac{1}{1-e^{-\tau_1 t}}\right\|$
$\mathbf{T_1} \sim U[T_1 - \epsilon_1, T_1 + \epsilon_1]$	$f_{M_z}(m_z) = \frac{1}{2\epsilon_1} \left\|\frac{t}{(\tau_0 - m_z)\log^2 (\frac{\tau_0 - m_z}{M_0})}\right\|$

Table 9.5: $f_{m_y}(n_y)$. RF process. Rotation frame.

RV	$m_y(n_y)$ **1-PDF RF process. Rotation frame**
τ_0	$f_{m_y}(n_y) = \frac{1}{\sqrt{2\pi\sigma_{M_0}^2}} e^{-\frac{1}{2}\left(\frac{\frac{n_y}{\sin(\gamma B_1 t)} - \mu_{M_0}}{\sigma_{M_0}}\right)^2} \left\lvert \frac{1}{\sin(\gamma B_1 t)} \right\rvert$
$\mathbf{B_1}$	$f_{m_y}(n_y) = \frac{1}{\sqrt{2\pi\sigma_{B_1}^2}} e^{-\frac{1}{2}\left(\frac{\frac{\arcsin\frac{n_y}{\tau_0}}{\gamma t} - \mu_{B_1}}{\sigma_{B_1}}\right)^2} \left\lvert \frac{1}{\gamma t\sqrt{\tau_0^2 - n_y^2}} \right\rvert$

Table 9.6: $f_{m_z}(n_z)$. RF process. Rotation frame.

RV	$m_z(n_z)$ **1-PDF RF process.Rotation frame**
τ_0	$f_{m_z}(n_y) = \frac{1}{\sqrt{2\pi\sigma_{M_0}^2}} e^{-\frac{1}{2}\left(\frac{\frac{n_z}{\cos(\gamma B_1 t)} - \mu_{M_0}}{\sigma_{M_0}}\right)^2} \left\lvert \frac{1}{\cos(\gamma B_1 t)} \right\rvert$
$\mathbf{B_1}$	$f_{m_z}(n_z) = \frac{1}{\sqrt{2\pi\sigma_{B_1}^2}} e^{-\frac{1}{2}\left(\frac{\frac{\arccos\frac{n_y}{\tau_0}}{\gamma t} - \mu_{B_1}}{\sigma_{B_1}}\right)^2} \left\lvert \frac{-1}{\gamma t\sqrt{\tau_0^2 - n_y^2}} \right\rvert$

Table 9.7: $f_{M_x}(m_x)$. RF process. Laboratory frame.

RV	$M_x(m_x)$ **1-PDF RF process. Laboratory frame**
τ_0	$f_{M_x}(m_x) = \frac{1}{\sqrt{2\pi\sigma_{M_0}^2}} e^{-\frac{1}{2}\left(\frac{\frac{m_x}{\sin(\gamma B_1 t)\sin(\gamma B_0 t)} - \mu_{M_0}}{\sigma_{M_0}}\right)^2} \left\lvert \frac{1}{\sin(\gamma B_1 t)\sin(\gamma B_0 t)} \right\rvert$
$\mathbf{B_0}$	$f_{M_x}(m_x) = \frac{1}{\sqrt{2\pi\sigma_{B_0}^2}} e^{-\frac{1}{2}\left(\frac{\arcsin\left(\frac{m_x}{\tau_0 \sin(\omega_1 t)}\right) - \gamma t \mu_{B_1}}{\gamma t \sigma_{B_1}}\right)^2} \left\lvert \frac{1}{\gamma t \sqrt{\tau_0^2 \sin \omega_1 t^2 - m_x^2}} \right\rvert$
$\mathbf{B_1}$	$f_{M_x}(m_x) = \frac{1}{\sqrt{2\pi\sigma_{B_1}^2}} e^{-\frac{1}{2}\left(\frac{\arcsin\left(\frac{m_x}{\tau_0 \sin(\omega_0 t)}\right) - \gamma t \mu_{B_1}}{\gamma t \sigma_{B_1}}\right)^2} \left\lvert \frac{1}{\gamma t \sqrt{\tau_0^2 \sin \omega_0 t^2 - m_x^2}} \right\rvert$

Table 9.8: $f_{M_y}(m_y)$. RF process. Laboratory frame.

RV	$M_y(m_y)$ **1-PDF RF process. Laboratory frame**
τ_0	$f_{M_y}(m_y) = \frac{1}{\sqrt{2\pi\sigma^2_{M_0}}} e^{-\frac{1}{2}\left(\frac{\frac{m_y}{\sin(\gamma B_1 t)\cos(\gamma B_0 t)} - \mu_{M_0}}{\sigma_{M_0}}\right)^2} \left\lvert \frac{1}{\sin(\gamma B_1 t)\cos(\gamma B_0 t)} \right\rvert$
$\mathbf{B_0}$	$f_{M_y}(m_y) = \frac{1}{\sqrt{2\pi\sigma^2_{B_0}}} e^{-\frac{1}{2}\left(\frac{\arccos\left(\frac{m_y}{\tau_0 \sin(\omega_1 t)}\right) - \gamma t \mu_{B_0}}{\gamma t \sigma_{B_0}}\right)^2} \left\lvert \frac{-1}{\gamma t \sqrt{\tau_0^2 \sin^2 \omega_1 t^2 - m_y}} \right\rvert$
$\mathbf{B_1}$	$f_{M_y}(m_y) = \frac{1}{\sqrt{2\pi\sigma^2_{B_1}}} e^{-\frac{1}{2}\left(\frac{\arcsin\left(\frac{m_y}{\tau_0 \cos(\omega_0 t)}\right) - \gamma t \mu_{B_1}}{\gamma t \sigma_{B_1}}\right)^2} \left\lvert \frac{1}{\gamma t \sqrt{\tau_0^2 \cos^2 \omega_0 t - m_y^2}} \right\rvert$

Table 9.9: $f_{M_xy}(m_{xy})$. RF process. Laboratory frame.

RV	$M_{xy}(m_{xy})$ **1-PDF RF process. Laboratory frame**
τ_0	the same as $f_{m_y}(n_y)$
$\mathbf{B_1}$	the same as $f_{m_y}(n_y)$

Table 9.10: $f_{M_z}(m_z)$. RF process. Laboratory frame.

RV	$M_z(m_z)$ **1-PDF RF process. Laboratory frame**
τ_0	$f_{M_z}(m_z) = \frac{1}{\sqrt{2\pi\sigma^2_{M_0}}} e^{-\frac{1}{2}\left(\frac{\frac{m_z}{\cos(\gamma B_1 t)} - \mu_{M_0}}{\sigma_{M_0}}\right)^2} \left\lvert \frac{1}{\cos(\gamma B_1 t)} \right\rvert$
$\mathbf{B_1}$	the same as $f_{m_z}(n_z)$

Bibliography

[1] Balac, S. and Chupin, L. *Fast approximate of Bloch equation for simulation of RF artifacts in Magnetic Resonance Imagin.* Mathematical and Computer Modelling 48 1901–1913 (2008) 10.1016/j.mcm.2007.05.021

[2] Hazra, A. Lube, G. and Raumer, H.G. *Numerical simulation of Bloch equations for dynamic magnetic resonance imaging.* Applied Numerical Mathematics 123 241–255 (2018) 10.1016/j.apnum.2017.09.007

[3] Jurczuk, K. *Computational modeling of MR flow imaging by the lattice Boltzmann method and Bloch equation.* Magnetic Resonance Imaging 31 1163–1173 (2013) 10.1016/j.mri.2013.01.005

[4] Wei, J. Wang, X. and Geng, X. *Periodic and rational solutions of the reduce d MaxwellBloch equations.* Commun Nonlinear Sci Numer Simulat 59 1–14 (2018) 10.1016/j.cnsns.2017.10.017

[5] Balac and S. Caloz, G. *Mathematical modelling and numerical simulation of magnetic susceptibility artifacts in magnetic Resonance Imaging.* Comput Methods Biomech Biomed Engin 3(4) 335–349 (2000) 10.1080/10255840008915276

[6] Gafner, A. *Construction of NMR Equipment to be used in the Physical Properties Measurement System (PPMS, Quantum Design).* Zürich. (2006).

[7] Cordes, C. *Efficient Simulation of Magnetic Resonance Imaging.* Germany. Optimus Verlag (2015). ISBN 978-3-86376-052-6

[8] McRobbie, D. Moore, E. Graves, M. and Prince, M. *MRI From Picture to Proton.* UK. Cambridge University Press (2006). ISBN-13 978-0-511-34944-7

[9] Lars G. *Introduction to Magnetic Resonance Imaging Techniques.* Denmark. Danish Research Centre for Magnetic Resonance (DRCMR) (2009).

[10] Hazra, A. *Numerical Simulation of Bloch Equations for Dynamic Magnetic Resonance Imaging.* India. Doctoral program (2016).

[11] Erdogmusa, D. Larssona, E. Yana, R. Principea, J. and Fitzsimmons, J. *Measuring the signal-to-noise ratio in magnetic resonance imaging: a caveat.* Signal Processing 84 1035–1040 (2004) 10.1016/j.sigpro.2004.03.006

[12] Ocali, O. and Atalar, E. *Ultimate intrinsic signal-to-noise ratio in MRI.* Magnetic Resonance in Medicine 39 462–473 (1998) PMID: 9498603

[13] Stanisz, G. Odrobina, E. Pun, J. Escaravage, M. Graham, S. Bronskill, M. and Henkelman, M. *T1, T2 relaxation and magnetization transfer in tissue at 3T.* Magnetic Resonance in Medicine 54 507–512 (2005) 10.1002/mrm.20605

[14] Epstein, C. and Wehrli, F. *Magnetic Resonance Imaging.* USA. Encyclopaedia of mathematical Physics, Elsevier, 367–375 (2005).

[15] Epstein, C. *Introduction to the Mathematics of Medical Imaging.* USA. Society for Industrial and applied Mathematics (2007). ISBN 978-0-89871-642-9

[16] Oleaga, L. and Lafuente, J. *Aprendiendo los Fundamentos de la Resonancia Magnética.* Argentina. Editorial Médica Panamericana (2006). ISBN 84-7903-899-3

[17] Hoult, D. , Bhakar, B. *NMR Signal Reception: Virtual Photons and Coherent Spontaneous Emission.* Canada. John Wiley & Sons, Inc. (1997). CCC 1043-7347/97/050277-21

[18] *Pulse Nuclear Magnetic Spectrometer.* USA. TeachSpin, Inc. (1997). `http://www.teachspin.com`

[19] Soong, T. *Random Differential Equations in Science and Engineering.* USA. Mathematics in Science and Engineering, vol.103 Academic Press Inc. (1973). ISBN-13 9780126548501

[20] Casabán, M.C. Cortés, J.C. Romero, J.V. and Roselló M.D. *Determining the first probability density function of linear random initial value problems by the Random Variable Transformation (R.V.T.) technique: A comprehensive study.* Abstract and Applied Analysis, vol. 2014 art. ID248512 1–25. (2014) 10.1155/2014/248512

[21] Casabán, M.C. Cortés, J.C. Romero, J.V. and Roselló M.D. *Probabilistic solution of random homogeneous linear second-order difference equations.* Mediterranean Journal of Mathematics. Issue 6 3817–3836 (2016) 10.1007/s00009-016-0716-6

[22] Grafakos, L. *Classical Fourier Analysis.* USA. Springer vol. 249 173–240 (2014). ISBN 978-1-4939-1194-3

[23] Hsieh, P. and Sibuya, Y. *Basic Theory of Ordinary Differential Equations.* USA. Springer (1999). ISBN 978-1-4612-1506-6

[24] Coddington, E. and Carlson, R. *Linear Ordinary Differential Equations.* USA Society for Industrial and Applied Mathematics (1997). ISBN 0-89871-388-9

[25] Grant, C. *Theory of Ordinary Differential Equations.* USA (2008). ISBN 13: 9781502911407

[26] Mkolesia, A. C. Kikawa, C. R. and Shatalov, M. Y. *Estimation of the Rayleigh Distribution Parameter.* Transylvanian Special Issue Review. Vol. 24(8) 1158–1163 (2016).

[27] Benoit-Cattin,H. Collewet,G. Belaroussi, B. Saint-Jalmes, H. and Odet,C. *The SIMRI project: a versatile and interactive MRI simulator.* Journal of Magnetic Resonance vol. 173 97–115 (2004). 10.1016/j.jmr.2004.09.027

[28] Christos G. Xanthis, Member, IEEE, Ioannis E. Venetis, A. V. Chalkias, and Anthony H. Aletras *MRISIMUL: A GPU-Based Parallel Approach to MRI Simulations.* IEEE Trans Med Imaging. 33(3) 607–17 (2013). 10.1109/TMI.2013.2292119

[29] Geiser, J. *Multicomponent and Multiscale Systems. Chapter 2: Functional Splitting.* Switzerland Springer International Publishing (2016). ISBN 978-3-319-15117-5

[30] Liang-Der, J. Rem, V.T. Stanley, A. and Saloner, D. *Calculation of the magnetization distribution for fluid flow in curved vessels.* Magnetic Resonance in Medicine vol.35(4) 577–584 (1996) 10.1002/mrm.1910350418

[31] Ern, A. and Guermond, J.-L. *Theory and Practice of Finite Elements.* Applied Mathematical Sciences vol. 159 (2004). ISBN 978-1-4757-4355-5